January 2015

Additives for Heat Transfer Enhancement in High Temperature Thermal Energy Storage Media: Selection and Characterization

Philip D. Myers Jr.
University of South Florida, philipmyers@mail.usf.edu

Additives for Heat Transfer Enhancement in High Temperature Thermal Energy Storage Media:

Selection and Characterization

by

Philip D. Myers, Jr.

A dissertation submitted in partial fulfillment
of the requirements for the degree of
Doctor of Philosophy
Department of Chemical and Biomedical Engineering
College of Engineering
University of South Florida

Co-Major Professor: D. Yogi Goswami, Ph.D.
Co-Major Professor: Elias Stefanakos, Ph.D.
Venkat Bhethanabotla, Ph.D.
Babu Joseph, Ph.D.
George Philippidis, Ph.D.

Date of Approval:
June 26, 2015

Keywords: PCM, sensible heat, inorganic salts, conduction, thermal radiation

DEDICATION

This work is dedicated to my family—my parents, Jocelyn and Philip, and my sister Amanda—for their endless love and support, and also to Kerri, for being a wellspring of affection, sympathy, and constructive criticism throughout the development of this work.

ACKNOWLEDGMENTS

I would like to first acknowledge the help and support of my friends and colleagues at the University of South Florida's (USF's) Clean Energy Research Center (CERC), including—but certainly not limited to—Saeb Besarati, Tanvir Alam, Abhinav Bhardwaj, Antonio Ramos Archibold, Emre Demirocak, Prashanth Sridharan, Chennan Li, Chatura Wickramaratne, Innocent Udom, Rajeev Kamal, Jamie Trahan, Mehdi Zeyghami, and Yang Yang Zhang. I am likewise indebted to many other fellow students at the USF College of Engineering who were not mentioned above.

Special thanks is owed to my advisors D. Yogi Goswami and Elias Stefanakos, without whose counsel and contributions none of this work would be possible. I am very much in their debt, and I remain exceedingly grateful at their willingness to freely share of their expertise as they direct me in my studies and future endeavors.

I would be remiss to not acknowledge the efforts of many others at USF and CERC. Barbara Graham deserves special mention, for her tireless work in helping all the CERC students navigate their way through USF and beyond. Charles Garretson, laboratory supervisor, was invaluable in assisting my experimental work, and I hope he's enjoying his much-deserved retirement. There are too many other students, professors, and staff to dutifully mention here, and so I sincerely apologize to any who have been overlooked.

Thank you all!

TABLE OF CONTENTS

LIST OF TABLES

LIST OF FIGURES

ABSTRACT

Inorganic salts are very promising as high-temperature heat transfer fluids and thermal storage media in solar thermal power production. The dual-tank molten salt storage system, for example, has been demonstrated to be effective for continuous operation in solar power tower plants. In this particular storage regime, however, much of the thermal storage potential of the salts is ignored. Most inorganic salts are characterized by high heats of fusion, so their use as phase-change materials (PCMs) allows for substantially higher energy storage density than their use as sensible heat storage alone. For instance, use of molten sodium-potassium eutectic salt over a temperature range of 260 to 560°C (the approximate operating parameters of a proposed utility-scale storage system) allows for a volumetric energy storage density of 212 kWh_{th}/m^3, whereas the use of pure sodium nitrate (T_m = 307°C) over the same temperature range (utilizing both sensible and latent heat) yields a storage density of 347 kWh_{th}/m^3.

The main downside to these media is their relatively low thermal conductivity (typically on the order of 1 W/m-K). While low conductivity is not as much an issue with heat transfer fluids, which, owing to convective heat transfer, are not as reliant on conduction as a heat transfer mode, it can become important for PCM storage strategies, in which transient charging behavior will necessarily involve heating the solid-phase material up to and through the process of melting. This investigation seeks to develop new methods of improving heat transfer in inorganic salt latent heat thermal energy storage (TES) media, such as sodium / potassium nitrates and chlorides. These methods include two basic strategies: first, inclusion of conductivity-enhancing additives, and second, incorporation of infrared absorptive additives in otherwise transparent media. Also, in the

process, a group of chloride based salts for use as sensible storage media and/or heat transfer fluids has been developed, based on relevant cost and thermophysical properties data.

For direct conductivity enhancement, the idea is simple: a PCM with low conductivity can be enhanced by incorporation of nanoparticulate additives at low concentration (~5 wt %). This concept has been explored extensively with lower temperature heat transfer fluids such as water, ethylene glycol, etc. (e.g., nanofluids), as well as with many lower temperature PCMs, such as paraffin wax. Extension of the concept to high temperature inorganic salt thermal storage media brings new challenges—most importantly, material compatibility. Also, maintenance of the additive distribution can be more difficult. Promising results were obtained in both these regards with nitrate salt systems.

The second heat transfer enhancement strategy examined here is more novel in principle: increasing the infrared absorption of a semitransparent salt PCM (e.g., NaCl) with a suitable additive can theoretically enhance radiative heat transfer (for sufficiently high temperatures), thereby compensating for low thermal conductivity. Here again, material compatibility and maintenance of additive dispersion become the focus, but in very different ways, owing to the higher temperatures of application (>600°C) and the much lower concentration of additives required (~0.5 wt %). Promising results have been obtained in this case, as well, in terms of demonstrably greater infrared absorptance with inclusion of additives.

CHAPTER 1 INTRODUCTION

It is widely agreed that the increased development and implementation of renewable energy (e.g., solar, wind, biomass) will benefit the environment, principally due to the decline in greenhouse gas emissions expected from phasing out fossil fuels. Furthermore, so-called clean energy technologies afford additional benefits—namely, decreased emissions of other pollutants. Solar energy in particular seems ideal for aiding in the transition from non-renewable to renewable energy sources, as over much of the planet the sun is an abundant and easily accessible resource.

When contemplating the strengths and weaknesses of various energy technologies, it is worthwhile to examine the energy picture as it stands today. In Figure 1, the total yearly electricity generation for the U.S. across various resource types is plotted for the years of 2013 and 2014, using data taken from the U.S. Energy Information Administration (EIA) [1]. According to these data, renewable energy sources account for approximately 13.7% of the total electricity generation for 2014. Solar is seen to comprise a comparatively small part of the total electricity market; however, its generation grew by 116% from 2013 to 2014—more than any other resource type. In other words, solar energy has the most room to grow and the greatest potential for growth of any renewable energy source.

However, renewable energy technologies in general, including solar energy, suffer from intermittency. As an illustration, the solar irradiance as a function of the hour of the day and month of the year for Tampa, Florida (27.96°N, 82.54°W) is plotted in Figure 2, using the ASHRAE Clear Sky Model [2, 3]. Data for a single day, October 21, are extracted and plotted in Figure 3 with measured data obtained from the National Solar Radiation Database (NSRDB) [4]. In this

way, two types of solar resource intermittency are demonstrated: the ASHRAE model shows the daily and seasonal variations due to the earth's rotation and orbit around the sun, while the NSRDB data show the additional, generally unpredictable variation due to other factors—in this case, weather events. Other renewable energy technologies, such as tidal and wind power, also suffer from intermittency. For example, electricity generated by wind is plotted with total consumption in Figure 4 for two weeks in Denmark in January 2000 [5]. It is seen that wind power yields rather irregular generation patterns (some days there is no generation, and some days wind power accounts for over one third of the peak consumption), and these patterns are considerably less predictable than the consumption patterns. The key to overcoming intermittency is energy storage: during peak output (in excess of demand) energy is stored; later, when output declines (below the demand), the energy is redistributed to compensate for the shortfall. An example of such a strategy specific to solar energy utilization is depicted in Figure 5. This dissertation will investigate materials with potential for use in thermal energy storage (TES), specifically with solar power generation in mind.

Inorganic salts are already very promising as high-temperature heat transfer fluids and thermal storage media in solar thermal power production. Recent efforts in Arizona have demonstrated 6 hours nighttime generation from dual-tank molten salt storage, and similar plants elsewhere in the American southwest—solar power tower with dual-tank molten salt storage—are projected to be completed in the near future. Yet in this particular storage regime, much of the potential of inorganic salts as storage media is ignored. These materials are characterized by high heats of fusion, so their use as phase-change materials (PCMs) allows for substantially higher energy storage density than their use as sensible heat storage alone. For instance, use of molten sodium-potassium nitrate eutectic salt over a temperature range of 260 to 560°C (the approximate

operating parameters of a proposed utility-scale storage system) allows for a volumetric energy storage density of 212 kWh_{th}/m^3, whereas the use of pure sodium nitrate (T_m = 307°C) over the same temperature range (utilizing both sensible and latent heat) yields a storage density of 347 kWh_{th}/m^3. Also of interest, chloride salts, including sodium chloride and the eutectic system formed by sodium and potassium chloride, display both higher melting temperatures and higher latent heats than their nitrate counterparts. Taking into account the relatively low cost of NaCl, it seems likely that these salts will find greater application as solar energy conversion strategies develop toward greater operating temperatures and efficiencies.

These materials, however, are significantly hampered by their relatively low thermal conductivity (typically on the order of 1 W/m-K). While low conductivity is not as much an issue with heat transfer fluids, which, owing to convective heat transfer, are not as reliant on conduction as a heat transfer mode, it can become important for PCM storage strategies, in which transient charging behavior will necessarily involve heating the solid-phase material up to and through the process of melting. This research discusses novel strategies for overcoming the typically low thermal conductivities of inorganic salt PCMs—namely, direct enhancement of thermal conductivity or radiative heat transfer through inclusion of appropriate additive materials.

In Chapter 2, a review of potential PCM heat transfer enhancement techniques is presented, including a treatment of prior work on radiative transfer enhancement. In this chapter, as well, a PCM screening process is described, whereby the salts of interest in this study, nitrates and chlorides, are selected. In Chapter 3, case studies based on direct conductivity enhancement are presented, elucidating the potential for direct enhancement of thermal conductivity through addition of high conductivity particles. In Chapter 4, a more detailed survey of the chloride salts is performed, with the goal of identifying promising pure salts and multicomponent systems for

either latent or sensible TES. In Chapter 5, enhancement of heat transfer by increasing infrared absorption via addition of IR-absorptive particles in some of these salt systems is examined. In Chapter 6, numerical techniques for studying these systems are explored, and the potential performance enhancement using these techniques is quantified. Finally, in Chapter 7, conclusions of this work are summarized.

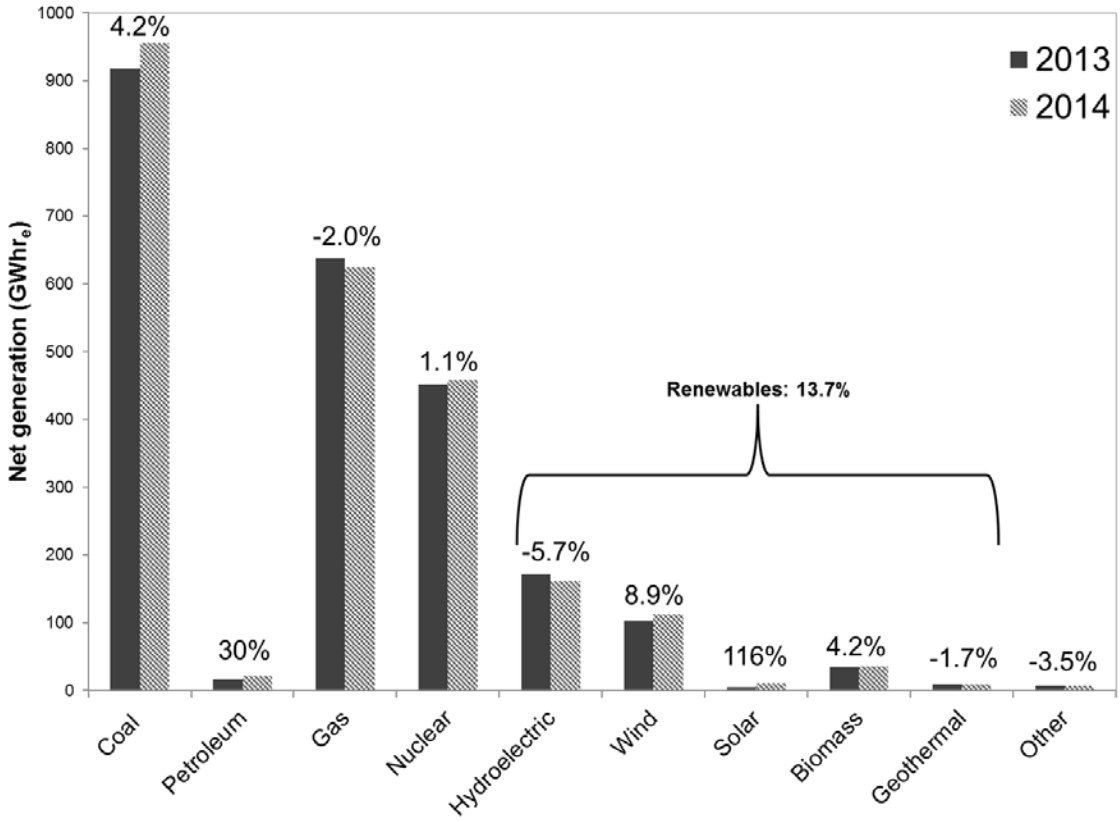

Figure 1 Total yearly electricity generation, U.S. The percent change in generation capacity from 2013 to 2014 is shown above each category.

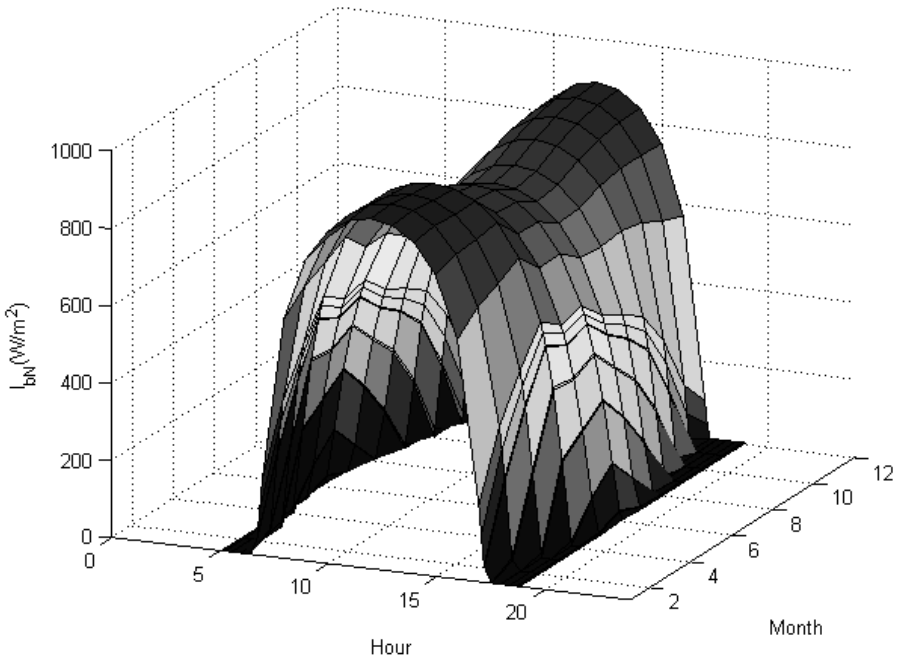

Figure 2 Solar irradiance for Tampa, Florida. Calculated using the ASHRAE Clear Sky Model.

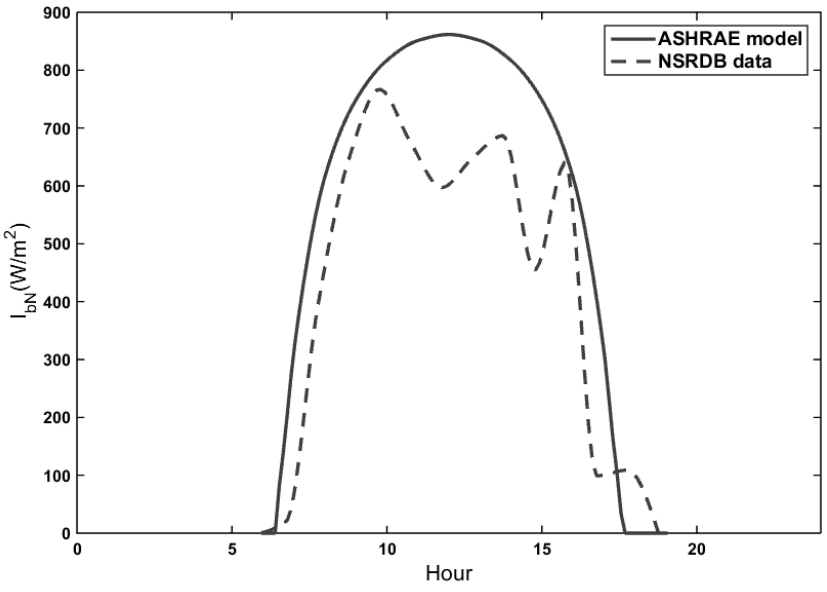

Figure 3 Solar irradiance for Tampa, Florida, on October 21.

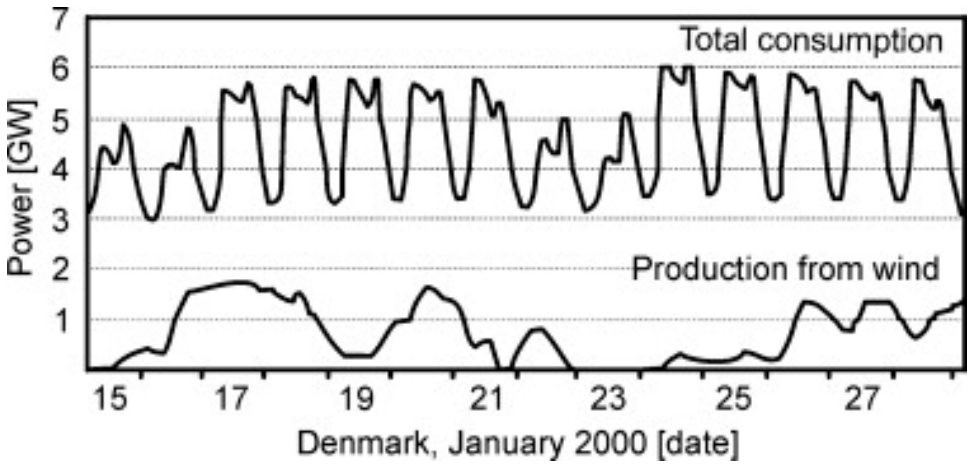

Figure 4 Electricity generation via wind versus total consumption, Denmark, January 2000 [5].

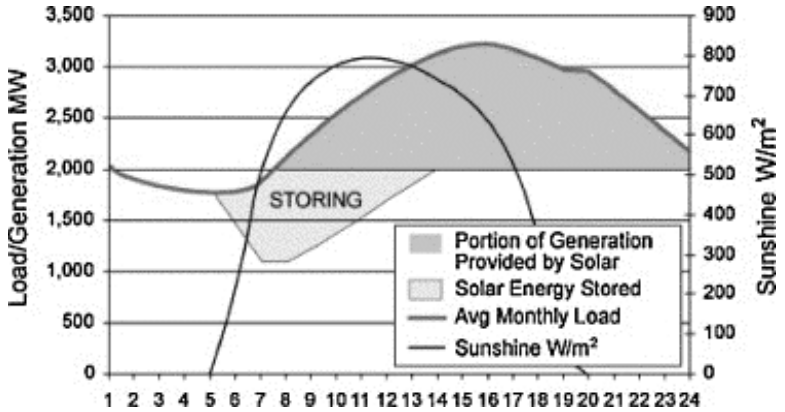

Figure 5 Energy storage scheme for a solar power plant [6, 7].

CHAPTER 2 LITERATURE REVIEW

2.1 Introduction

This chapter examines various strategies for overcoming the typically low thermal conductivities of inorganic salt PCMs—namely, inclusion of conductivity-enhancing additives, encapsulation / dispersal for increased heat transfer area, and enhancement of other modes of heat transfer. Particular attention is paid to the work proposed for this research:

- Thermal conductivity enhancement through addition of high conductivity particles
- Thermal radiative transfer enhancement through addition of infrared (IR-) absorptive materials.

Additionally, at the conclusion of the chapter, a discussion of the selection of PCM for study is presented.

2.2 Background

TES will likely play an important role in the renewable technology development of the near future. It may find applicability in utilizing process / waste heat, aiding in temperature regulation of sensitive electronics, building heating / cooling, and power conversion—in each case allowing for improved overall efficiencies over conventional technologies [8, 9]. It has been said that the oldest form of TES took the form of ice harvested from lakes and rivers in the winter for cooling during warmer months. This type of "seasonal" TES itself entails a phase change process (melting of the ice), and the Hungarian parliament building is still air-conditioned in part by this TES scheme [10]. TES is especially important in power generation, and has advantages over technologies such as mechanical (e.g., compressed air storage) or chemical (e.g., batteries) in that

it generally entails lower capital cost [11, 12]. Solar thermal power possesses a versatility unique among renewable energy technologies: the ability to dovetail with existing and widely prevalent fossil fuel conversion systems in combined cycle schemes. Further, for solar thermal power plants, TES is a simple, efficient, and cost effective way to store energy by converting sunlight to heat as an intermediate step, holding it until it is needed, at which time it can be fed to a heat engine [13]. More information on the technological details on solar power plants can be found in the review by Barlev et al [14]; extensive review of the importance and practical design concerns of TES in concentrating solar power plants can be found in the work by Kuravi et al [12].

TES can generally be divided into three distinct categories: sensible heat, latent heat, and thermochemical energy [3]. Sensible heat is perhaps the most familiar; it stored by heating a mass of material of constant phase (e.g., does not melt or evaporate) from a lower temperature to a higher temperature, and its quantification requires knowledge of the material's specific heat capacity (c_p), which itself may vary with temperature. Latent heat, on the other hand, stems from a phase change and attendant change in enthalpy of the storage medium—that is, a solid-solid phase change [crystallographic reorientation of sodium nitrate ($NaNO_3$) at 276°C], a solid-liquid phase change (e.g., melting of $NaNO_3$ at the temperature of 306°C), a solid-gas phase change (i.e., sublimation, as ice to water vapor, for instance), or a liquid-gas phase change (e.g., evaporative cooling). In this way latent heat storage makes use of phase-change materials (PCMs), and they have potential to offer great improvements over sensible heat storage alone, owing to the typically large quantities of energy required for phase change and the potential to store / deliver heat a consistent temperature (i.e., the phase-change temperature) [15]. TES via thermochemical energy is illustrated in Figure 6. Thermochemical storage is very promising because of its potential for

significant energy storage capacity (mass basis) [13]; however, it faces a number of technical challenges, and it will not be discussed further in this dissertation.

As a matter of practicality, solid-liquid PCMs have received the most attention—evaporative processes tend to require more rigorous containment controls (either pressurized containers or substantially larger containment volumes) [16], and solid-solid phase change enthalpies tend to be significantly lower in magnitude than those of solid-liquid phase changes [17]—but it is important to be aware of the potential energetic contributions of other phase changes near the melting point of the material in question. Complications such as this may arise in, for example, the $NaNO_3$ system, which has its solid-solid transition only approximately 34 degrees below its melting point, or in the NaCl system, which, although it has no solid-solid phase transition, has a comparatively high vapor pressure upon melting, and thus any NaCl that evaporates (without condensing) will bring about an additional source of absorbed heat [18, 19].

The focus of this study is PCM-based TES—that is, primarily the latent heat contribution. It is possible to divide such materials into two general categories, organic and inorganic, and further to divide the inorganic storage media into salt hydrates, anhydrous salts, and metallic materials [16, 17]. This research mainly focuses on TES for concentrating solar power plants, which tend to result in working fluid temperatures well in excess of 200°C [20]. At these temperatures, organic materials are difficult if not impossible to work with, so organic PCMs will not be considered here. Salt hydrates similarly are limited to lower temperatures, and so they will be neglected [21]. (For a more information on lower temperature PCMs, including salt hydrates and organic PCMs, the reader is referred to the reviews by Farid and A. Sharma [9, 22].) The remaining candidate materials are anhydrous salts (either pure or in eutectic or near-eutectic mixtures) or metals (either pure or alloyed). Metals are desirable for a number of reasons, including

high latent heat of fusion per volume, small change in volume upon melting, and relatively low vapor pressures. However, they are generally more expensive than anhydrous salts and much more prone to oxidative degradation. Hence, we will focus here on anhydrous salts as PCM thermal storage materials. (For discussions on the use of metals as PCMs, the reader is referred to the works of Sharma et al, Kenisarin, and Cárdenas and León [9, 17, 23].)

Inorganic salts have already found widespread use as storage media in a sensible heat storage arrangement, such as in the system depicted in Figure 7. Molten salts in utility scale storage systems—the two-tank storage system design—are well-established [24]. Indeed, multiple power plants soon to come online will make use of this storage strategy, including the Crescent Dunes project in Tonopah, Nevada [13]. In this scheme, molten salts, typically either the ternary eutectic system of sodium nitrite, sodium nitrate, and potassium nitrate, or the binary eutectic system of sodium nitrate and potassium nitrate, are stored in the molten state in two different tanks: a hot tank and a cold tank. The cold salt is pumped through heat exchangers which transfer heat from the solar field to the salt; after heating, the salt is stored in the hot tank. When production lags (e.g., due to cloud cover or off-daylight hours), the process is run in reverse, with the hot salt heating the heat transfer fluid (HTF) to run the power block before returning to the cold tank, having released its accumulated thermal energy.

Technically speaking, the storage scheme described above is an example of indirect two-tank storage; that is, the fluid used in the storage system (molten salt) is segregated from the HTF in the solar field (e.g., thermal oil) [25]. As concentrating solar power plants have achieved higher temperatures (and correspondingly higher power block efficiencies), a simpler arrangement has drawn attention: direct two-tank storage. This arrangement is being investigated extensively for fluids with lower melting temperatures. It is important to note that the conventional indirect storage

system, when applied to molten salt storage for a thermal oil HTF, requires high pressure on the HTF side (high vapor pressure oil) and rather low pressure on the molten salt side (low vapor pressure nitrate salts); heat exchangers may therefore be required to accommodate a pressure difference of 15 bar or more [26]. The motivation in moving to direct storage is simple: by employing the same molten salts as both HTF and TES media, the capital costs savings in eliminating these heat exchangers will bring the overall cost of storage down.[1] Also, in some cases, the heat exchanger involved in the indirect storage arrangement has been shown to decrease exergetic efficiency [13].

The latent heat of fusion of salts such as these provides a new largely unexplored avenue to greater energy storage density. For instance, use of molten sodium-potassium eutectic salt over a temperature range of 260 to 560°C (the approximate operating parameters of a proposed utility-scale storage system) allows for an volumetric energy storage density of 212 kWh/m^3, whereas the use of pure sodium nitrate (T_m = 307°C) over the same temperature range (utilizing both sensible and latent heat) yields a storage density of 347 kWh/m^3 (thermophysical properties data obtained from FactSage [27]).

To better illustrate, a generalized phase change process for a hypothetical pure substance is depicted in Figure 8. In this process, the pure substance undergoes a solid-solid transition (i.e., from α to β morphology), followed by melting and then vaporization. The areas of the plot showing rising temperature correspond to sensible heating of the various pure phases—that is, α-phase solid, β-phase solid, liquid, and vapor. The areas of the plot showing invariant temperature represent the various phase transitions, each requiring a certain amount heat to completely convert

[1] Other considerations come into play, of course; piping, pumps, and other equipment may need to be redesigned to ensure compatibility with the salt(s) as transfer fluid. A detailed economic analysis is required to balance any additional costs against the savings of eliminating the heat exchangers.

the pure substance from its lower temperature phase to its higher temperature phase. The figure is not meant to be quantitative, but it does show qualitatively that the solid-solid transition is less in quantity of heat required than the solid-liquid transition, which itself is less than the liquid-vapor transition, on a per mole basis.[2]

For our purposes, it suffices to focus on the solid-liquid transition. In this case, it has been shown that the total heat stored in a storage system making use of media elevated from temperature, T_1, to temperature, T_2, can be quantified as follows [3].

$$Q = \int_{T_1}^{T_m} mc_{p,s}dT + m\Delta H_{fus} + \int_{T_m}^{T_2} mc_{p,l}dT \tag{2.1}$$

Here, T_m represents the phase change temperature, m is the mass of the material, ΔH_{fus} is the latent heat of fusion, and c_p is the specific heat capacity, either of the solid (*s*) or liquid (*l*) phase. As such, the second term of the equation captures the phase transformation heat, while the first and the third terms of the equation account for sensible heating of the solid and liquid phases, respectively.

It is worth noting that, as with all sensible storage media, a wider range of temperature elevation will result in a greater amount of heat stored; however, the advantage of PCMs as storage media is greater for narrower operating temperatures. As an illustration, consider the abovementioned comparison between $NaNO_3$ PCM as sensible and latent heat storage and KNO_3-$NaNO_3$ eutectic liquid as sensible heating alone. The PCM was shown to give approximately 64% greater volumetric storage density (347÷212=1.637). Let us consider instead a narrower operating range—say, 260 to 360°C. In this case, the purely sensible heating media decreases markedly in

[2] This is not to say that the liquid-vapor transition is more favorable from a thermal energy storage standpoint; owing to the significantly greater molar volume in the vapor phase, storage systems based on a liquid-vapor transition would have much less volumetric energy storage density than those based on the solid-liquid transition.

volumetric storage density, from 212 to 77.1 kWh/m^3; this is due to the much smaller temperature range for very nearly the same specific heat capacity and density.[3] The PCM, while also decreasing, is still substantially higher in storage density at 186 kWh/m^3. So, for this smaller temperature range, the PCM offers over 140% more volumetric storage density (186÷77.1=2.412). For related reasons, many PCM containment designs stipulate a kind of cascade scheme, where higher melting PCMs are placed upstream of lower melting PCMs during charging (i.e., hot HTF first encounters the highest melting PCM before flowing to lower melting materials), so that in a practical sense narrower temperature ranges pertain to individual PCMs—high melting PCM collects heat from the hottest fluid stream, lower melting PCM collects heat from a lower-temperature fluid stream, etc. [28]. In this way, PCM materials can be a significant improvement over conventional sensible heat storage technologies, allowing for greater volumetric energy storage density and narrower operating temperatures (greater exergetic efficiency) [13].

Typical arrangements for PCM TES units may take many forms. The packed-bed arrangement, pictured in Figure 9, entails a number of capsules containing some amount of PCM which are packed in a container through with the HTF flows. Another arrangement is a cylindrical shell storage unit, pictured in Figure 10. In this case, the PCM is encapsulated in cylindrical tubes housed within a larger cylindrical shell; through this shell, the HTF flows (tube-side PCM). An alternative but similar arrangement is shown in Figure 11. Here, the PCM is contained in the shell, while the HTF flows through the tubes (shell-side PCM). These are just a few of the arrangements possible for TES units; more discussion of such geometries and their impact on performance may be found in Chapter 6.

[3]In point of fact, both the specific heat and the density of the liquid eutectic salt vary with respect with temperature, and this variation has been accounted for in the calculations. The specific heat increases slightly over the temperature range, while the density decreases. However, the gains in volumetric capacity by having a lower temperature (denser) fluid are negligible compared to the sensible heating capacity lost with the much shorter span in temperature.

2.3 PCM Selection Criteria

A list of the basic requirements that any potential PCM storage media should meet has been presented by Kenisarin [23]:

- Appropriate melting temperature. The temperature must be within the operating range of interest—ideally comfortably within that range, so as to provide a buffer for any transient effects (e.g., supercooling). Appropriate temperatures can be obtained by eutectic combinations of salts, either binary or ternary.
- High specific heat, enthalpy of fusion, and density. In other words, the PCM should have a high thermal storage capacity, as would be expected of any successful candidate thermal storage medium.
- Congruent phase change. Congruent phase change results in equal compositions of PCM constituents in both (solid and liquid) phases.
- Reliable convertibility after repeated cycling. As may be the case with incongruent phase change, or if phase change occurs in the presence of labile impurities, repeated thermal cycling may compromise the thermophysical properties of the PCM. It has been demonstrated that both the enthalpy of fusion and the melting temperature of various eutectic salts and metal alloys can decline markedly after thermal cycling on the order of 1000 times [23]. Single-component salt PCMs seem less prone to this problem.
- High thermal conductivity. The thermal conductivity will dictate the transient behavior of the storage system, although convective heat transfer effects will play a major role, as well [29].

- Tolerable volume change upon phase change. Salts tend to have significant volume changes upon melting, and it is up to the designer to choose among candidate PCMs appropriately and account for this effect.
- Insignificant supercooling. Supercooling is the phenomenon whereby a system can cool to below its phase change temperature without undergoing a phase transition, usually the result of a metastable state forming due to a lack of nucleation points [30]. Such behavior is characteristic of crystalline salts, and can lead to rather drastic transient effects.
- Chemical stability. The PCM must remain chemically inert over the life of its use—ideally on the order of many years.
- Compatibility with construction / container / encapsulation materials. Material compatibility can be a problem with salts especially, many of which have a high tendency to corrode common construction materials such as iron. As such, extensive research has been conducted investigating potential encapsulation techniques for use with these PCMs [8].
- Tolerable toxicity. The toxicity of these compounds warrants attention—the inclusion of adequate health and safety measures in the manufacturing design may introduce unforeseen costs.
- Flame and fire safety. Again, additional health and safety measures to contain the threat posed by flammable or explosive candidate PCMs will likely introduce unforeseen costs. Thus, these materials should be avoided where prudent.

- Cost. A principal goal of this project is to reduce the cost of thermal storage as much as is practicable. As such, high cost PCM materials (e.g., lithium salts as opposed to sodium salts) is not advisable.

It is prudent to amend two of these criteria. Firstly, further elaboration is called for concerning congruent phase change. Congruent melting stipulates that there is no change in composition in undergoing the phase transition—for instance, a eutectic mixture would melt congruently, with the same composition of chemical components in the solid phase prior to melting reflected in the homogeneous liquid phase after melting. However, the phase change need not be perfectly congruent. A so-called "semi-congruent" transition is also tolerable, in the sense that it allows for complete melting of the PCM material, despite the fact that it may be slightly off-eutectic, for instance, in composition [21]. In this case, however, the phase change may occur over some range of temperatures, which would be acceptable if it remains small and within the range of operating temperatures of the system [31]. Semi-congruent phase change systems will generally involve pure PCMs with very small concentrations of impurities (this may be the case with many commercially available salts, for instance) or eutectic mixtures of PCMs with some slight excess of one or more components (this may occur during industrial scale preparation of PCM mixtures).

Next, there is the problem of conductivity. Most salts considered in the context of PCMs display relatively low thermal conductivities, on the order of 1 W/m-K [23]. In focusing on inorganic salt PCMs, therefore, this report must address the inherent problem of low conductivity. Use of adjuncts or additives that improve the conductivity of these materials has been investigated—specifically, graphite-salt composites show much improved conductivity, while generally retaining desired phase change characteristics [32]. Container ribbing or incorporation of fins are other possible means of improving heat transfer in poorly conductive PCMs [33].

Ultimately, the goal of this research is to improve the heat transfer characteristics of the PCM materials proposed for TES. Below is presented a summary of various heat transfer enhancement techniques, with particular emphasis placed on the enhancement of radiative transfer.

2.4 Heat Transfer Enhancement

In a comprehensive review of latent heat thermal storage system performance enhancement, Jegadheeswaran and Pohekar cite four classifications of enhancement techniques: 1) use of extended surfaces; 2) incorporation of multiple PCMs; 3) enhancement of thermal conductivity; and 4) micro-encapsulation of PCMs [34]. To this we add only the following: encapsulation in a more general sense and enhancement of other modes of heat transfer.

It is important to differentiate between micro-encapsulation and encapsulation in general. The benefits of micro-encapsulation in enhancement of heat transfer are clear—a much greater surface area to volume ratio will necessarily increase the rate of heat transfer. However, micro-encapsulation carries with it a complication with regard to another mode of heat transfer: convection. Clearly on the PCM side of the encapsulant, natural convection is hindered by virtue of the smaller characteristic dimensions of the PCM; more importantly, though, this complication can apply to the HTF, as well. Depending on the packing of the micro-encapsulated PCM, the encapsulant matrix may be so rigid as to prevent significant convective currents from forming in the HTF, thereby decreasing the overall heat transfer rate in spite of the increase in heat transfer area [15]. An additional downside is the relative cost of encapsulant—much greater surface area relative to PCM volume necessitates much more encapsulation material [8].

Alternatively, larger scale encapsulation (e.g., spheroidal pellets on the order of 1 inch in diameter) can provide an improvement over the simplistic case of the bulk PCM, but it is not a trivial improvement. Encapsulation of pellets in the range of 0.5 to 8.0 cm in diameter has shown

to yield distinct benefits in lieu of another promising design, the heat pipe [35]. Furthermore, the dimensions of the pellets may allow for improved convective transfer from the HTF, i.e., in the pores of a packed bed.

Enhancement of thermal conductivity of PCMs represents the seemingly most direct route to heat transfer improvement. However, it has been demonstrated by numerous studies that focusing entirely on the conductive mode of heat transfer, at the expense of other modes, can be ultimately deleterious. As alluded to above, the best example of this is seen in the importance of convective heat transfer in the melting process of PCMs [36]. In short, conductivity enhancing materials may improve the sensible heating regime of the solid phase, but if they significantly increase the viscosity of the liquid PCM, they may hinder both the melting process and sensible heating of the liquid.

Conduction typically predominates over convection during the process of solidification. Here, we have the reverse situation as with melting: we begin with a completely liquid material. As the temperature cools, depending on the liquid's viscosity, it should transport heat mainly by natural convection currents within the liquid. However, as soon as it starts to solidify, there is less liquid to provide this mode of transport. Moreover, because the solidification happens along the walls of the container, one can expect the convection to be limited to a smaller and smaller region within the material (i.e., as the solid layers accumulate on the walls). These solid layers form a new barrier to heat transfer from the outer wall of the container to the inner liquid, limiting heat transfer according to the solid-state thermal conductivity of the PCM [37]. Similar results were demonstrated in the numerical and experimental work of Lamberg et al [38, 39].

It is clear, then, that conduction alone is not generally determinative in the phase change processes of these heat storage systems. As such, strategies for enhancement of other modes of

heat transfer—namely, convection and radiation—open up new avenues for optimizing charging / discharging times. Increasing the effectiveness of convective heat transfer is well known: such considerations come into play in designing containers (geometry, areas of heat transfer, etc.) and also, often, in the incorporation of extended surfaces. As pointed out by Jegadheeswaran and Pohekar in their review of work in this field, use of extended surfaces within PCMs must promote natural convection in the systems or else provide such a preponderance of additional heat transfer area (e.g., by conduction and convection) to overcome any loss in convection caused by their presence [34]. In as much as convection is an inherent concern in the design of PCM containers and extended surfaces, we will not treat convective heat transfer enhancement as a separate category.

Radiative heat transfer enhancement, however, is worth additional attention, if only for its novelty in this field. While much work has been done in the study of lower temperature PCMs (organic materials, salt hydrates, etc.), work on PCMs formulated from inorganic salts, such as nitrates, is relatively recent. Furthermore, much of this work has focused on relatively low melting salts—say, below the temperature of 600°C. As such, little attention has been paid to thermal radiation as a heat transfer mode in the melting / solidification of these materials. The potential for improving radiative transfer in these materials as a heat transfer enhancement will therefore be discussed as a separate category.

To summarize, the following categories of heat transfer enhancement will be discussed:

- Extended surfaces
- Encapsulation
- High thermal conductivity additives / matrices
- Radiative transfer enhancement

Before continuing, it is worthwhile to mention “direct contact” PCM storage. Direct contact thermal storage units—that is, storage units where the HTF is bubbled through the PCM material—have been proposed for lower temperature systems, such as salt hydrates [40]. However, this is generally not acceptable for use with high temperature inorganic salt PCMs. Firstly, it is likely that HTFs employed would react with the salt PCMs. Consider high temperature organic HTFs, which may work well with nitrate-based PCMs if segregated through a heat exchange system, but would likely be degraded by the highly oxidative nitrate salts [41]. Alternately, if molten salt (e.g., KNO_3-$NaNO_3$ eutectic) is used as the HTF, there will undoubtedly be some miscibility and/or ion exchange with the PCM salt, thereby rendering the heat storage unit impractical. In short, it is highly likely that heat storage unit making use of these anhydrous inorganic salt PCMs will need containment to segregate the PCM from the HTF.

2.4.1 Extended Surfaces

Perhaps the simplest idea of extended surfaces in the design of PCM TES systems are embedded pipes—that is, pipes conveying the HTF through a volume of PCM material. Tao et al studied this concept and in particular examined three pipe geometries: dimpled, cone-finned, and helically finned [42]. They demonstrated that all three performed better (i.e., faster melting times) than the smooth pipe, with the helically finned tube showing the greatest improvement relative to the smooth pipe. Tamme et al describe such a system with water / steam as the HTF and KNO_3-$NaNO_3$ eutectic as the PCM storage material [43]. At least during discharging, thermal conductivity of the PCM will largely determine the rate of heat transfer, as solid PCM begins to accumulate on the embedded pipes. Their analysis shows that even a small increase in the thermal conductivity of the PCM will significantly decrease the required number of pipes for a specified heat flow demand. As such, they examined a variety of ways of incorporating relatively high

conductivity graphite into the PCM, including the use of graphite foil, which showed resistance to corrosion by nitrate salts, as a kind of conductive fin between sandwiched layers of PCM material [44].

Fins are very promising as heat transfer enhancing surfaces, and they can be employed on either the PCM or HTF side [34]. Common fin arrangements in a latent heat storage system are shown in Figure 12. Focusing on lower temperature PCM materials (namely, paraffin), Bugaje showed the effectiveness of fins in improving heat transfer rates, with fins performing better than star-shaped matrices and improving phase change times for both melting and freezing, with the effect more pronounced during solidification [45]. Steinmann examined systems with both graphite and aluminum fins [46]. Both systems displayed improved heat transfer. Moreover, a pilot-scale heat storage unit with aluminum fins was operated for more than 4000 hours (168 thermal cycles) with no obvious degradation of the aluminum fins; no mention was made of any decline in performance over the course of the pilot study.

A more novel example of extended surfaces in PCM storage unit design is the heat pipe [47]. As with embedded tubes, the PCM can either surround tubes or be placed within them, in either case with HTF flowing on the other side; a schematic showing the PCM outside the tubes is shown in Figure 13. In either case, the heat pipes are best arranged so as to be perpendicular to the HTF flow (i.e., see Figure 14). The heat pipe serves as a high conductivity bridge between the PCM and the HTF. It has an additional fluid within it, whose evaporation and condensation increases the effective conductivity of the heat pipe. Extensive work on this topic has been undertaken by Nithyanandam and Pitchumani [48, 49]. In a subsequent economic analysis, however, they show that storage systems based on encapsulated PCM had lower capital cost, lower levelized cost of electricity (LCOE), higher exergetic efficiency, and higher capacity factor then

optimized systems using heat pipes [35]. It is important to note, however, that there study was based on an initial study using paraffin wax as the PCM, and they make no mention of materials / fluid selection in light of the higher temperature nitrate salt PCM considered in their work.

Whatever strategy is employed with extended surfaces, it is important to be mindful of the impact extended surfaces for conductive transfer may have on convective transfer. It has been pointed out in the design of fins for improved heat transfer that there is typically an optimum point that balances the increased surface area for heat transfer with the decreased degree of natural convection caused by the addition (number / size) of fins [34]. Owing to the nature of phase change, this is a necessary optimization analysis that must be performed on a case-by-case basis.

2.4.2 Encapsulation

As mentioned above, one can think about encapsulation in terms of micro-encapsulation or macro-encapsulation [22]. Most of the work on micro-encapsulation pertains only to lower temperature PCM materials; hence, it will not be addressed here. From this point forward, macro-encapsulation shall be referred to simply as encapsulation.

There are clear advantages to an encapsulated PCM storage unit, including more effective heat transfer (due to increased heat transfer area), potential for greater exergetic efficiency (i.e., in a cascaded PCM arrangement), and reduced tankage cost (may require only a single tank) [13]. Unfortunately, comparatively little work has been done concerning encapsulation of higher temperature PCM materials of interest for concentrating solar power applications. Some numerical work has been done, however, and it is described here.

Shiina and Inagaki performed a numeral study on the thermal conductivity and melting characteristics of a variety of PCM materials, including lithium carbonate and NaCl [50]. However, this study focused on inclusion of high conductivity matrices for increase in thermal

conductivity, and little attention is given to encapsulation. Zhao et al performed a similar numerical analysis of encapsulated PCM [51]. For the eutectic of NaCl and magnesium chloride considered in this study, nickel and stainless steel (pre-formed) shells were deemed necessary. They also point out the likely need for unconventional HTFs for such high temperature PCM materials (T_m = 444°C).

2.4.3 High Conductivity Additives / Matrices

Many studies have been undertaken on high conductivity particles / matrices incorporated within lower temperature PCM materials, including organics (e.g., paraffin) and salt hydrates, such as that by Velraj [37]. For a description of some of these works, the reader is referred to the review by Jegaheeswaran and Pohekar [34].

Tamme et al extended the concept of graphite dispersions in paraffin to the KNO_3-$NaNO_3$ eutectic salt PCM [43]. Among different methods of preparation examined, they demonstrated a nearly one order of magnitude increase in thermal conductivity using a graphite weight fraction of only 0.05. Further study demonstrated substantial improvement in conductivity of both this eutectic salt and a eutectic mixture of KNO_3 and lithium nitrate using either of two methods of preparation: infiltration of a graphite matrix by molten salt, and compaction of a mixture of dry PCM and expanded graphite flakes [52]. It was demonstrated, however, that the compacted graphite-PCM mixtures showed varied conductivity upon thermal cycling. Pincemin's work shows similar behavior for mixtures of graphite of various morphologies in nitrate salts [32, 53]. Also, Acem et al describe a similar compaction technique, and describe the measured thermophysical properties of composites with KNO_3-$NaNO_3$ with concentrations of graphite between 15 and 20 wt % [54].

Of primary importance in the design of these additive-salt systems is the adequacy of additive dispersion. Fukai et al discuss the impact of orientation of carbon nanostructures (in this case, fibers), and a very dramatic decrease in heat transfer rate can be observed for such anisotropic systems, depending on the geometry of heat transfer [36, 55]. Also, there is tradeoff involved in using higher conductivity particles for improved heat transfer. As elucidated by Siegel, in the process of solidification, the increase in conduction provided by the particles is coupled with a decrease in volume occupied by the PCM (and hence, an increase the distance over which heat must traverse) [56]. Hence, for reasonable concentrations (20% by volume), addition of particles may only yield a removal rate (for plane geometry) of 10-20%. However, extrapolated over an entire heat storage unit, and over the life of the unit, this improvement would nonetheless be appreciable.

While a number of studies have examined the use of metallic nanoparticles (see, for example, Zeng et al [57]), these materials have not been examined with higher temperature anhydrous salt based PCM materials, likely because of the propensity for oxidative degradation. Indeed, this is a concern for carbon-based materials, as well [41]. In a study by Sure et al, it is shown that graphite has a relatively low resistance to corrosion by chloride salts, although glassy carbon and pyrolytic graphite show improved resistance [58].

To conclude, the use of this strategy requires maintenance of additive dispersion, appropriate balance of the concentration to avoid excessive loss of PCM volume, and appropriate material selection to prevent degradation of the additive.

2.4.4 Radiative Heat Transfer Enhancement

The objective of radiative transfer enhancement in PCM materials is to incorporate infrared absorptive additives in an otherwise semi-transparent PCM. Hence, depending on the

concentration of the additive, a varying degree of infrared radiation will pass through the PCM, being absorbed and transferring heat in the process. In order for this concept to work, temperatures must be sufficient to render radiation an important mode of heat transfer—as a rough rule, greater than 600°C. Because there is a relative lack of research on this concept, a brief description of relevant scientific principles follows.

Potential PCMs falling within this range include NaCl (phase transition at 800.7°C) and the eutectic of potassium chloride (KCl) and NaCl (phase transition at 658°C) [19, 59]. These materials are known to be transparent in much of the infrared [60]. While the focus here is on these two salt systems, the concept could theoretically be extended to other semi-transparent salts (e.g., other chlorides, fluorides, and their eutectics).

In analyzing the radiative properties of the PCMs and potential absorptive media in question, it was necessary to determine a spectral range of interest. It is evident from Planck's distribution law [61],

$$e_{b\lambda} = \frac{2\pi c^2 h}{\lambda^5} \frac{1}{e^{ch/\lambda\kappa T} - 1} \tag{2.2}$$

that approximately 90 percent of blackbody emissive power falls within the region of 2.0 to 13.0 μm at the melting point of the eutectic salt (T_m = 658°C); this is depicted graphically in Figure 15. Similarly, approximately 93% of blackbody emissive power falls within the range of 0.5 to 10 μm at the melting point of pure NaCl (T_m = 800.7°C); this is depicted graphically in Figure 16. Both these salt systems are largely transparent in these regions. The implication, of course, is that 90% or more of the total emissive power of an ideally black container would pass through the container-PCM interface, attenuating as it transfers heat further into the medium than would be possible by conduction alone over a finite amount of time.

For real (i.e., non-ideal) containment materials, the situation is more complex. In Figure 17, for example, the normal spectral emissivity for alumina at 600°C and two different purities is plotted, using data taken from [62]. The normal spectral emissivity can be defined as [61]

$$\epsilon_\lambda(\theta = 0, T) = \frac{I_\lambda(\theta = 0, T)}{I_{b\lambda}(T)} \tag{2.3}$$

In other words, the normal spectral emissivity is the ratio of actual emitted radiant intensity normal to the surface to that emitted by a blackbody (the blackbody radiative emittance is, by definition, isotropic). From the behavior shown in Figure 17, it is clear that ideal blackbody emittance (as demonstrated in Figure 15 and Figure 16) will be somewhat higher than the actual emittance in a real application with alumina as the containment material; additionally, the departure from ideality will be greater (i.e., emittance will be less) at shorter wavelengths (< 5 μm, approximately). This characteristic is verified by independent measurements of two crucible materials, porcelain and alumina, which are shown in Figure 18. Here, normal total emissivity is plotted versus temperature over the range of 400°C to 700°C. Measurements were made with a Jasco FTIR-6300 spectrometer with emission accessory and MCT detector. The emittance of the sample was compared to a blackbody reference manufactured by Infrared Systems Development Corporation of Winter Park, Florida. The normal total emissivity is generally defined as [61]

$$\epsilon(\theta = 0, T) = \frac{\int_0^\infty I_\lambda(\theta = 0, T)d\lambda}{\int_0^\infty I_{b\lambda}(T)d\lambda} = \frac{I(\theta = 0, T)}{\sigma T^4} \tag{2.4}$$

However, given the limited range of the detector (approximately 2 to 16 μm), the normal total emissivity was calculated as

$$\epsilon_{eff}(\theta = 0, T) = \frac{\int_{\lambda_1}^{\lambda_2} I_\lambda(\theta = 0, T)d\lambda}{\int_{\lambda_1}^{\lambda_2} I_{b\lambda}(T)d\lambda} \tag{2.5}$$

where λ_1 and λ_2 are the upper and lower bounds, respectively, of the detector, and the subscript "eff" is used to denote this quantity as an "effective" emissivity. As temperature increases, the blackbody curve shifts its peak and with it a larger portion of its emissive power to shorter wavelengths. Because these ceramic material have lower spectral emissivity at these wavelengths, their total emissivity decreases as the temperature increases. It should be noted that the hemispherical emissivity—that is, the directional emissivity integrated over all directions emanating from the container surface—is a more relevant measure for our purposes, although for nonmetallic surfaces the normal emissivity is a close approximation of this quantity [63]. The radiative properties of potential containment materials will not be explored in great detail here; for further information the reader is referred to relevant data compilations [62, 64-68].

This study shall focus on the radiative properties of the TES materials themselves. The data available in the literature concerning the radiative properties of potential storage materials are often incomplete, in the sense that alternatively spectral emissivity, reflectivity, and transmissivity are measured with varied experimental methodologies [60]. To maintain a consistent basis of comparison, this review attempts to quantify the radiative properties of potential candidate materials using their hemispherical spectral quantities (i.e., directionality is neglected where possible). Further, for the sake of simplicity, any such data gleaned from the literature is converted where possible to a hemispherical total value, using a weighted integral. This integral for hemispherical total emissivity would typically be evaluated as follows [61].

$$\epsilon(T) = \frac{\int_0^\infty \epsilon_\lambda(\lambda,T) e_{b\lambda}(\lambda,T) d\lambda}{\int_0^\infty e_{b\lambda}(\lambda,T) d\lambda} = \frac{\int_0^\infty \epsilon_\lambda(\lambda,T) e_{b\lambda}(\lambda,T) d\lambda}{\sigma T^4} \tag{2.6}$$

Here, the second equality is a direct result of the Stefan-Boltzmann law. Unfortunately, data over the entire effective spectral range is rarely available. In these cases, this integral must be evaluated as follows, again in the case of emissivity.

$$\epsilon_{eff}(T) = \frac{\int_{\lambda_1}^{\lambda_2} \epsilon_\lambda(\lambda, T) e_{b\lambda}(\lambda, T) d\lambda}{\int_{\lambda_1}^{\lambda_2} e_{b\lambda}(\lambda, T) d\lambda} \tag{2.7}$$

The nomenclature "effective total emissivity" is used to emphasize the narrower spectral range of integration. In the ideal case, this range is the 0.5 to 20 microns range of interest described above; the range may be narrower depending upon the availability of applicable data. Additionally, it should be noted that due to the discrete nature of radiative property measurements considered here, the numerator of the effective total emissivity expression above must be evaluated using polynomial interpolation and quadrature. The denominator, on the other hand, can be more precisely calculated, owing to the well-defined Planck distribution.

The available solid-state thermal radiative properties were compiled from Touloukian and DeWitt [60]. Unfortunately, radiative data in the temperature range of interest (600 – 1000°C) were not available. The majority of the effective emissivity, reflectivity, and transmissivity data tabulated below were obtained from measurements taken at approximate room temperature (298K), with the following exceptions. The effective emissivity data for potassium bromide (KBr) and rubidium bromide (RbBr) were measured at 373K. The remaining data for rubidium bromide were measured at 313K. The effective emissivity data for NaCl and KCl were measured at 373K. All data for rubidium chloride (RbCl) and rubidium iodide (RbI) were measured at 313K.

The above data hold for the solid-state thermal radiative properties of the salts in question. Additional research concerning the thermal radiative properties of molten alkali metal (lithium, sodium, and potassium) chlorides [69] and carbonates [70] has been conducted. It was demonstrated that while a substantial semi-transparent region existed for lithium chloride (wavelengths of approximately 0.5 microns to 8 microns), both NaCl and KCl were nearly completely transparent.

Appropriately selected nanoparticles or fibers of solid additives will control transmittance by their manner of dispersion in the PCM. Additives will be dispersed within the bulk PCM by one of four methods: controlled amounts of dissolved materials, suspended (insoluble) additive particles of similar density to the molten PCM, a fibrous matrix distributed across the PCM pellet, or absorptive foam which is impregnated by molten PCM. In the third case, the similarity in densities is necessary so as to allow natural convection to maintain an adequate dispersion of the additive particles. Suspended additives should have densities similar to the molten PCM to minimize precipitation, as well. Potential additives of interest will be discussed in the final chapter.

At this point it is prudent to consider the prior work on this topic. As stated previously, not much work has been done on the inclusion of infrared absorptive particles / materials within infrared transparent PCM thermal storage media, but some has been done in increasing solar availability of such materials—that is, adding particles to enhance the absorption of the media in the ultraviolet, visible, and near infrared spectral regions. The motivation behind such work is to render these materials as better HTFs for direct absorption of solar radiation in a solar absorber.

Arai proposed what he called a “volume heat-trap” solar collector; the heat transfer mechanism is illustrated in Figure 19 [71]. The collector used a liquid diethylphthalate suspension of fine particles of various types: graphite, carborundum, and silicon dioxide [71]. In this case, the particles were not nano-sized, but rather sieved to a range of 5 μm or less. Perhaps more relevant to our focus here on inorganic salts, the work of Drotning demonstrated the potential for transition metal oxides—namely cupric oxide (CuO) and cobaltic oxide (Co_3O_4)—to increase solar absorption in the molten eutectic of sodium nitrite, sodium nitrate, and potassium nitrate (wt % 40:7:53) [72]. In both these studies, the emphasis was placed on absorption of solar radiation,

which is predominately in the ultraviolet, visible, and near infrared, according to Planck's distribution [61].

To extend the concept to the infrared radiation characteristic of the high temperature thermal storage units considered here, information about potential additives' infrared absorption characteristics is needed. Indeed, such data for many of the materials considered here are currently available [73]. Perhaps more robustly, independent measurement of these quantities (i.e., absorption coefficient, emissivity) should be performed, using transmission, reflection, and / or emission spectroscopy in the infrared.

2.5 Conclusions and Investigative Focus

For direct conductivity enhancement, this research will focus on the nitrate salts currently widely in use in many solar power plants, either as HTFs or thermal storage media [25]. Three salts are considered: sodium nitrate ($NaNO_3$), potassium nitrate (KNO_3), and the KNO_3-$NaNO_3$ eutectic, with melting points of approximately 334, 306, and 222°C, respectively [27]. While these materials, especially the eutectic salt, may find great applicability as HTFs, the primary focus of this research will be upon their value as PCMs. This latter scenario holds the added benefit of much higher storage density, owing to the outsized latent heat capacity of molten salts relative to their sensible heat capacity over the range of practicable operating temperatures. For the second part of this research, thermal radiative transfer enhancement, the chloride salts identified previously will be used: NaCl and the KCl-NaCl eutectic, with melting points of approximately 800.7 and 658°C, respectively [19, 59]. Both KCl and NaCl are listed in Table 2 with other higher temperature PCM candidates and relevant thermophysical properties data. It can be seen that they compare favorably with many of the other candidates in terms of latent heat of fusion. For example, as can be seen from Figure 20, many lithium compounds are seen to have higher latent heat values,

but they are also correspondingly more expensive, with lithium carbonate more than double the cost KCl, quadruple the cost of NaCl on a per kWh_{th} basis [74]. The eutectic, KCl-NaCl, has somewhat lower latent heat [31]. Nonetheless, because it makes use of relatively inexpensive components, and because it has a melting temperature intermediate to NaCl and many of the lower temperature nitrate salts currently in use, it will be selected for further study here.

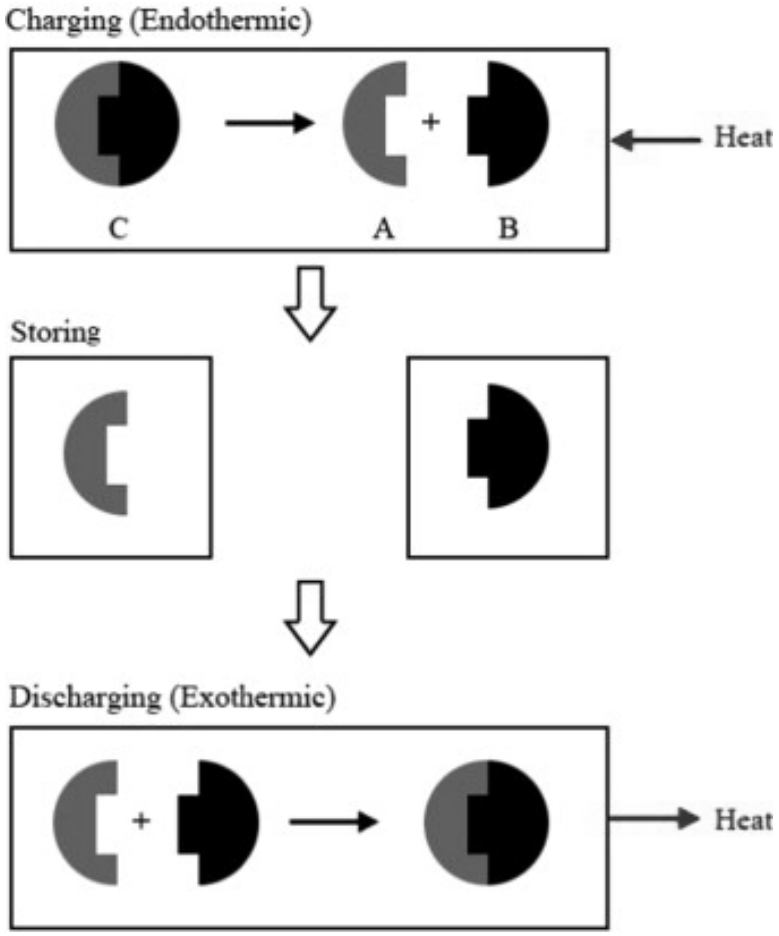

Figure 6 Thermochemical heat storage process [11].

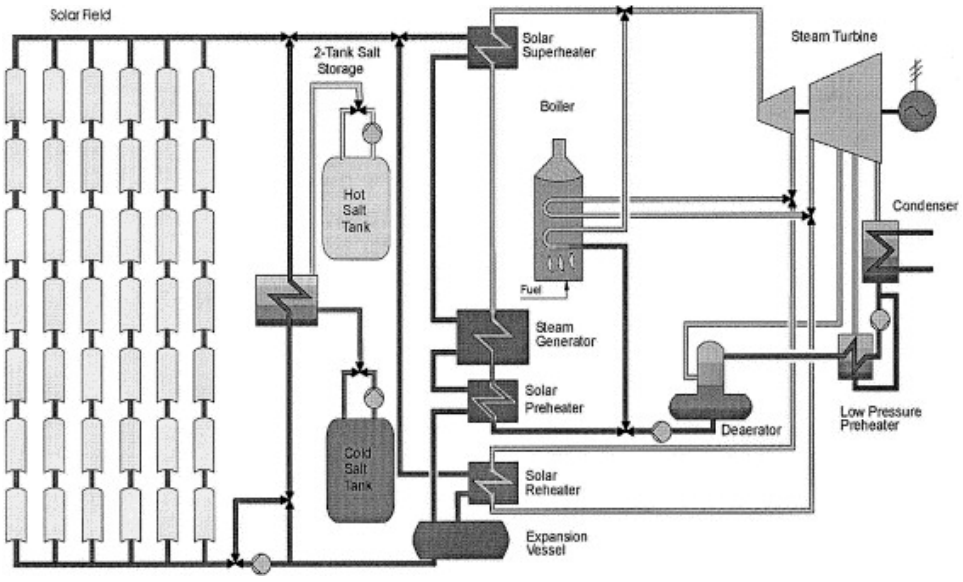

Figure 7 A potential configuration of inorganic salts used as sensible storage media [25].

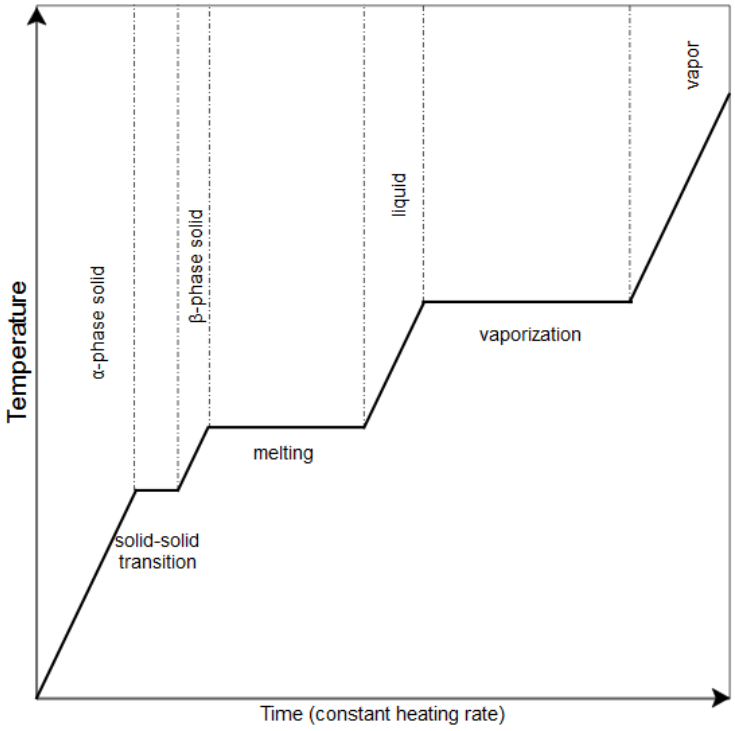

Figure 8 Generalized phase-transitions for a hypothetical pure substance.

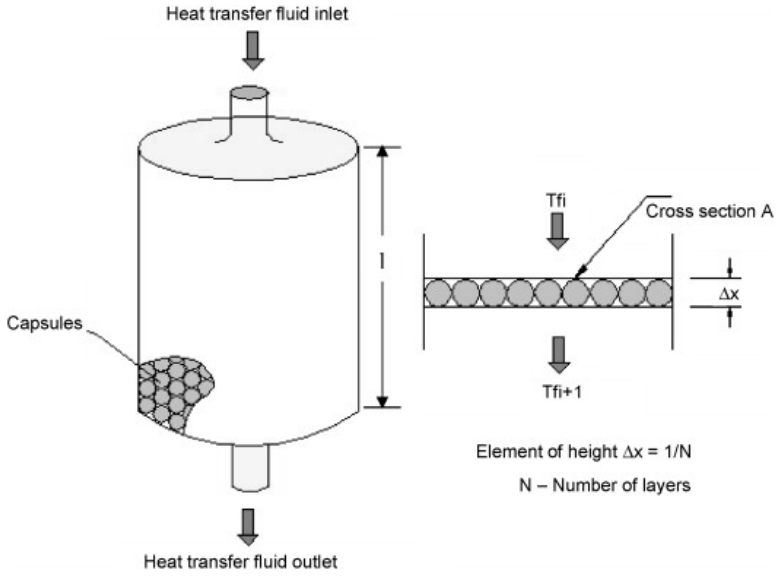

Figure 9 Packed-bed TES unit arrangement [15].

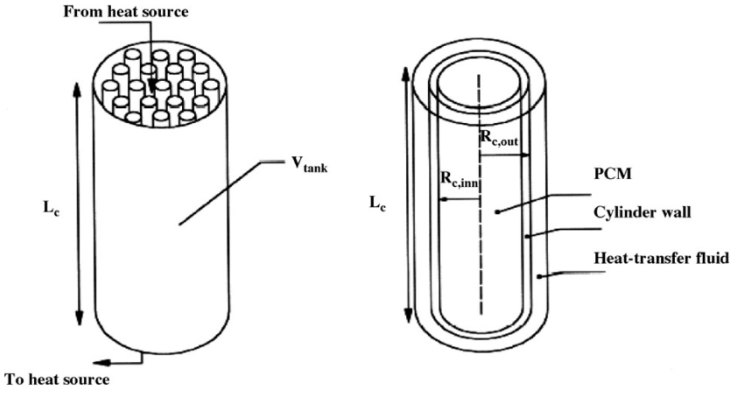

Figure 10 Cylindrical shell TES unit arrangement, tube-side PCM [9].

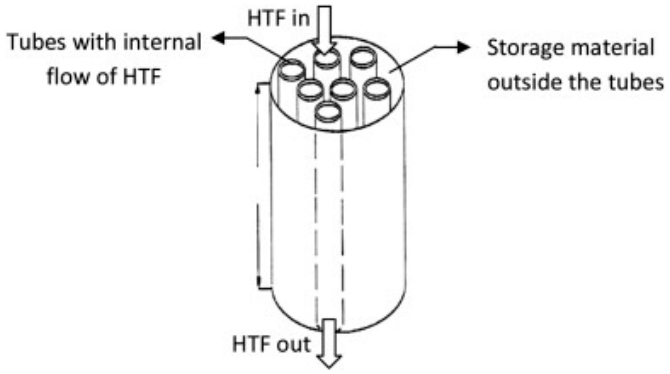

Figure 11 Cylindrical TES unit, PCM shell-side [12].

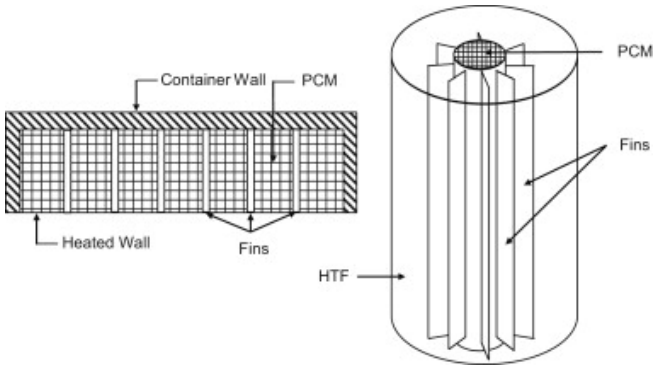

Figure 12 Common fin arrangements in latent heat storage systems [17].

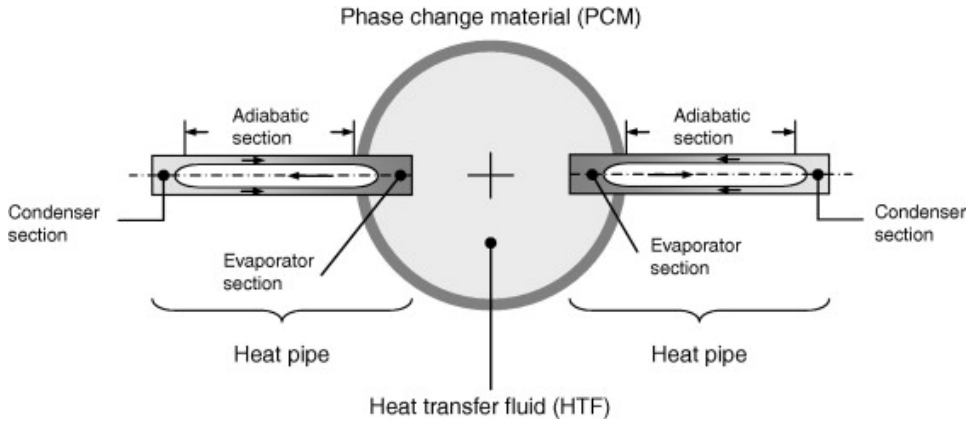

Figure 13 Schematic of heat pipe-enhanced storage unit with tube-side HTF [47].

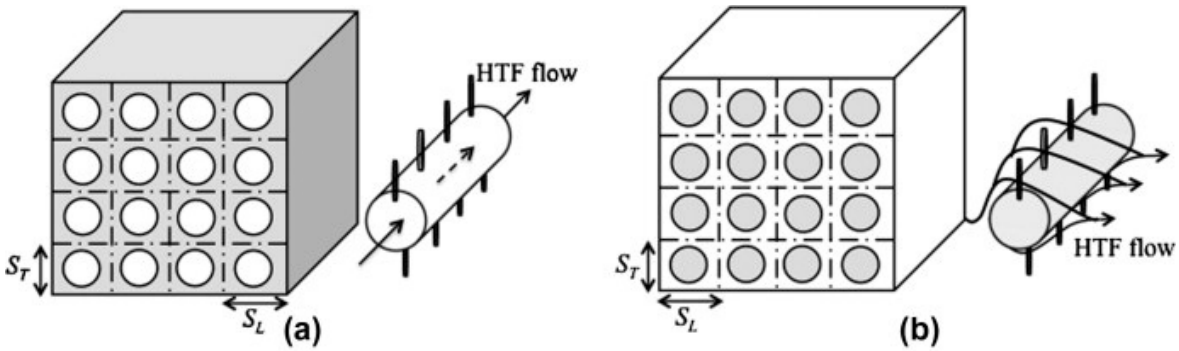

Figure 14 HTF flow configuration for heat-pipe enhanced storage units. Tube-side HTF is shown in (a) and tube-side PCM is shown in (b).

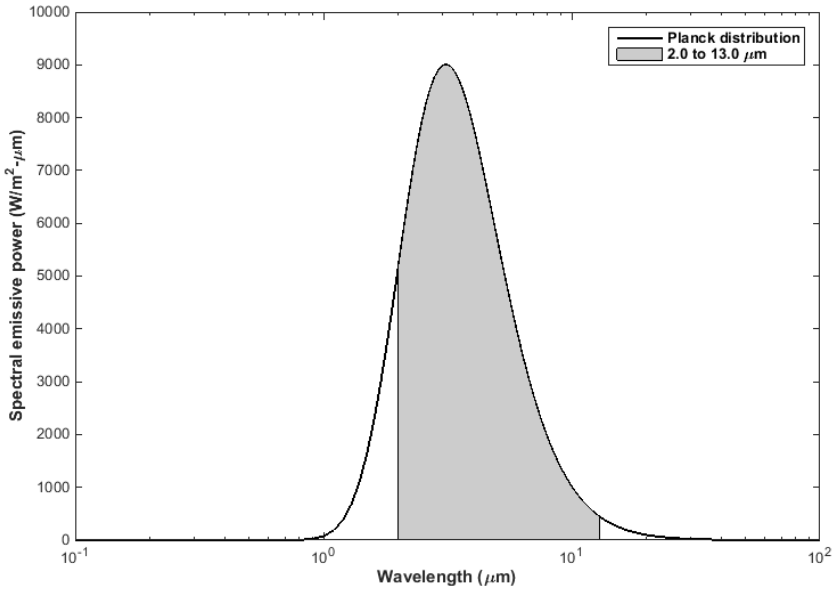

Figure 15 Blackbody radiation at 658°C. 90% of total emissive power is generated within the shaded region.

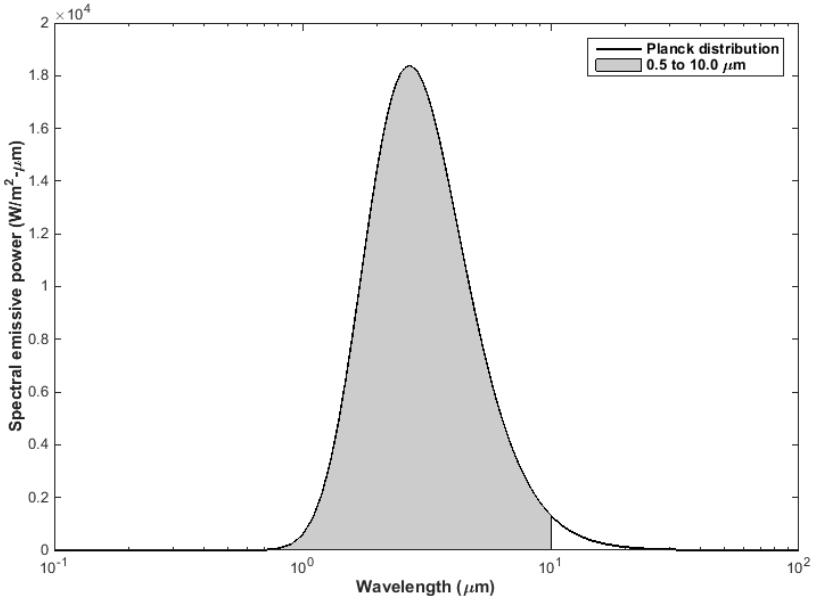

Figure 16 Blackbody radiation at 800.7°C. 93% of total emissive power is generated within the shaded region.

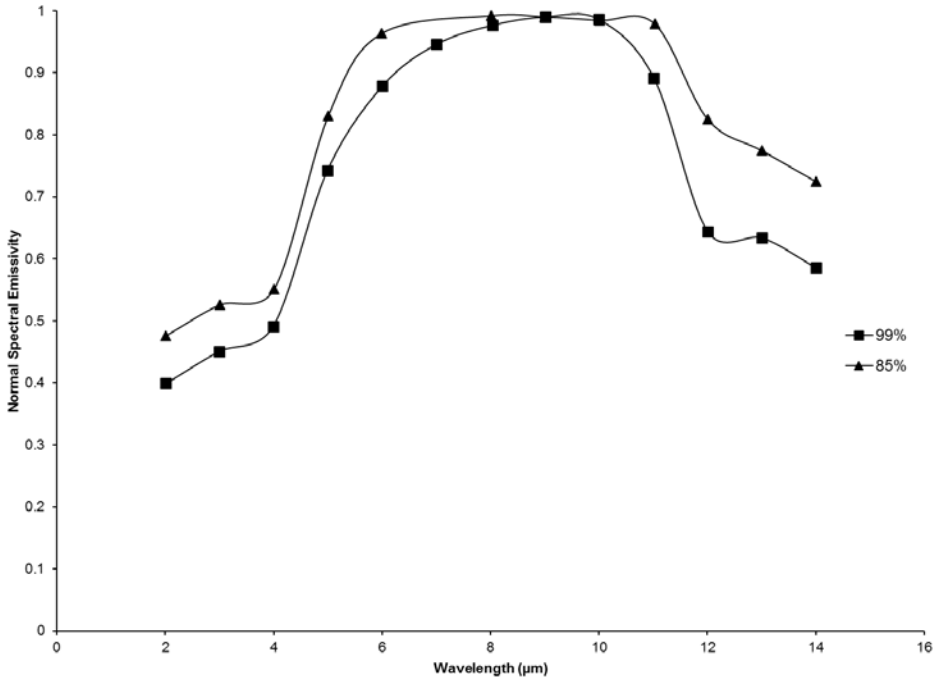

Figure 17 Normal spectral emissivity of alumina at 600°C. Two different concentrations are shown: 99% and 85%. Data taken from [62].

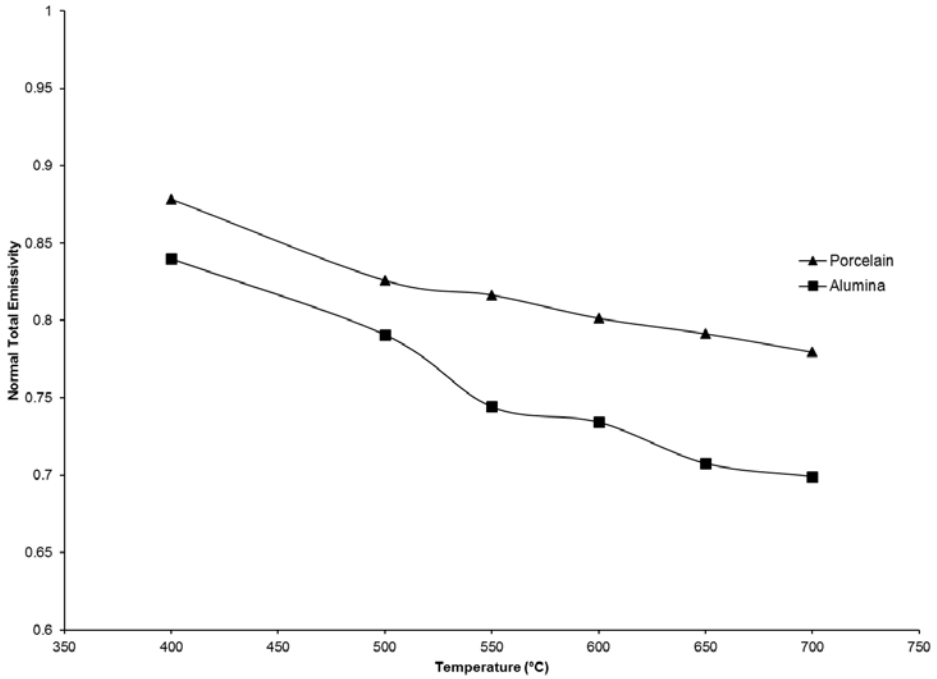

Figure 18 Normal total emissivity for porcelain and alumina.

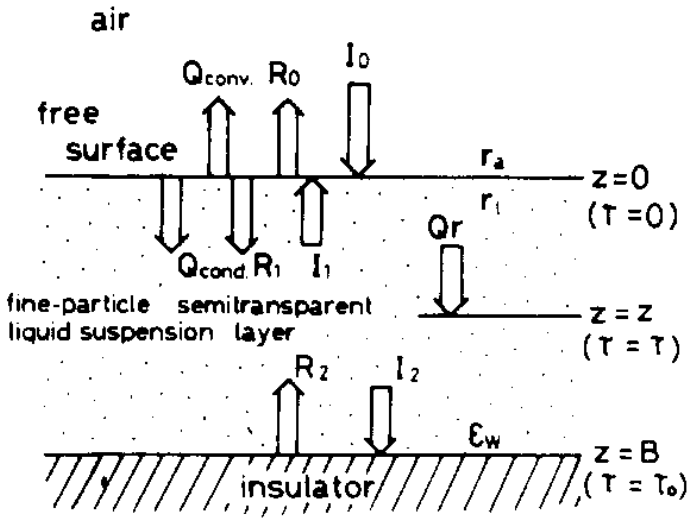

Figure 19 Heat transfer in a volume heat-trap collector, as articulated by Arai [71].

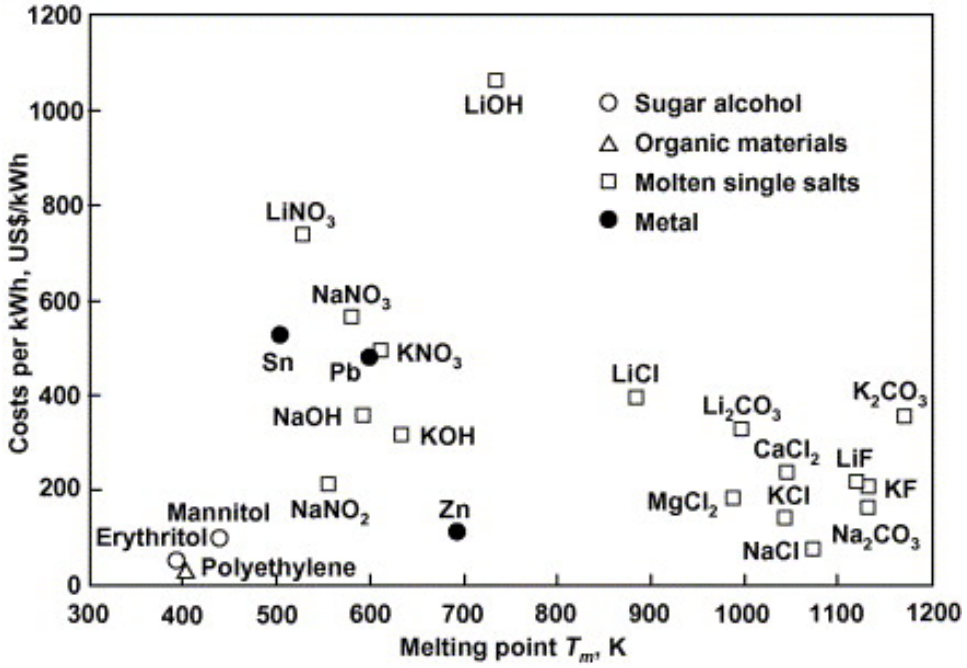

Figure 20 Cost per kWh_{th} latent heat of various PCM materials, circa 2005 [74].

Table 1 Selected radiative properties of potential PCM materials

Name	**T_m (°C)**	**ε_{eff}**	**ρ_{eff}**	**τ_{eff}**
Bromides				
KBr	734	0.04	-	0.9
RbBr	692	0.05	0.057	0.91
CsBr	636	-	0.08	0.8
$MgBr_2$	711	-	0.08	-
Carbonates				
Na_2CO_3	856	-	0.45	-
$BaCO_3$	811	-	0.99	-
Chlorides				
NaCl	800.7	0.08	0.03	0.92
KCl	771	0.03	0.03	0.9
RbCl	724	-	0.053	0.94
Fluorides				
LiF	848.2	-	0.3	0.9
NaF	996	-	0.02	0.9
Iodides				
KI	681	-	-	0.85
RbI	656	-	-	0.8
CsI	632	-	0.09	0.86

Table 2 Thermophysical properties of inorganic salt PCMs

Name	T_m (°C)	ΔH_{fus} (kJ/kg)	ρ_s (g/mL)	ρ_l (g/mL)	Capacity (kWh_{th}/m^3)
Bromides					
NaBr	747	256	3.200	2.342	167
KBr	734	212	2.74	2.127	125
RbBr	692	141	3.35	2.715	106
CsBr	636	111	4.43	3.133	97
$MgBr_2$	711	213	3.72	2.62	155
$CaBr_2$	742	146	3.38	3.111	126
$SrBr_2$	657	42.4	4.216	3.70	44
$BaBr_2$	857	108	4.781	3.991	120
Carbonates					
Li_2CO_3	732	606	2.11	1.80	303
Na_2CO_3	856	280	2.54	1.972	153
K_2CO_3	899	200	2.29	1.89	105
Rb_2CO_3	873	130	-	2.84	103
Cs_2CO_3	793	95	4.24	-	112
$MgCO_3$	990	700	3.010	-	585
$BaCO_3$	811	200	4.308	-	239
Chlorides					
LiCl	610	467	2.07	1.502	195
NaCl	800.7	482	2.17	1.556	208
KCl	771	353	1.988	1.527	150
RbCl	724	202	2.76	2.248	126
CsCl	646	121	3.988	2.79	94
$MgCl_2$	714	453	2.325	1.68	211
$CaCl_2$	775	252.7	2.15	2.085	146
$SrCl_2$	874	102.3	3.052	2.727	77
$BaCl_2$	961	76.12	3.9	3.174	67
Chromates					
Na_2CrO_4	794	152	2.72	-	115
K_2CrO_4	974	170	2.73	-	129
Cs_2CrO_4	963	92	4.24	-	108
Fluorides					
LiF	848.2	1044	2.64	1.81	525
NaF	996	794	2.78	1.948	430
KF	858	468	2.48	1.91	248
RbF	795	247	3.2	2.87	197

Table 2 (Continued)

Name	T_m (°C)	ΔH_{fus} (kJ/kg)	ρ_s (g/mL)	ρ_l (g/mL)	Capacity (kWh_{th}/m^3)
CsF	703	143	4.64	3.649	145
Iodides					
NaI	661	158	3.67	2.742	120
KI	681	145	3.12	2.448	99
RbI	656	104	3.55	2.904	84
CsI	632	99	4.51	3.197	88
MgI_2	634	93	4.43	3.05	79
CaI_2	783	142	3.96	3.443	136
BaI_2	711	67.8	5.15	4.26	80
Molybdates					
Li_2MoO_4	702	281	2.66	-	208
Na_2MoO_4	687	109	3.28	2.72848	83
K_2MoO_4	919	163	2.34	2.343184	106
Rb_2MoO_4	958	140	-	-	-
Cs_2MoO_4	956.3	75	-	-	-
Sulfates					
Li_2SO_4	860	82	2.21	2.003	46
Na_2SO_4	884	168	2.7	2.069	97
Tungstates					
Li_2WO_4	740	157	3.71	-	162
Na_2WO_4	695	107	4.18	3.679985	109
K_2WO_4	921	86	3.12	3.11784	74
Rb_2WO_4	952	78	-	-	-
Cs_2WO_4	953	63	-	-	-
Others					
MoO_3	802	338	4.7	-	441
NaCl50-KCl50	658	280	2.0776	1.588	124

CHAPTER 3 DIRECT CONDUCTIVITY ENHANCEMENT[4]

3.1 Introduction

Perhaps the most direct route to improving the thermal conductivity and therefore the performance of TES media is via the inclusion of higher conductivity materials. In this chapter we examine this concept in greater detail, specifically via the addition of various high conductivity particles in the following nitrate salts: $NaNO_3$, KNO_3, and the $NaNO_3$-KNO_3 eutectic system. Relevant thermophysical properties of these materials are presented in Table 3, taken from the thermodynamic database software FactSage [27], unless otherwise noted.

To begin, the abovementioned nitrate salts are mixed with approximately 2.0% volume cupric oxide, CuO, nanoparticles. The thermophysical properties of this additive material are discussed, as are those of other potential oxide-based additives. The properties of the nanoparticle-enhanced salts are measured and compared with those of the pure salts. Also, temperature-variant IR spectroscopy is used to verify that the additives do not facilitate the degradation of the salts.

Next, we give a brief treatment of dispersion properties of additive materials in these salts. Whereas as some research has shown that some transition metal oxides form stable suspensions in nitrate salts [76], our efforts showed some difficulty in maintaining the suspension at the concentrations necessary to achieve an appreciable increase in thermal conductivity.

Finally, in response to some of the issues raised concerning additive dispersions, graphene is examined as a potential conductivity enhancing additive. Although graphene is more expensive

[4] Section 3.2 has been submitted to *Applied Energy* for publication [75].

than the metal oxides considered here, it was found that a comparatively small mass of graphene nanoflakes led to a significantly higher increase in thermal conductivity, relative to the CuO nanoparticles.

3.2 CuO Nanoparticle-Enhanced Nitrate Salt TES Media

In this section, experimental investigations of CuO-nanoparticle enhanced nitrate salt TES media are discussed. The first consideration in selecting CuO as the conductivity-enhancing additive is, of course, the additive's thermal conductivity. CuO has also been reported to have a much higher thermal conductivity (76.5 W/m-K) than the salts studied here [77]. While there is a lack of data on the solid-state thermal conductivity of these salts, it has been found sodium nitrate, for example, that the thermal conductivity is less than 1 W/m-K for the temperature range of room temperature to the melting point [78]. Further, through examination of a separate study involving conductivity enhancement in borosilicate glass, it was found that addition of CuO resulted in the greatest conductivity increase per concentration by weight of any of several transition metal oxides studied [79]. As a note of caution, one would not expect a close equivalence of the borosilicate glass and the crystalline nitrate salts, although under certain conditions nitrate salts can form glasses [80].

In Table 4, relevant thermophysical properties of CuO and other potential oxide-based additives are compared. Density and specific heat data are taken from FactSage [27]. Thermal conductivity data, where available, are taken from the compilation of Touloukian and coworkers [81], unless otherwise noted. It should be recognized that all data reported here are for the bulk material. Heat transfer for particles whose dimensions are on the order of the mean free path is potentially reduced, due to localized heating effects [82]. Nonetheless, the bulk properties are a good starting point with which to judge potential additive materials.

The quantity in the last heading of Table 4, ρc_p, can be conceptualized a volume-based heat capacity. The importance of this quantity is seen in the definition of the thermal diffusivity:

$$\alpha = \frac{k}{\rho c_p} \tag{3.1}$$

The flow of heat in a one-dimensional problem depends on both the conductivity (according to Fourier's law, how quickly heat will flow in a given direction) and the heat capacity (how much heat will be absorbed by a given spatial element). So, in the effort to increase heat flow in the pure TES media, it is generally desirable to have high thermal conductivity and low heat capacity in the additive material. Of course, if the heat capacity of the additive is lower than that of the pure salt, some sensible heat capacity of the storage media is lost, and due to the fact that the additive presumably will not participate in the salt's phase change, latent heat capacity is also lost. In either case, this loss should be proportional to the concentration of the additive, although, in working with nanomaterials, the bulk material properties may not be a good predictor of the loss [83]. The bulk thermal diffusivity of materials for which data were available is plotted in Figure 21. It is clear from the limited data available that CuO is the most promising of the candidate oxide additives considered based on potential heat transfer enhancement.

Another important consideration in selection of the additive material is thermochemical stability. Whereas prior studies have examined graphite and aluminum as potential conductivity enhancing additives for salt TES media, corrosion was found to be an issue. Graphite-salt composites prepared by Pincemin et al, for example, were shown to steadily decrease in melting endotherm peak upon initial cycling, stabilizing after at least 40 cycles [32]. It is quite possible that this change behavior is the result of degradation of a small proportion of the nitrate to the nitrite salt [76, 84], which would shorten and stretch the endothermic peak. CuO, owing to its high

oxidation state, is expected to remain stable in a mixture with the salt, preventing degradation of the nanoparticle or the nitrate (i.e., to a nitrite).

The remainder of this section summarizes efforts into investigating the CuO nanoparticle-enhanced nitrate salts systems. First, diffusivity data are presented. Using properties obtained from the literature, the thermal conductivity of these systems is also calculated. Next, measured thermophysical properties of the systems are summarized. Finally, the stability of the nanoparticle-salt systems is demonstrated through spectroscopic methods.

3.2.1 Methodology

CuO nanoparticles (spherical, approximately 40 nm; obtained from SkySpring Nanomaterials) were added to each salt in a volume ratio (solid state) of approximately 0.02. This particular volume fraction was chosen based on prior studies of lower temperature nanofluids, which showed demonstrable increases in thermal conductivity with this concentration of CuO [85]. This volume fraction translates to weight fractions of approximately 0.058, 0.054, and 0.056 for the KNO_3, $NaNO_3$, and eutectic salt, respectively.

The thermal diffusivity of the pure salts and additive-salt mixtures was measured using laser flash analysis (LFA). The samples were prepared by first melting the salt at approximately 20C above its melting point, then grinding the solidified material in a ball mill, and finally pressing the material in a hydraulic press. To minimize moisture infiltration, milled material was kept in a drying oven prior to pressing; samples were pressed under vacuum under force of approximately 18,000 lb (the limit of the sample die). The resultant samples were cylindrical in shape, approximately 1.3 mm thick with diameter of 13.0 mm. The thermal diffusivity was measured with a Linseis XFA500 LFA instrument. The instrument is calibrated with a graphite standard to a stated accuracy of ± 6% [86].

The technique behind the measurement was introduced by Parker and coworkers and has become a widely used technique for determining the thermal diffusivity of homogeneous materials based on the flash method [87, 88]. The instrument uses a laser to deliver a radiant energy pulse to heat one surface of the sample; the temperature of the opposite side is measured, and the diffusivity is calculated by the transient temperature response [89]. Parker's formula was implemented to calculate thermal diffusivity as follows.

$$\alpha = \frac{0.1388\, d^2}{t_{0.5}} \tag{3.2}$$

Here, α is the thermal diffusivity in cm^2/s, d is the sample thickness in cm, and $t_{0.5}$ is the time taken in seconds to reach approximately half the maximum temperature [86]. Using this equation, thermal diffusivity can be calculated over a wide range of temperatures. Because we are primarily concerned with the solid phase thermal conductivity (i.e., because it largely determines the solidification time of the PCMs), we will restrict our attention to temperatures below the melting points of the pure nitrate salts: 223, 306.5, and 334°C for the eutectic salt, $NaNO_3$, and KNO_3, respectively.

Differential scanning calorimetry (DSC) measurements were performed with a TA Instruments SDT Q600 Simultaneous DSC / Thermogravimetric Analyzer (TGA). The DSC temperature signal was calibrated to tin (T_m = 231.93°C) and zinc (T_m = 419.53°C) calibration standards. The heat flow calibration was performed with a sapphire calibrant with known specific heat capacity. Platinum crucibles were selected for the measurement based on their high conductivity and resistance to attack by nitrate salts. Samples were prepared then dried prior to measurement; TGA measurements indicated negligible weight lost, suggesting moisture did not significantly impact the calorimetric measurements. All measurements were run under dry nitrogen at a flow rate of approximately 100 ml/min. Approximately 5 mg samples were used, and

three to five runs were performed for each salt / salt composite system studied. The melting point of the samples was assessed as the extrapolated onset of the melting endotherm [90]. The enthalpy change on melting was determined by integrating the corresponding endothermic peak using the extrapolated baseline [91].

Temperature variant FTIR measurements of the pure salt and salt composite systems were made using a Jasco FTIR-6900 spectrometer with a diffuse reflectance accessory provided by Pike Instruments. The diffuse reflectance accessory was equipped with a heating element and thermocouple to control the sample temperature. The spectrometer utilized a mercury-cadmium-telluride (MCT) detector, and while it is able to achieve spectrometric data at wave numbers as high as approximately 8000 cm^{-1}, measurements were limited to the range of 4000 to 600 cm^{-1} after preliminary measurements indicated negligible infrared activity at higher wave numbers. Samples were prepared by dispersion in KBr at approximately 1.0 wt %, followed by homogenization in agate mortar. The samples were placed in a porous ceramic cup, which allowed purge gas (dry nitrogen, approximately 100 ml/min) to continually pass through the sample. The sample and heating element were encased under a zinc selenide (ZnSe) window, and all spectra were obtained relative to pure KBr baseline samples at the relevant measurement temperature.

The spectra of KNO_3 and $NaNO_3$ are well known [92]. FTIR spectroscopy can be used to determine degradation of the salt by analyzing IR spectra for the presence of nitrite peaks, as the nitrite would be a product of the nitrate degradation reaction. In the case of KNO_3, the presence of nitrite can be determined by peaks at 2560, 1335, or 1235 cm^{-1}. In the case of $NaNO_3$, the presence of nitrite can be determined by 1335 or 1250 cm^{-1}. In the case of the eutectic salt, the presence of nitrite can be determined by a peak at 1335 cm^{-1} or potentially by any of the peaks of the pure nitrite salts listed above.

All spectrophotometric measurements were performed on the nitrate salt systems both prior to and after melting. To melt the salts, approximately 10 g of each were heated in a muffle furnace to a temperature approximately 20°C higher than the presumed melting point, then dwelled isothermally for approximately 2 hr.

3.2.2 Results and Discussion

Scanning electron microscope (SEM) images of the post melting salt-CuO composites are shown in Figures 22 – 24. The SEM images suggest that some agglomerates on the order of 100-300 nm in size were present. It is possible that the agglomerates formed via natural convection currents in the liquid phase of the salt; however, the nanoparticles were found to maintain their distribution in the salt after melting, as judged by visual inspection (i.e., salt appears homogeneous).

The diffusivity measurements comparing the pure and additive enhanced salt systems are plotted in Figures 25 – 27. For reference, the solid phase transitions for both KNO_3 (130°C) and the eutectic (109°C) are indicated by a horizontal dashed line [27]; these transition temperatures were verified by DSC measurement of the pure salts. Note that diffusivity measurements were not made above the solid-solid transition temperature of $NaNO_3$, 276°C [93].

The eutectic system displays the greatest improvement in thermal diffusivity upon addition of CuO nanoparticles, and it also is the only system that shows statistically significant (i.e., greater than two standard deviations) improvement over the entire temperature range considered. KNO_3 showed the next highest improvement, and the increase in diffusivity was generally statistically significant, with exception to the highest temperature data point (i.e., 300°C). $NaNO_3$ showed the lowest relative increase in thermal diffusivity, and the increase was statistically significant only

for temperature below 150°C. Statistical significance has been judged by the error bars on the data, which represent plus / minus one standard deviation from each measured diffusivity value.

In an effort to clarify the behavior observed in the thermal diffusivity measurements, an effort was made to estimate the thermal conductivity of the systems based on these measurements and known property values. The thermodynamic properties of the pure salts have been extensively studied; for the sake of simplicity, such data for these salts—namely, values for density and specific heat as a function of temperature—were all obtained from the thermodynamic property database software FACTSage [27]. To calculate the density of the composite systems, the following formula was used.

$$\rho_{composite} = f_{v,CuO}\rho_{CuO} + \left(1 - f_{v,CuO}\right)\rho_{salt} \tag{3.3}$$

The specific heat of the composite material was calculated using a volume-weighted average of the component heat capacities [94].

$$c_{p,composite} = \frac{f_{v,CuO}\rho_{CuO}c_{p,CuO} + \left(1 - f_{v,CuO}\right)\rho_{salt}c_{p,salt}}{\rho_{composite}} \tag{3.4}$$

Short of rigorous measurement, these calculations provide an estimate of the change in thermal conductivity in the composite salt systems relative to the pure salts.

The results of the thermal conductivity estimation are plotted Figures 28 – 30. The behavior is similar to that displayed in the diffusivity measurements. All the salts show an increase in thermal conductivity with addition of the CuO nanoparticles. The eutectic system shows the greatest improvement, and $NaNO_3$ shows the least improvement. The increase in the NaNO3-CuO system is only statistically significant for temperatures below 150°C. In this case, however, all the data points considered for KNO_3 show a statistically significant increase in conductivity. It should be noted that the errors displayed here do not account for any potential error in Equations (3.3) and (3.4).

Thermophysical properties measured by DSC are shown in Table 5. The data measured for this study agree well with the literature values shown in Table 3, with possible exception to the melting point of the pure eutectic salt. The measured melting point of the eutectic system was approximately 221°C, whereas the reported value was 223°C. Moreover, the measured properties of the CuO-nitrate salt mixtures closely agree with those of the pure salts. A slight but not statistically significant decrease in temperature is noted in each salt upon addition of the additive; this may be an indication of solubility. In regard to the enthalpy of fusion, one would expect some decrease in the latent heat upon addition of the additives if they did not participate in the phase change, and this decrease would be directly proportional to the additive concentration; however, within the error of the measurement, the latent heat of the additive-salt mixtures is approximately the same as that of the pure salts.

In an effort to assess the stability of the molten salt systems, spectrophotometric measurements were made of CuO nanoparticle-enhanced salts both prior to and after melting. The results of the FTIR studies are shown in Figures 31 – 33. The FTIR measurements were taken at three different temperatures for each salt: 150, 200, and 215°C for the eutectic salt, and 200, 250, and 300°C for both KNO_3 and $NaNO_3$. The pre-melt salt mixture is shown in the left column, (a), while the post-melt salt mixture is shown in the right column, (b).

In each case, the intensity of the IR signal decreased with temperature, so the lowest curves represent the highest temperatures. In general it is clear that the infrared spectra vary little with temperature, and appear to change little after melting. None of the characteristic peaks for nitrites (see: 3.2.1 Methodology) are visible before or after melting. There are some differences between the pre-melt and post-melt spectra for the eutectic salt; this is likely due to the eutectic salt forming a new macroscale structure (e.g., lamellar) after the first melting and solidification.

3.2.3 Conclusions

The improvements in diffusivity and conductivity are clearly demonstrated for the inclusion of small amounts (2% by volume) CuO nanoparticles in nitrate salts. In all measurements, CuO was shown to increase the thermal diffusivity and thermal conductivity, although in some cases the increase was not significant, given the error of the measurement. Statistically significant increases in thermal diffusivity were measured over there entire temperature range of study for the eutectic salt system; significant increases in diffusivity for KNO_3-CuO were observed for temperature below 300°C; and significant increases in diffusivity for $NaNO_3$-CuO were observed for temperatures below 150°C. Statistically significant increases in thermal conductivity were observed for both the eutectic salt and pure KNO_3 systems over the entire temperature range of study; significant increases in conductivity for $NaNO_3$ were observed only for temperatures under 150°C. It should be noted, however, that the calculation of thermal conductivity involved estimates of the systems' density and specific heat capacity that were not verified by independent measurement.

Additionally, the systems' were shown to not degrade under thermal cycling, as demonstrated by FTIR studies of the materials before and after melting. No peaks characteristic of nitrite, the decomposition product of the nitrate salts, were observed after melting.

There are multiple areas in which additional research should be pursued. These include:

- Study of the thermophysical properties of the composite salt systems in the molten state. These would be of much more relevance to the use of the systems as HTFs.
- Dispersion studies of the nanoparticles within the salt matrices.
- Better characterization of the behavior of CuO within the salt matrix.

Nonetheless, this additive shows promise in that relatively small amounts (2% by volume) yield significant increases in thermal diffusivity and appear to remain chemically stable.

3.3 Additive Dispersion

A determining factor in the maintenance of a dispersion of nanoparticles in a liquid medium (e.g., a molten salt) is the tendency toward sedimentation. As the PCM undergoes phase change to a liquid state, care must be taken to ensure the particles do not aggregate and settle to the bottom. A method of estimating the potential for particle settling is to employ the methods used for Stokes fluid flow, also known as creeping flow [95]. In this approximation, the settling velocity of the particles is assumed to be sufficiently slow ($\mathrm{Re} < 0.1$) so as to preclude the formation of eddies downstream of the settling particles. Balancing the gravitational force with the buoyancy force and the viscous force, we obtain the following relation for terminal sedimentation velocity.

$$v_t = \frac{2}{9}\frac{r^2 \Delta \rho g}{\mu} \tag{3.5}$$

If we arbitrarily take a settling distance of 2 cm, we can calculate a settling time for the nanoparticles. Taking the example of CuO nanoparticles (40 nm in diameter) in sodium nitrate, a settling time of approximately 6 months is obtained. Aggregation is seen to be a major problem. If the particles aggregate to some degree, resulting in a modest effective diameter increase of 400nm, the settling time becomes approximately 10 hours.

In Figure 34, a bisected pellet of $NaNO_3$ and NiO nanoparticles (<50 nm) is shown, following 5 thermal cycles (i.e., melting and solidification). The concentration of nanoparticles in the pellet was approximately 2 wt %. It can be seen that the nanoparticles have accumulated at the bottom of the pellet. It is likely that some degree of aggregation has occurred prior to the settling of the particles; this may have been exacerbated by natural convection currents and the process of phase separation during solidification.

It seems worthwhile to investigate other ways to ensure additive dispersion. Examining Equation (3.5), we see that the settling time can be increased by decreasing the quantity $\Delta\rho$—that is, by using less dense nanoparticles. As has been mentioned previously, graphite has been investigated as a potential conductivity enhancing additive [32]. Below, a preliminary study of another carbonaceous material, graphene, is described.

3.4 Graphene Nanoflakes for Conductivity Enhancement

Previous work shows some promise for CuO nanoparticles for conductivity enhancement, although the increase in conductivity in $NaNO_3$ was not shown to be as dramatic as in the other nitrate salts. Furthermore, because CuO has a relatively high density, there is some concern about the ability of the salt-CuO mixture to maintain adequate dispersion of the nanoparticles. In this section, we discuss some preliminary work with graphene nanoflakes, which have a lower density and higher conductivity than the CuO nanoparticles.

In Figure 35, the thermal diffusivity of approximately 2.0 wt % graphene-$NaNO_3$ mixtures is plotted with the diffusivity of the pure salt. Increased diffusivity is shown, but it is only statistically significant for the room temperature data point. With only a 1.0 wt % increase, however, to 3.0 wt % graphene, there is significant improvement, as shown in Figure 36.

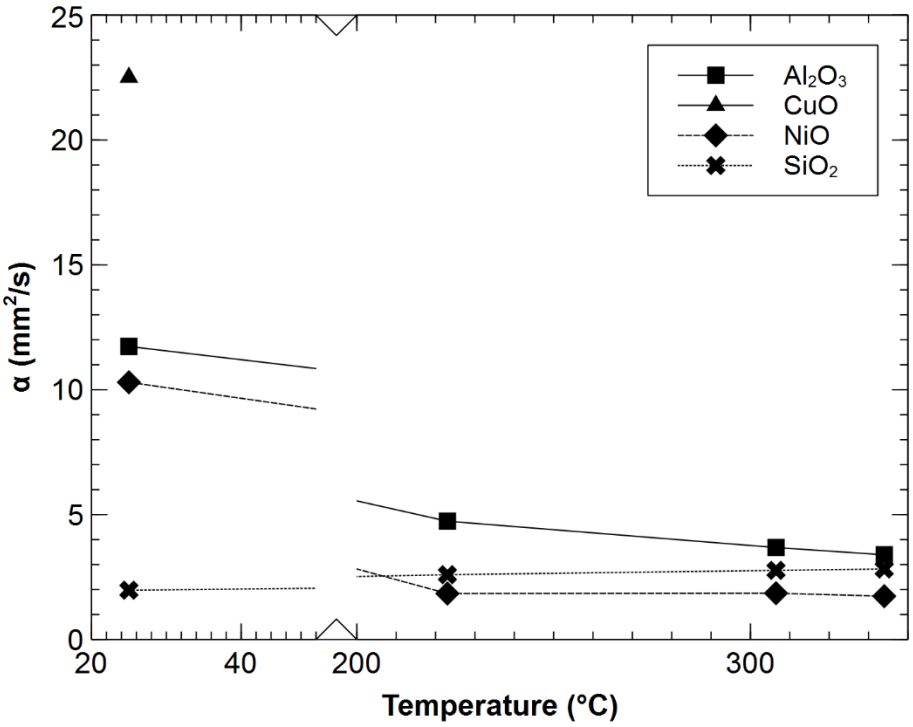

Figure 21 Thermal diffusivity of potential conductivity enhancing additives. Density and heat capacity data taken from FactSage [27]; thermal conductivity data taken from other sources [77, 81].

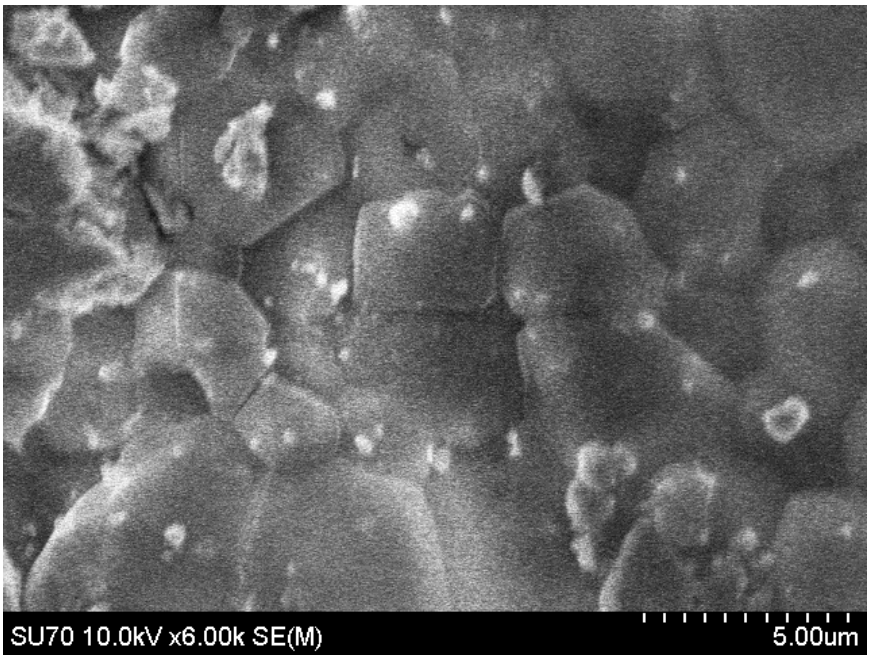

Figure 22 SEM image of eutectic salt with CuO nanoparticles.

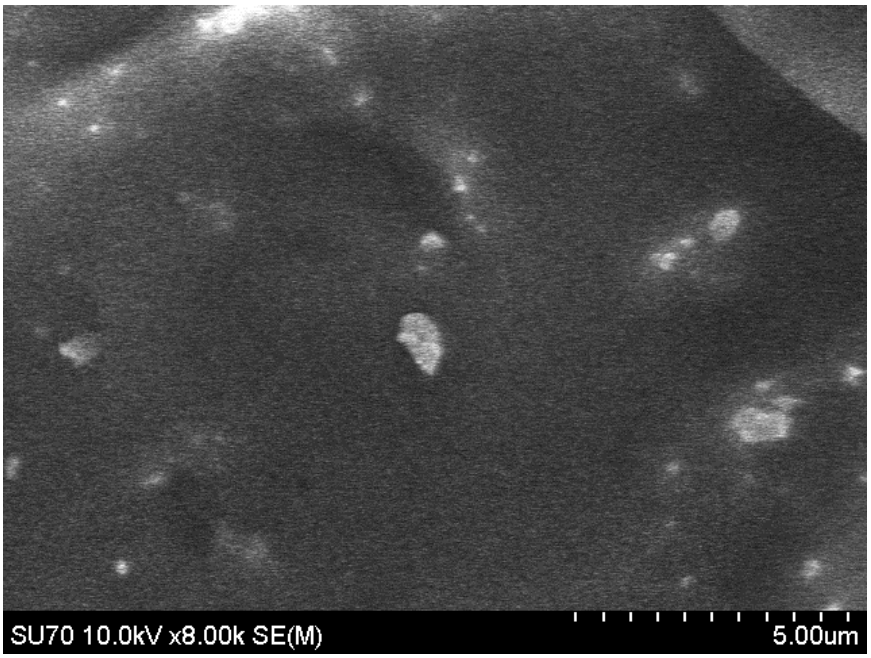

Figure 23 SEM image of KNO_3 with CuO nanoparticles.

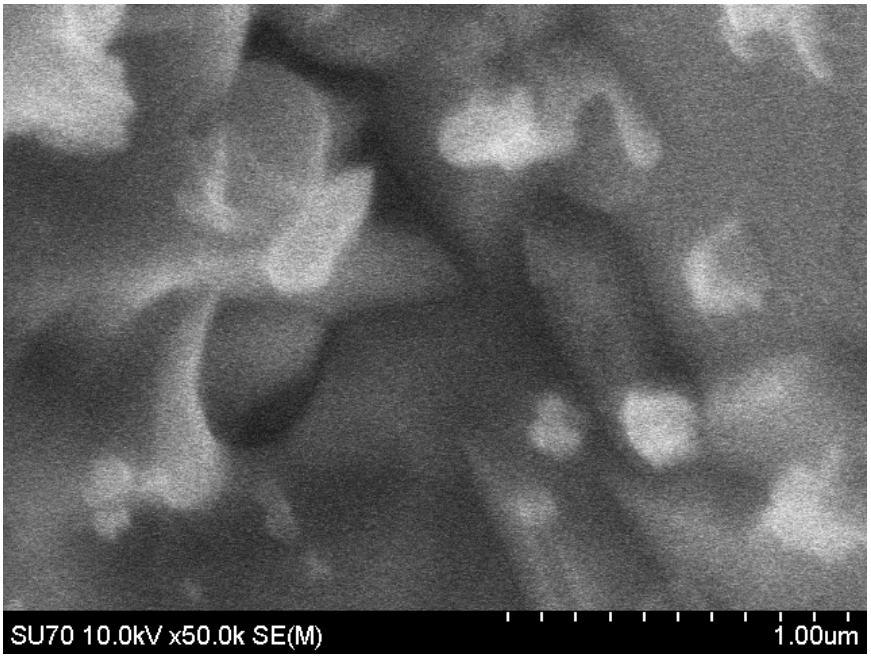

Figure 24 SEM image of $NaNO_3$ with CuO nanoparticles.

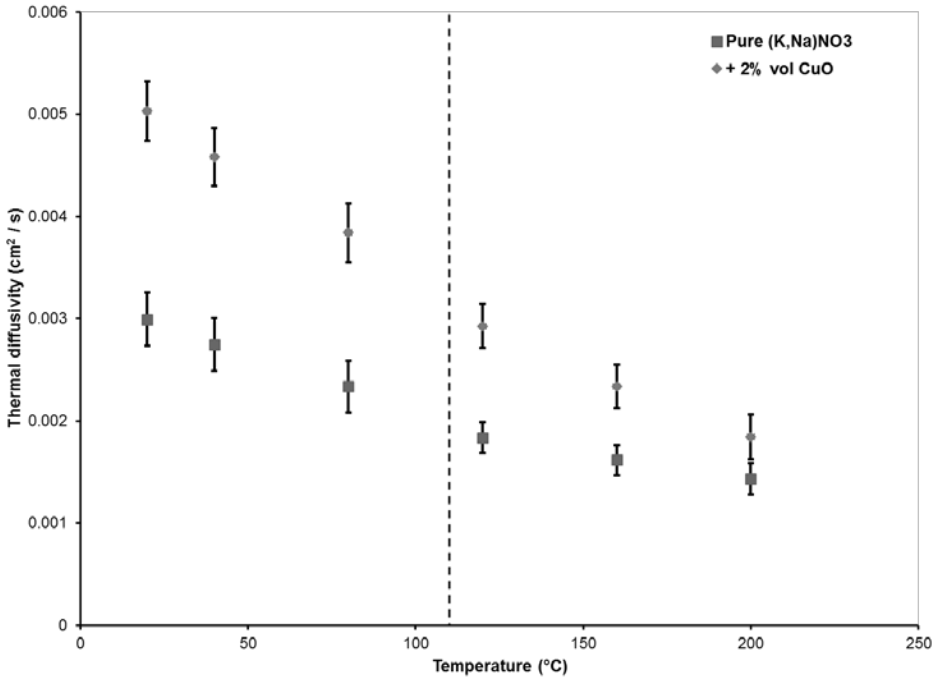

Figure 25 Thermal diffusivity of pure nitrate eutectic salt and eutectic-CuO system.

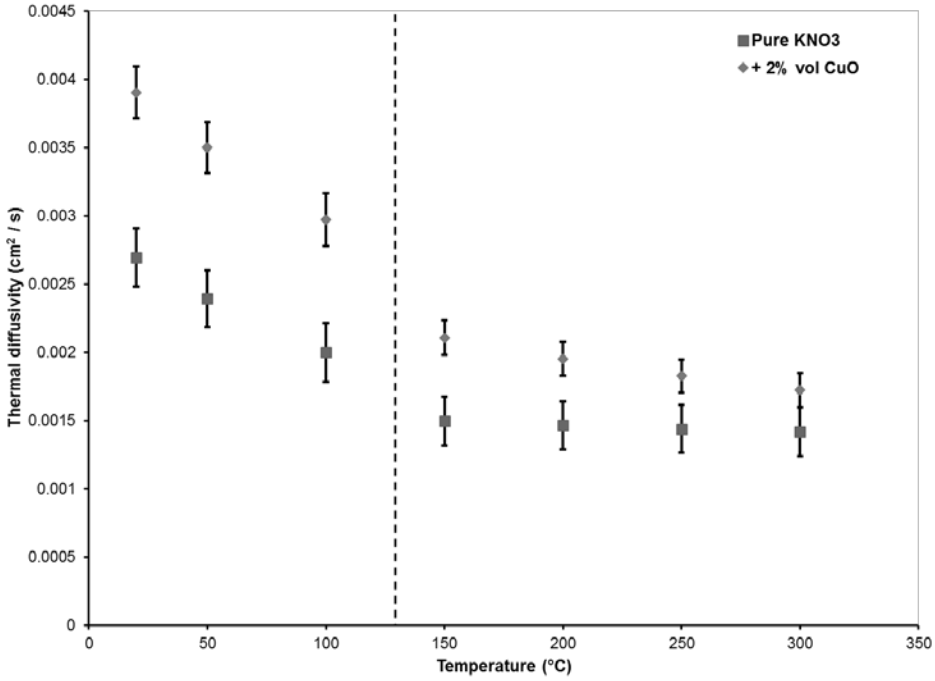

Figure 26 Thermal diffusivity of pure KNO_3 and KNO_3-CuO system.

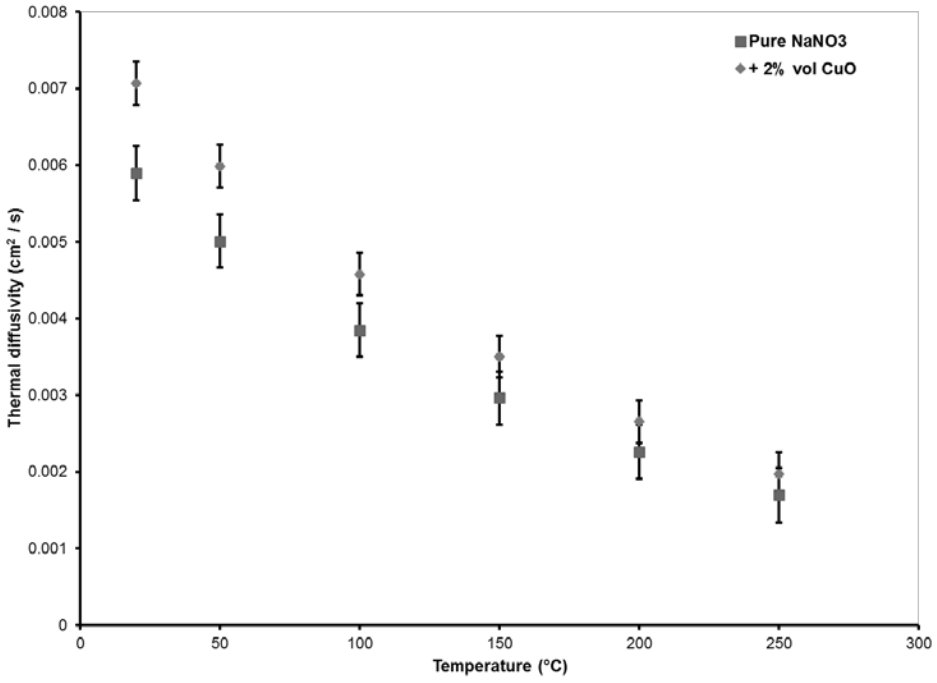

Figure 27 Thermal diffusivity of pure $NaNO_3$ and $NaNO_3$-CuO system.

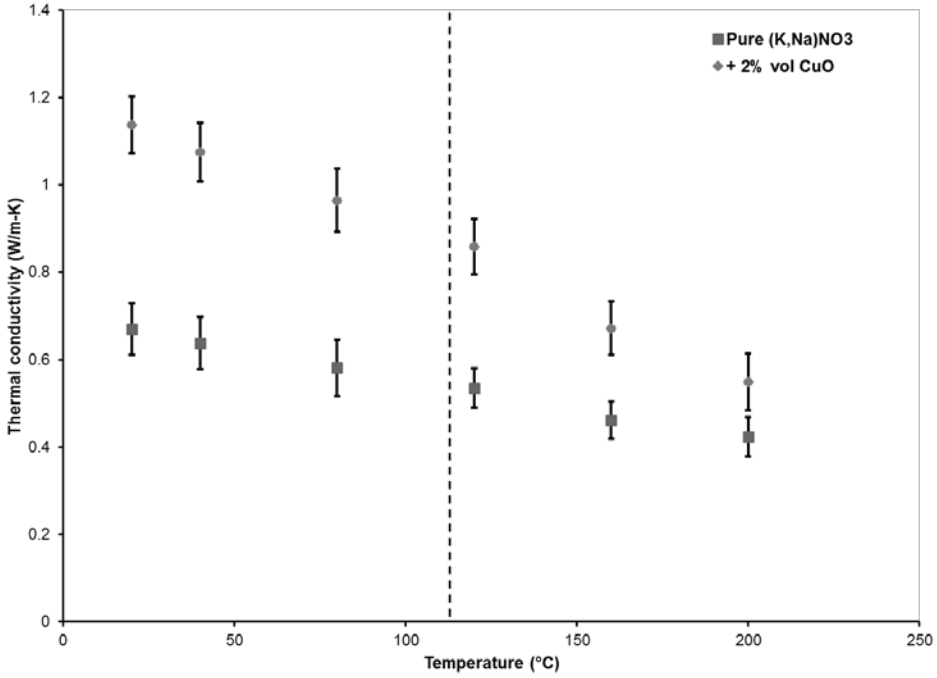

Figure 28 Thermal conductivity of pure nitrate eutectic salt and eutectic-CuO system.

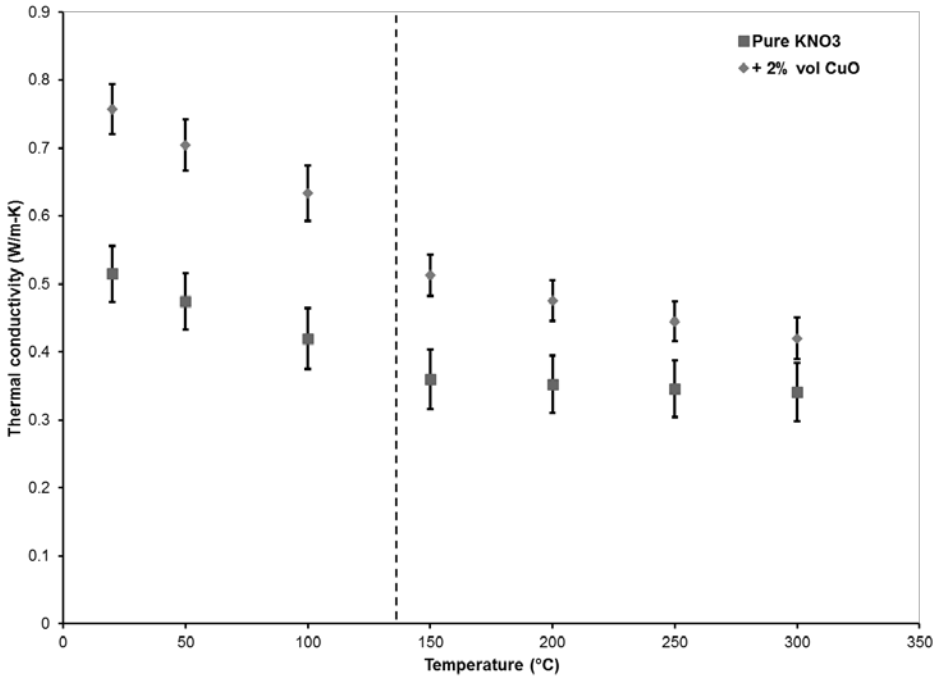

Figure 29 Thermal conductivity of pure KNO_3 and KNO_3-CuO system.

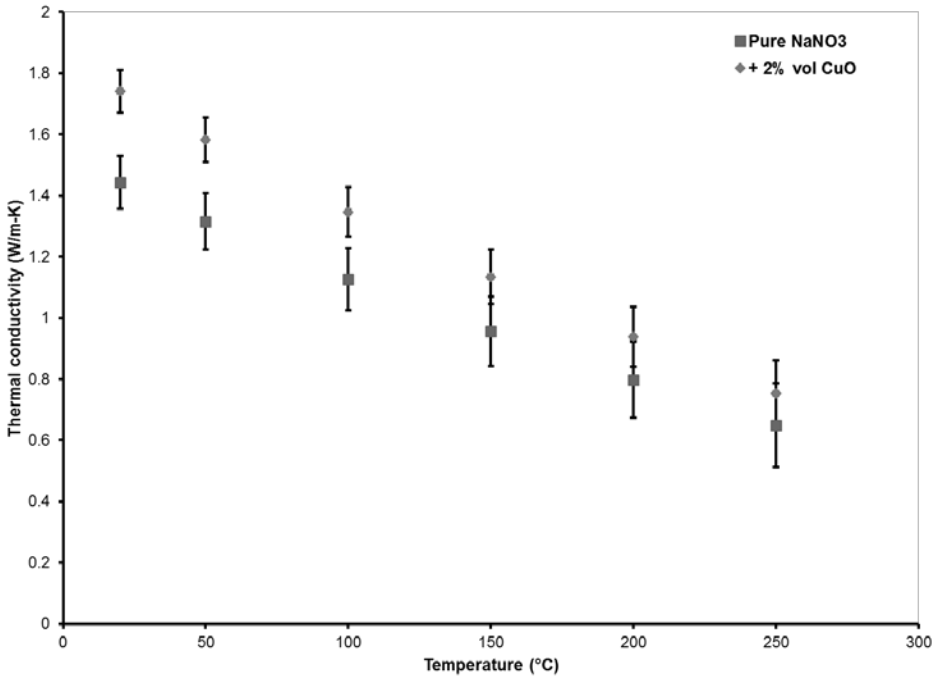

Figure 30 Thermal conductivity of pure $NaNO_3$ and $NaNO_3$-CuO system.

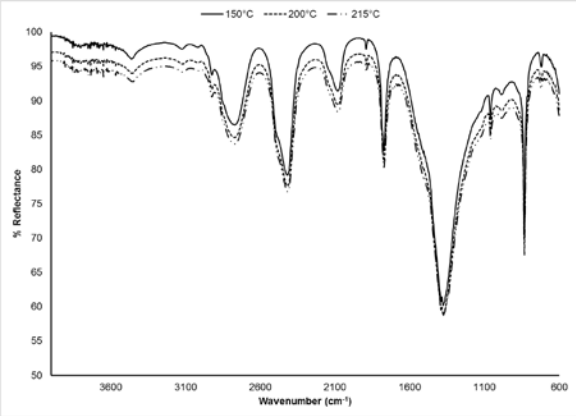

(a)

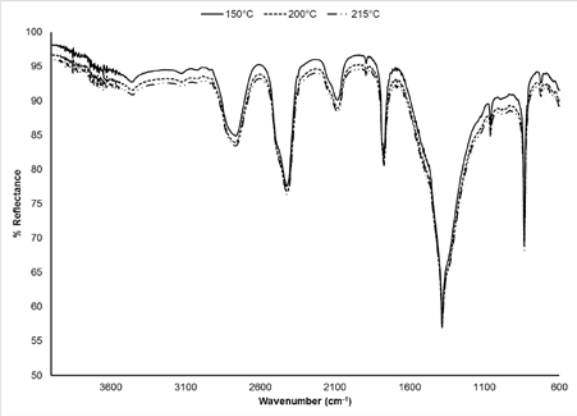

(b)

Figure 31 IR spectra of eutectic salt with CuO nanoparticles. Measurements made before (a) and after (b) melting.

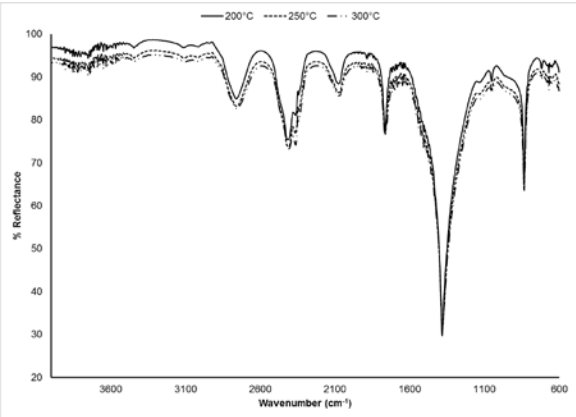

(a)

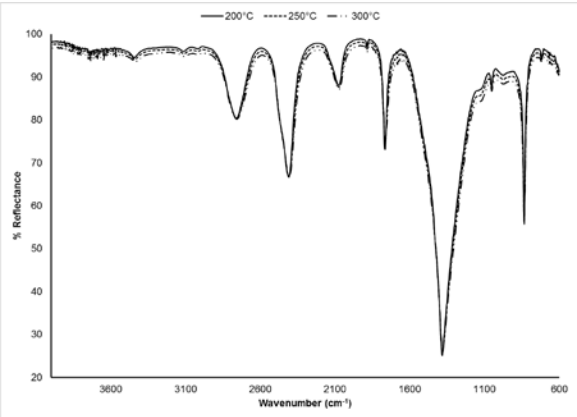

(b)

Figure 32 IR spectra of KNO_3 with CuO nanoparticles. Measurements made before (a) and after (b) melting.

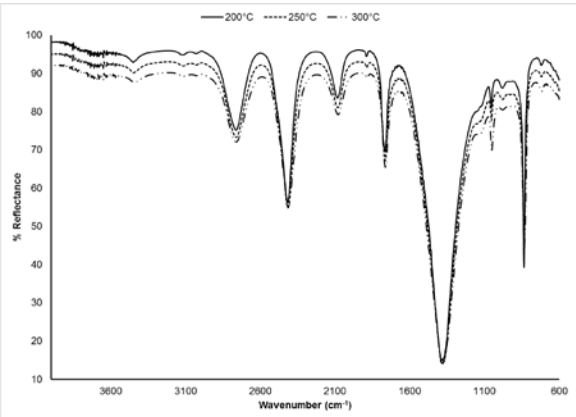

(a)

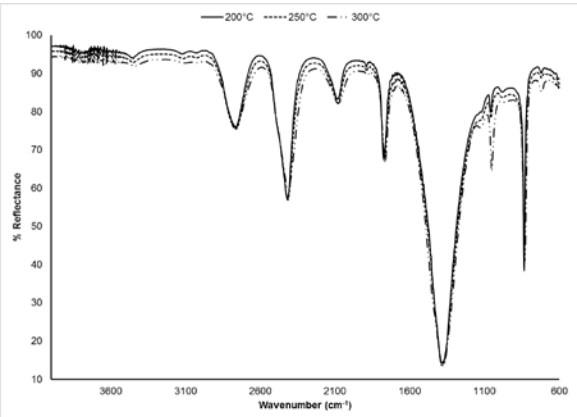

(b)

Figure 33 IR spectra of $NaNO_3$ with CuO nanoparticles. Measurements made before (a) and after (b) melting.

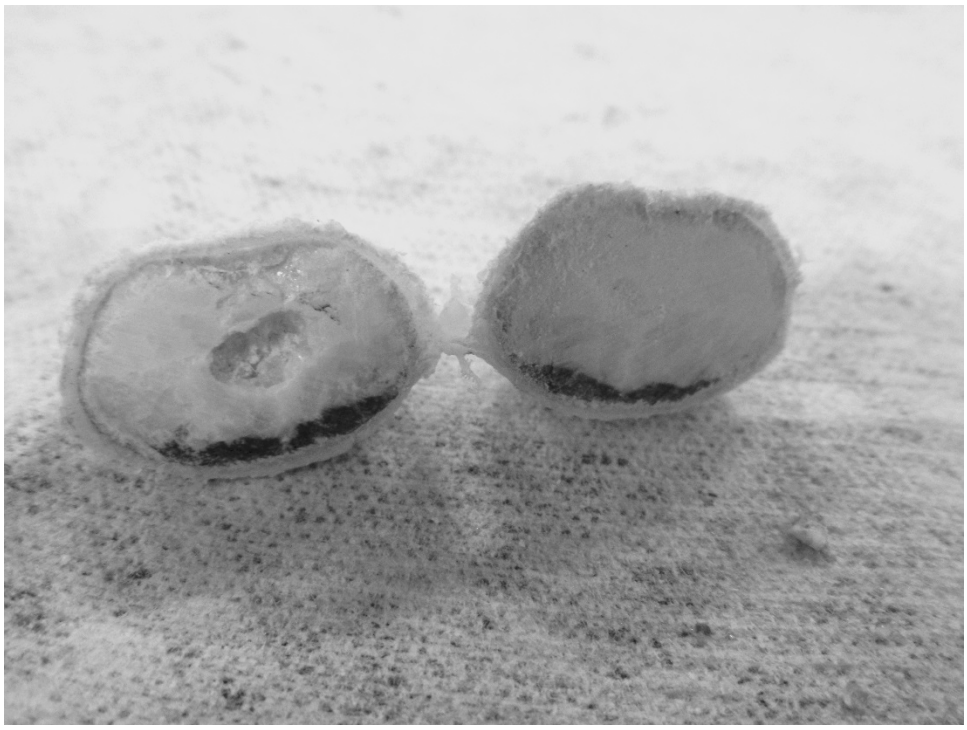

Figure 34 Bisected pellet containing sodium nitrate and 2 wt % NiO nanoparticles. The NiO is seen as the black material at the bottom of the pellet.

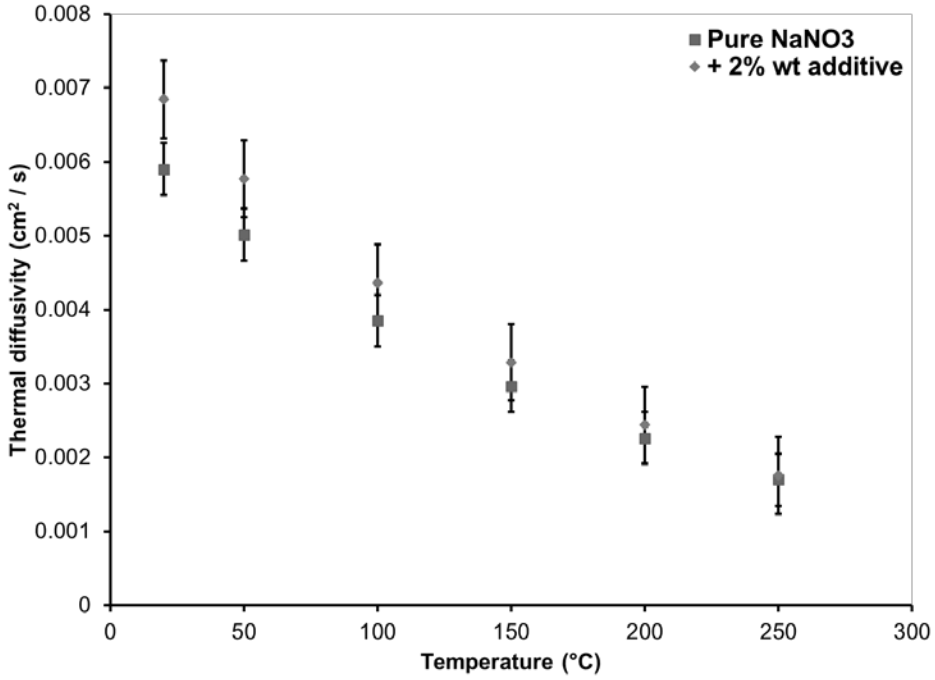

Figure 35 Thermal diffusivity of pure $NaNO_3$ and 2.0 wt % $NaNO_3$-graphene system.

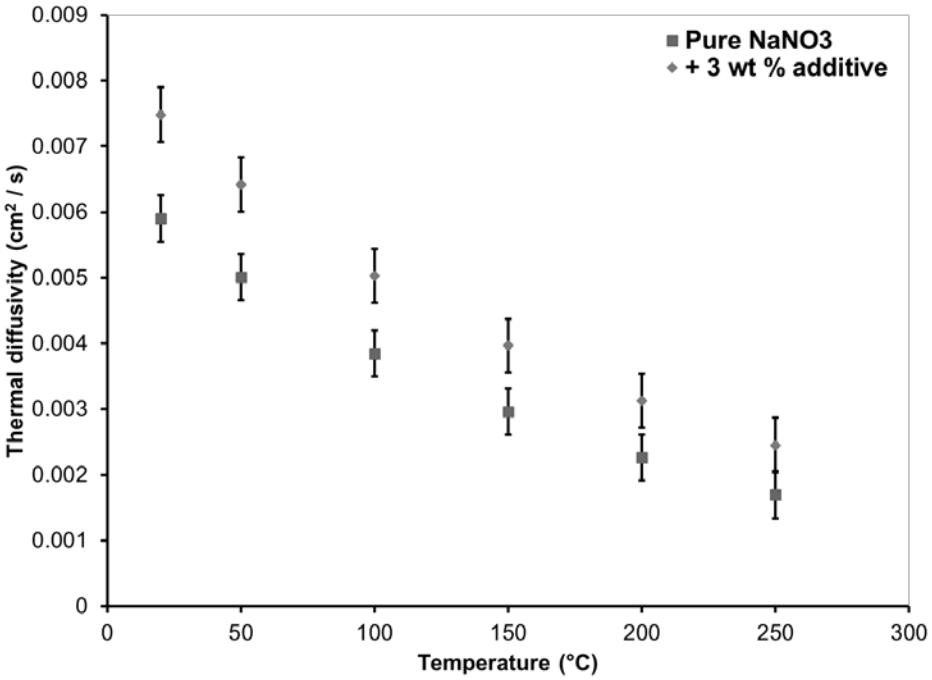

Figure 36 Thermal diffusivity of pure $NaNO_3$ and 3.0 wt % $NaNO_3$-graphene system.

Table 3 Thermophysical properties of nitrate eutectic salt and constituents. $T = 200$°C and $T = 250$°C correspond to solid and liquid phases, respectively. Data are taken from FactSage [27], unless otherwise noted.

Salt	**Mole % (KNO_3:$NaNO_3$)**	**T_m (°C)**	**ΔH_{fus} (J/g)**	**c_p (J/g-K)**		**Density (g/ml)**	
				T = 200°C	*T = 250°C*	*T = 200°C*	*T = 250°C*
KNO_3	100:0	334 [59]	95 [59]	1.19		2.11	
$NaNO_3$	0:100	306.5 [59]	182 [59]	1.56	1.69	2.26	
$(K,Na)NO_3$	51.8:48.2	223.01	125.8	1.35	1.41	2.18	1.94

Table 4 Thermophyiscal properties of potential additives. Thermal conductivity data are taken from [81], unless otherwise noted. All other data are taken from FactSage [27], unless otherwise noted.

Additive	**k (W/m-K)**				**Density (g/cm^3)**			**c_p (J/g-K)**			**ρc_p (J/cm^3-K)**		
	T = 25°C	*223°C*	*306.5°C*	*334°C*	*T = 223°C*	*306.5°C*	*334°C*	*T = 223°C*	*306.5°C*	*334°C*	*T = 223°C*	*306.5°C*	*334°C*
Al_2O_3	36.3	20.4	16.7	15.6	3.97	3.96	3.96	1.09	1.14	1.16	4.32	4.54	4.59
CoO	-				6.45			0.72	0.72	0.72	4.66	4.66	4.66
CuO	76.5 [77]	-			6.40			0.62	0.64	0.64	3.96	4.07	4.11
Fe_2O_3	-				5.24	5.23	5.22	0.82	0.86	0.87	4.29	4.50	4.57
NiO	41	10.5	8.6	8.0	6.67			0.85	0.69	0.69	5.69	4.61	4.64
SiO_2	8.3	5.0	4.3	4.1	2.63	2.62	2.62	0.99	1.06	1.08	2.59	2.77	2.82

Table 5 Thermophysical properties of pure nitrate salts and nitrate-CuO mixtures. Properties were measured by DSC.

Salt	T_m (°C)	ΔH_{fus} (J/g)
$(K,Na)NO_3$	220.52 ± 0.04	124 ± 3
$(K,Na)NO_3$ + CuO	220.35 ± 0.03	120 ± 6
KNO_3	334.48 ± 0.02	91 ± 6
KNO_3 + CuO	333.90 ± 0.06	87 ± 2
$NaNO_3$	306.21 ± 0.03	186 ± 4
$NaNO_3$ + CuO	306.14 ± 0.05	186 ± 4

CHAPTER 4 CHLORIDE SALTS FOR THERMAL ENERGY STORAGE[5]

4.1 Introduction

Increased implementation of renewable energy technologies and, in particular, the next generation of concentrating solar power (CSP) plants require the development of new means to ensure these technologies provide consistent and reliable power generation. It is expected that the next generation of CSP plants will allow for higher operating temperatures and correspondingly increased operating efficiencies. In recent years central receivers for the solar power tower configuration produced working fluid temperatures in excess of 950°C [97]. The central receiver design is limited in operating temperature by material constraints, but it is generally regarded that gaseous fluids (e.g., air) can be reliably heated to 800 – 1100°C [98]. Also crucial to the development of such plants are advanced TES systems capable of meeting nighttime loads and improving general dispatchability. Higher operating temperatures and thermal storage strategies are crucial to allowing CSP technologies to achieve the goals put forth by the U.S. Department of Energy Sunshot Initiative—namely, levelized cost of electricity (LCOE) of $0.06/kWh or less [20].

This paper investigates a group of materials, chloride salts, that hold great potential for use in the next generation of CSP plants. Inorganic salts in general are well suited to address both the higher operating temperature needs of solar power towers and the attendant need for TES, as they can be used as HTFs and/or thermal storage media in advanced high-temperature CSP plants [99,

[5] This chapter has been submitted to the *Journal of Solar Energy Engineering* for publication [96].

100]. In current plants, however, only nitrate-based salts have been utilized, either as the working fluid in the central receiver or as molten salt sensible heat storage media (i.e., dual tank storage) [25, 101]. At the lower temperatures of their current use, nitrate salts possess favorable thermophysical properties, low vapor pressure, and comparatively low cost [26]. They are, however, limited in their application to temperatures below 600°C, and thus would be inappropriate as working fluids or TES media for central receivers operating at higher temperatures [102]. Many chloride salts, however, are stable at these higher temperatures, and tend to have low vapor pressure up to 801°C [103].

This paper examines a set of chloride salts and their mixtures particularly relevant to high temperature (>400°C) applications for solar power tower plants—as a working fluid, as sensible TES, or as latent heat thermal energy storage (LHTES). A preliminary screening of pure chloride salts based on available literature yields a list of promising candidate salts. Eutectic mixtures of these salts are also considered; the eutectic systems were modeled using the thermodynamic database software, FactSage [27]. Thermophysical properties, such as melting point, latent heat, etc., are summarized for each salt system. Given the higher temperatures of operation considered here, data for the radiative properties of these materials are also presented. Candidate containment materials and strategies are discussed, along with the attendant potential for corrosion. Last, cost data for these systems are used to assess the most promising storage media for individual applications.

4.2 Background

TES is especially important in power generation, and has a primary advantage over technologies such as mechanical (e.g., compressed air storage) or chemical (e.g., batteries) in that it generally entails lower capital cost [11, 12]. Further, for solar thermal power plants, TES is

preferable over other storage technologies because it allows for a smaller turbogenerator with less part-time operation [98]. Here, we briefly describe some of the general aspects of TES. More information on the technological details on solar power plants can be found in the review by Barlev et al [14]; extensive review of the importance and practical design concerns of TES in CSP plants can be found in the work by Kuravi et al [12].

TES can generally be divided into three distinct categories: sensible heat, latent heat, and thermochemical energy [104]. Sensible heat is perhaps the most familiar; it stores thermal energy by heating a mass of material of constant phase (e.g., solid, liquid, or vapor) from a lower temperature to a higher temperature, and its quantification requires knowledge of the material's specific heat capacity, which itself may vary with temperature. Latent heat, on the other hand, stems from a phase change and corresponding change in the enthalpy of the storage medium. In this way latent heat storage makes use of PCMs and has the potential to offer great improvements over sensible heat storage alone, due to the typically large quantities of energy required for phase change and the ability to store and deliver heat at a consistent temperature (i.e., the phase-change temperature) [15]. Thermochemical storage is very promising because of its potential for significant energy storage capacity (mass basis) [13]; however, it faces a number of technical challenges, and it will not be discussed in this paper.

This study examines a particular class of inorganic salts, chloride salts, for use in TES-equipped solar power generation. Inorganic salts have already found widespread use as storage media in a sensible heat storage arrangement. Molten salts in utility scale storage systems—the two-tank storage system design—are well-established [24]. Indeed, multiple power plants soon to come online will make use of this storage strategy, including the Crescent Dunes project in Tonopah, Nevada [13]. In this way, inorganic salts are very promising as high-temperature heat

transfer fluids and sensible thermal storage media in solar thermal power production. It is also important to note that these materials are characterized by high heats of fusion, so their use as PCMs in LHTES arrangements allows for substantially higher energy storage density than their use as sensible heat storage alone.

The operating temperature is a crucial factor in determining the potential upper-limit efficiency of a thermal power plant's power cycle, as well as the exergetic efficiency of any TES system meant to support the plant [13]. Higher operating temperatures and thermal storage strategies are therefore crucial to allowing CSP technologies to achieve the goals put forth by the U.S. Department of Energy Sunshot Initiative—namely, LCOE of $0.06/kWh or less [20]. Chloride salts are promising materials to meet the higher operating temperature needs of the next generation of CSP plants, mainly because they tend to have higher melting temperatures—NaCl, for instance, melts at 800.7°C [59]. Moreover, many chloride salts are comparatively inexpensive. The review conducted by Hoshi et al, for instance, shows chloride salts in general to be less expensive per kWh latent heat than corresponding nitrates, fluorides, hydroxides, carbonates [74].

To conduct a meaningful review and screening of potential chloride salt systems for application in solar power plants, there is a need for both cost and thermophysical properties data. Data for pure component melting points and latent heat of fusion are available in the CRC Handbook of Chemistry and Physics [59]. Other pure component thermophysical properties, including thermal conductivity, specific heat capacity, and radiative properties, can be found in the compilations of Touloukian et al [67, 81, 105]. A number of reviews have been conducted addressing the properties of inorganic salts as PCMs [8, 23, 74]. These reviews include relevant properties such as melting point, latent heat of fusion, and eutectic composition for select salt systems. As far as molten salt properties are concerned, the work of Janz et al provides much useful

information [84, 106-108]. Phase equilibria data (relevant for mixtures of the salts considered here) are found in numerous works undertaken to analyze and consolidate phase equilibrium diagrams [109-111]; particularly noteworthy is the CD-ROM database compiled by the American Ceramic Society and the U.S. National Institute of Standards and Technology [112].

In the process of screening potential salts based on estimated cost and sufficiently high melting temperature (>400C°), it became clear that, when considering mixtures of these materials, systems of interest would include mixtures with little thermophysical properties data immediately available in the literature. As such, the thermophysical properties database software, FactSage, was used to model the eutectic salt mixtures considered here [113, 114]. FactSage 6.4 was used with the database FTSalt to model the binary eutectic systems of the pure salts obtained from the first screening. Most of the eutectic systems considered here have been "optimized" by the software developers—that is, they have been closely correlated to experimental phase equilibria data from various literature sources. FTSalt contains data on all the pure salts except the chlorides of copper (CuCl, $CuCl_2$). If a binary salt system was shown to have no congruently melting eutectic composition (e.g., a monotectic system such as $MgCl_2$-$MnCl_2$), then that system was excluded from further consideration. Such a salt, while inappropriate for LHTES, may be used in the molten state as a working fluid or sensible heat storage medium, however.

4.3 Pure Salt Screening Process

There are, of course, numerous chlorides which may be considered as TES media. The general categories into which these materials fall are chlorides of alkali metals, alkaline earth metals, transition metals, *p*-block metals, and rare earth metals. For the purposes of this study, we limit ourselves to salts of higher melting temperatures—that is, greater than 400°C (ferric chloride, $FeCl_3$, for instance, would be neglected, as its melting temperature is 306°C). When combined in

eutectic mixtures, the resulting salt systems may melt at temperatures lower than 400°C; it is anticipated that these materials may still find use at elevated temperature as fused salt sensible storage media (i.e., as "solar salt," the eutectic of KNO_3 and $NaNO_3$, is used currently for dual tank storage in solar power plants [25]). Moreover, many of the pure salts considered exhibited costs well in excess of those of the preponderance of the other candidate salts (for example, chlorides of rare earth metals); as such, salts with costs on the order of $1000/kg or more were also excluded during this preliminary screening.

The results of this screening are shown in Table 6. The melting temperatures and enthalpy change of fusion for these substances were obtained from the same reference data compilation [59]; further, they were cross-referenced with other databases to assure validity (e.g., [110, 113, 115]). Costs were obtained by taking the lowest "bulk" price among the aggregate vendors on the chemical identification and supply website, SciFinder [116]. Prices reflect quotes obtained over the approximate period of October – December 2014. A variety of different purities were available, so prices for purities less than 95% were excluded from consideration (lower purity salts would give less reliable thermophysical properties, not the least of which would be melting temperature). It is worthwhile to note here that, even at purities of 95% and greater, impurities in the "as-received" salts may hinder the long-term performance of the TES unit utilizing these materials. As such, it may be necessary to pretreat the as received salts to remove or precipitate impurities prior to implementation [103]. For example, it was necessary to thermally treat the "solar salt" (KNO_3-$NaNO_3$ eutectic) working fluid in order to eliminate $Mg(NO_3)_2$ impurities at the Solar Two molten salt power tower installation [101].

The latent heat of these pure materials is plotted with respect to their costs in Figure 37. From this depiction, one can discern a distinct region of high latent heat / low cost materials that

would be ideal as storage media for LHTES. Materials with greater cost and lower latent heat would not be recommended for this purpose. In between, there are materials of less certain applicability—either relatively inexpensive but low in latent heat (e.g., $BaCl_2$), or high in latent heat but also expensive (e.g., $CoCl_2$). Any of the materials shown in this figure (or mixtures thereof) may find use as fused salt sensible heat storage media, depending on other thermophysical properties (melting temperature, density, specific heat, etc.) and their chemical stability.

The melting point, latent heat, and cost data for the pure salts obtained from the screening process are listed in Table 6, along with cost data obtained from the various vendors. Two types of costs are presented. The first, on a mass basis, is more appropriate for materials meant to be applied as either a working fluid or a molten salt-based sensible heat storage medium. For LHTES media, however, it is more appropriate to cost the materials based on the amount of energy they are capable of absorbing during phase change. Hence, the second cost column gives the cost per-kJ latent heat.

Next, we consider the binary eutectic mixtures of the pure salts listed in Table 6. As described in the prior section, the FactSage database, FTSalt has data on all the pure salts except the chlorides of copper (CuCl, $CuCl_2$). Data for systems involving these salts must be obtained directly from the literature. The binary systems of the remaining salts, however, were successfully modeled using the software, which yielded the appropriate eutectic composition and the melting point for each system. The binary eutectic mixtures of these salts are listed in Table 7, along with relevant thermophysical properties. As with the pure salts, the latent heat of fusion is a desired quantity to aid in the selection of LHTES storage media. To that end, the latent heat of fusion was estimated based on entropy additivity of its pure component salts [117]. This approximation can be articulated as follows [98].

$$\Delta H_{fus} = T_m \sum_i \frac{x_i \Delta H_{fus,i}}{T_{m,i}} \quad (4.1)$$

While approximate, this equation can allow for direct comparison among all the individual salt mixtures, for many of whom direct latent heat data are unavailable. These approximate values for latent heat of the mixtures are also presented in Table 7. As with the pure salts, two costs are listed: one with a mass basis (more appropriate for working fluid or sensible heat storage application), and the other with a latent heat basis (more appropriate for latent heat storage application).

4.4 Radiative Properties

The chloride salt systems studied in the paper are particularly useful for TES at higher temperatures. At sufficiently high temperature, radiative transfer becomes a major mode of heat transfer. For the temperatures considered here (approximately 1000°C or less), the bulk of this radiation is in the infrared. Moreover, if the molten salt is to be employed as the absorbing fluid in the receiver, information regarding its radiative properties in the ultraviolet and visible regions of the spectrum would be important for modeling solar absorption.

Radiative properties data, unfortunately, are not available for every system considered here. Data for selected pure chloride salts are obtained from the thermophysical properties compilation of Touloukian et al [67]; they are presented in Figure 38. Specifically, the normal spectral transmittance (measured at room temperature) is presented for CuCl, KCl, NaCl, and $PbCl_2$. The samples in these cases were single, polished crystals; in practice, these materials will likely experience additional attenuation due to impurities, fractures, grain boundaries, etc. Also, since the measurements were made at room temperature, one can expect the near- to mid- infrared absorption to rise with temperature, especially if lattice defects or dopants are present within the crystal [118]. Nonetheless, we gain a general picture of these materials' properties from the plotted normal spectral transmittance. The chloride salt data shown with the radiative properties of ionic

crystals, having one or more absorption bands in the mid- to far- infrared (*Reststrahlen* absorption) and several absorption bands near the ultraviolet (electronic excitation), as described by the Lorentz model [118].

4.5 Containment Materials / Methods

High temperature chlorides may require non-metallic containment, as most metals would be prone to corrosion in the presence of these materials and even small quantities of oxygen and/or moisture. One could justifiably predict that ceramic materials would be necessary for these uses, and in this case the importance of radiative transfer is amplified, for two reasons. On the one hand, ceramics are significantly less conductive than metals; on the other, metals tend to be less emissive than ceramics.

High temperature conditions (>400°C), cyclic thermal stress, and corrosive TES media present a unique challenge to the material selection process. Corrosion is a major consideration at these temperatures. Nickel-based alloys are frequently employed in corrosive applications. Various studies discuss the role of specialty alloys for corrosive applications. Vignarooban et al reported corrosion rates for various Hastealloys in NaCl-KCl-$ZnCl_2$ molten salt mixtures up to 500°C [119]. However, containment materials must not only protect against corrosion, but must also be cost-effective. While some nickel alloys may withstand these corrosive conditions, their selection is hindered by their high costs (4 times as high as stainless steel alloys [13]). Hence, steel or steel-based alloys could prove to be important contributors towards containment of the chloride-based TES systems.

It has been found that certain elements like Cr and Ni are conducive to improving corrosion resistance of low carbon microalloying steel [120]. Moreover, corrosion rates increase with increasing temperatures [121]. Hiramatsu et al. presented the effects of alloying elements of

stainless steels on NaCl induced corrosion in a temperature range of 450°C to 750°C. Austenitic stainless steels displayed better results than ferritic stainless steels [121]. SEM/EDXA analysis was conducted by Lehmusto et al to study the effect of solid KCl on superheater steels at elevated temperatures [122]. Nickel-based alloy 625-type steel was found to be more durable in terms of corrosion resistance as compared to ferritic 10CrMo-type steel. In case of the alloy 625 type steel, the thick oxide layer predominantly comprised of nickel oxide in the presence of KCl. Furthermore, a comprehensive analysis of various Fe-Cr-Ni alloys was conducted by Evans et al [123]. This study concluded that diffusion of Cr ions in the Cr_2O_3 scale was the rate controlling step in the temperature range of 700°C to 1100°C. The role of chlorides in hot corrosion of high alloy stainless steels was studied by Mohanty et al [124]. The authors concluded that thermal cycling, when superimposed on hot corrosion, caused spallation of the oxide layer while cooling.

Corrosion protection afforded by various protective coatings has also been evaluated in various studies. Shankar et al compared the performance of yttria-stabilized zirconia coating on 316L SS with respect to uncoated 316L SS [125]. The testing was carried out at elevated temperatures of 600°C and the coating was found to be instrumental in providing improved corrosion resistance. Uusitalo et al discussed results of experimental studies of boiler steels and protective coatings at high temperatures [126]. The coatings evaluated were high velocity oxy-fuel (HVOF) coatings, laser cladding, and diffusion chromized steel. In addition, two boiler steels were also analyzed. The performance of nickel-based high chromium coatings was found to be satisfactory.

In addition to developing new alloys and protective coatings, other techniques employed to improve the corrosion resistance of cost effective stainless steel based alloys include shot peening, cladding and internal insulation approach [13]. Shot peening is employed to change the

grain size and the structure of the alloy at the surface to improve its corrosion resistance. Smaller grain size provides a larger surface area for formation of passivating layers [127].

Cladding is a method bonding thin protective layers to a substrate through roll welding, explosive welding or laser application. Internal insulation approach employs thermally insulating refractory bricks as internal liner to the storage tank. Inexpensive insulation materials make this an economically attractive option. This approach has been employed in coal gasification industries [128].

4.6 Cost Comparison

In Figure 39, the cost per kg of the binary salt eutectic mixtures is plotted against melting temperature. The systems are labeled with their numbers as listed in Table 7. Also included for reference are cost data for the nitrate salts, $NaNO_3$ and KNO_3, which are now commonly used for sensible storage media. From this plot, it is clear which systems are preferable in terms of cost at each temperature of interest; in general, the systems involving the chlorides of sodium, potassium, and magnesium tend to be less expensive, as well as some systems involving chlorides of barium and calcium. In Figure 40, the cost per kJ latent heat (estimated) is plotted against melting temperature for the same binary systems (again, numbered as in Table 7). While the grouping of materials is qualitatively similar to that shown in Figure 39, differences that arise are illustrative of the different selection process required for latent heat media as opposed to that required for sensible heat media. For instance, it can be seen in Figure 40 that systems 2 and 3 (different eutectic compositions of BaCl2-CsCl) become relatively more expensive when judged on the basis of their heat storage capacity, which is to be expected owing to the relatively low latent heat of these systems. Last, we present all the chloride salt systems (pure or eutectic) that fall below $0.20 per kJ latent heat (Figure 41). These materials show most promise as PCMs in a LHTES arrangement.

It is clear from the plot that there are a wealth of salt systems which can cover the range of approximately 400 – 800°C (e.g., in a cascade latent heat storage system [28]). Based on this observation, it seems that more expensive salts (e.g., fluorides) or metals may be needed for latent heat storage media at higher temperatures; alternatively, sensible heat storage could be explored.

As an illustration of the information that can be gleaned from these charts, consider a cascaded latent heat system designed to heat a working fluid from 400 to 540°C. Consulting Figure 41, we see that the 43 → 44 → 6 → 7 cascade—that is, two eutectic mixtures of KCl-$MgCl_2$, followed by $BaCl_2$-LiCl and $BaCl_2$-$MgCl_2$—provides a suitable configuration with an approximate 20°C approach or greater and approximately 50°C separation between each PCM melting point.

4.7 Conclusions / Future Work

Inorganic salts are promising as TES media to increase dispatchability and capacity factor of CSP plants. Nitrate salts especially have found widespread use in this context. Chloride salts, however, have received less attention. This paper proposes various chloride salt systems for use in high temperature (>400°C) solar power plants, either as working fluid, sensible heat storage media, or latent heat storage media (i.e., PCMs). A group of 17 pure chloride salts was obtained from a preliminary screening process based on cost and melting temperature. An additional 64 systems, taken from the binary eutectic systems of the pure salts, were modeled using the thermodynamic database software, FactSage. Thermophysical properties, taken from the FactSage model and other literature sources, are presented for each of the salt systems. A cost comparison was performed for the systems in application as sensible heat storage media or latent heat storage media.

Lack of measured properties data for many of these systems is a distinct challenge, and future work is planned to address this problem. Also, potential downsides of some of these materials (containment compatibility, long-term thermal stability) need to be studied in greater

detail. Nonetheless, it is expected that chloride salts in general can find use in high temperature TES applications in the near future.

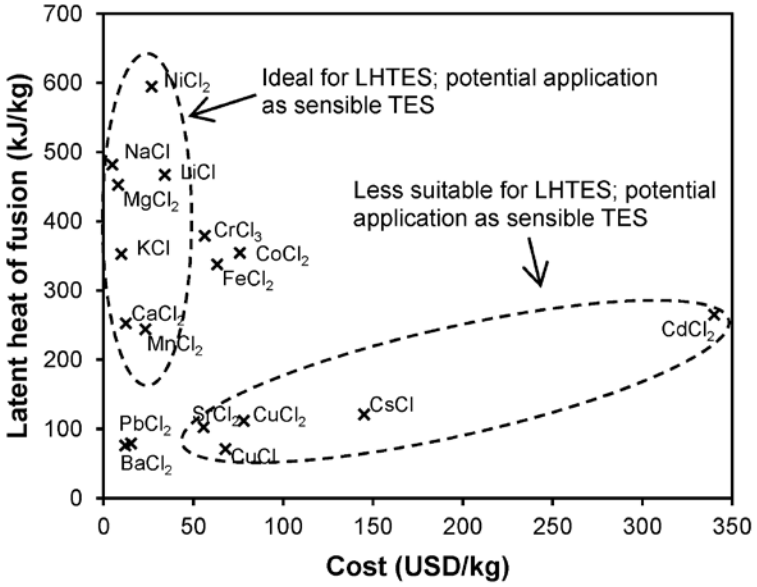

Figure 37 Latent heat plotted against cost for pure chloride salts

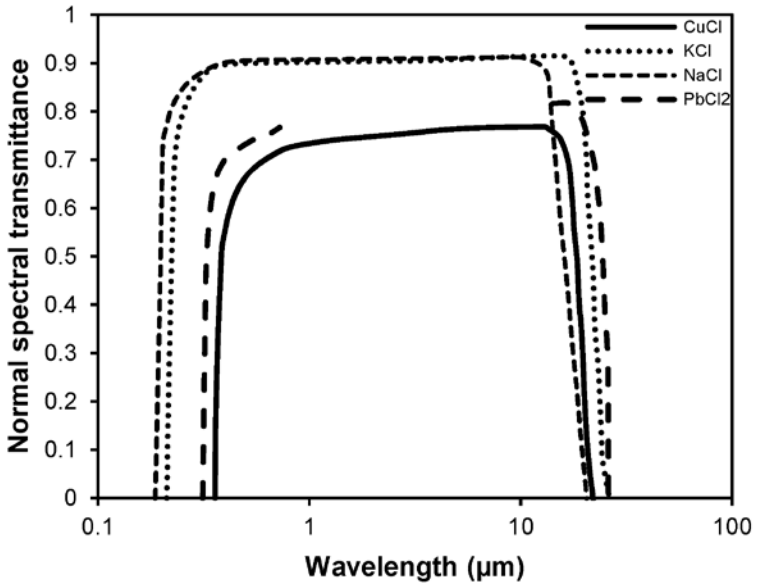

.

Figure 38 Normal spectral transmittance for select pure chloride salts. Data were taken from Touloukian [67].

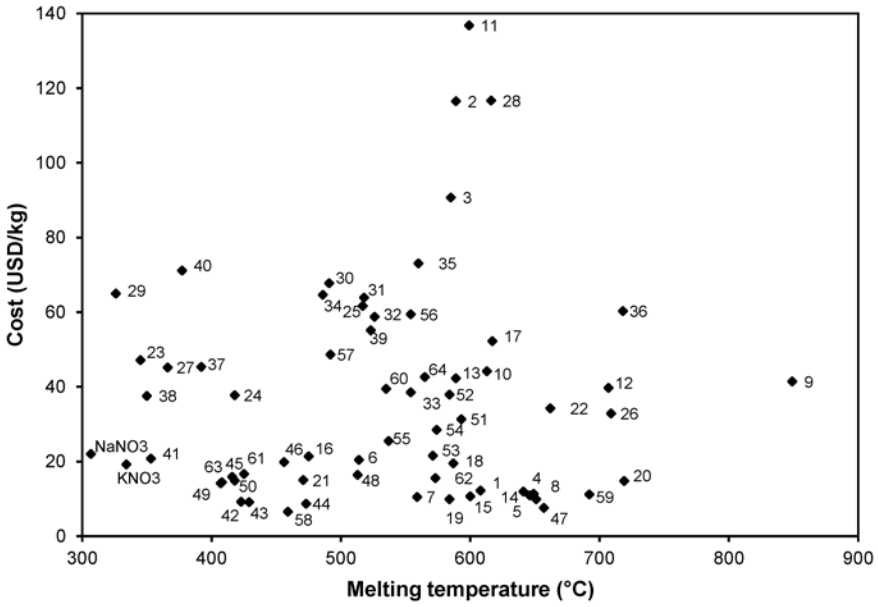

Figure 39 Cost per kg (e.g., sensible storage application) of chloride salt systems. Systems are presented as numbered in Table 7.

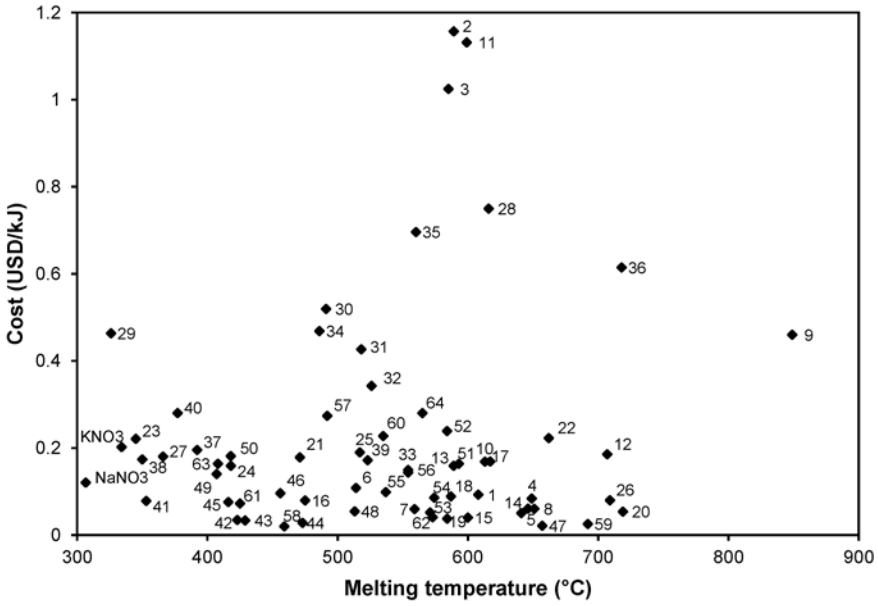

Figure 40 Cost per kJ (e.g., latent storage application) of chloride salt systems. Systems are presented as numbered in Table 7.

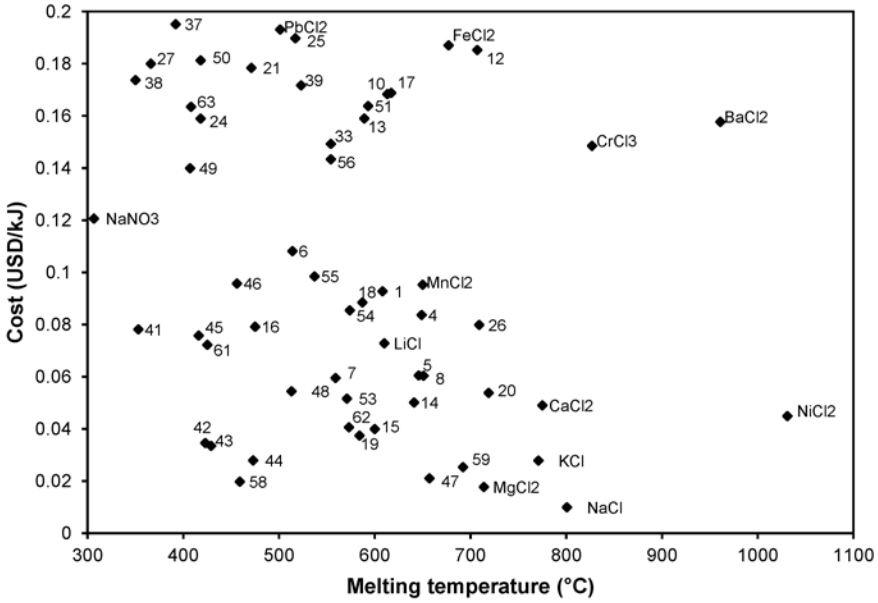

Figure 41 Pure salts and eutectics under $0.2 (USD) per kJ latent heat.

Table 6 Pure salts obtained from preliminary screening process

	T_m (°C)	ΔH_{fus} (kJ/kg)	Cost (USD/kg)	Cost (USD/kJ)
Alkali metal				
LiCl	610	467	$34	$0.07
KCl	771	353	$9.80	$0.03
NaCl	800.7	482	$4.76	$0.01
CsCl	646	121	$145	$1.20
Alkaline earth metal				
$MgCl_2$	714	453	$8.00	$0.02
$CaCl_2$	775	253	$12.38	$0.05
$SrCl_2$	874	102	$55.65	$0.54
$BaCl_2$	961	76	$12.00	$0.16
Transition metal				
$CrCl_3$	827	379	$56.25	$0.15
$MnCl_2$	650	244	$23.23	$0.10
$FeCl_2$	677	338	$63.20	$0.19
$CoCl_2$	737	354	$75.80	$0.21
$NiCl_2$	1031	595	$26.69	$0.04
$CuCl_2$	598	112	$78	$0.70
CuCl	423	71	$67.80	$0.95
$CdCl_2$	589	265	$340	$1.28
Other				
$PbCl_2$	501	79	$15.19	$0.19

Table 7 Thermophysical properties and cost data for the binary eutectic mixtures

		x_A	x_B	T_m (°C)	ΔH_{fus} (approximate) (kJ/kg)	Cost (USD/kg)	Cost (USD/kJ)
No.	*Eutectic mixture (A-B)*						
1	$BaCl_2$-$CaCl_2$	0.359	0.641	608	131	$12.18	$0.09
2	$BaCl_2$-CsCl	0.181	0.819	589	101	$116.45	$1.16
3	$BaCl_2$-CsCl	0.358	0.642	585	89	$90.71	$1.02
4	$BaCl_2$-KCl	0.445	0.555	649	135	$11.32	$0.08
5	$BaCl_2$-KCl	0.272	0.728	646	181	$10.92	$0.06
6	$BaCl_2$-LiCl	0.249	0.751	514	188	$20.37	$0.11
7	$BaCl_2$-$MgCl_2$	0.429	0.571	559	176	$10.49	$0.06

Table 7 (Continued)

		x_A	x_B	T_m (°C)	ΔH_{fus} (approximate) (kJ/kg)	Cost (USD/kg)	Cost (USD/kJ)
No.	*Eutectic mixture (A-B)*						
8	$BaCl_2$-NaCl	0.399	0.601	651	163	$9.85	$0.06
9	$BaCl_2$-$SrCl_2$	0.27	0.73	849	90	$41.38	$0.46
10	$CaCl_2$-$CoCl_2$	0.538	0.462	613	262	$44.16	$0.17
11	$CaCl_2$-CsCl	0.091	0.909	599	121	$136.79	$1.13
12	$CaCl_2$-CsCl	0.854	0.146	707	214	$39.69	$0.19
13	$CaCl_2$-$FeCl_2$	0.444	0.556	589	266	$42.29	$0.16
14	$CaCl_2$-KCl	0.74	0.26	641	237	$11.88	$0.05
15	$CaCl_2$-KCl	0.25	0.75	600	267	$10.66	$0.04
16	$CaCl_2$-LiCl	0.35	0.65	475	270	$21.35	$0.08
17	$CaCl_2$-$MgCl_2$	0.474	0.526	617	309	$52.16	$0.17
18	$CaCl_2$-$MnCl_2$	0.374	0.626	587	220	$19.49	$0.09
19	$CaCl_2$-NaCl	0.521	0.479	584	265	$9.89	$0.04
20	$CaCl_2$-$NiCl_2$	0.852	0.148	719	275	$14.79	$0.05
21	$CaCl_2$-$PbCl_2$	0.178	0.822	471	84	$14.97	$0.18
22	$CaCl_2$-$SrCl_2$	0.584	0.416	662	154	$34.20	$0.22
23	$CoCl_2$-KCl	0.428	0.572	345	213	$47.14	$0.22
24	$CoCl_2$-KCl	0.296	0.704	418	237	$37.70	$0.16
25	$CoCl_2$-LiCl	0.389	0.611	517	325	$61.63	$0.19
26	$CoCl_2$-$MgCl_2$	0.298	0.702	709	412	$32.86	$0.08
27	$CoCl_2$-NaCl	0.373	0.627	366	251	$45.20	$0.18
28	CsCl-KCl	0.625	0.375	616	156	$116.62	$0.75
29	CsCl-LiCl	0.42	0.58	326	140	$65.02	$0.46
30	CsCl-$MgCl_2$	0.807	0.193	491	130	$67.72	$0.52
31	CsCl-$MgCl_2$	0.726	0.274	518	150	$63.87	$0.43
32	CsCl-$MgCl_2$	0.626	0.374	526	171	$58.68	$0.34
33	CsCl-$MgCl_2$	0.316	0.684	554	258	$38.48	$0.15
34	CsCl-NaCl	0.65	0.35	486	138	$64.61	$0.47
35	CsCl-$SrCl_2$	0.856	0.144	560	105	$73.04	$0.70
36	CsCl-$SrCl_2$	0.22	0.78	718	98	$60.29	$0.61
37	$FeCl_2$-KCl	0.54	0.46	392	233	$45.38	$0.20
38	$FeCl_2$-KCl	0.389	0.611	350	216	$37.56	$0.17
39	$FeCl_2$-LiCl	0.467	0.533	523	321	$55.13	$0.17
40	$FeCl_2$-NaCl	0.44	0.56	377	254	$71.12	$0.28

Table 7 (Continued)

		x_A	x_B	T_m (°C)	ΔH_{fus} (approximate) (kJ/kg)	Cost (USD/kg)	Cost (USD/kJ)
No.	*Eutectic mixture (A-B)*						
41	KCl-LiCl	0.408	0.592	353	266	$20.74	$0.08
42	KCl-$MgCl_2$	0.698	0.302	423	265	$9.16	$0.03
43	KCl-$MgCl_2$	0.653	0.347	429	271	$9.07	$0.03
44	KCl-$MgCl_2$	0.416	0.584	473	310	$8.65	$0.03
45	KCl-$MnCl_2$	0.67	0.33	416	210	$15.90	$0.08
46	KCl-$MnCl_2$	0.37	0.63	456	206	$19.77	$0.10
47	KCl-NaCl	0.494	0.506	657	360	$7.56	$0.02
48	KCl-$NiCl_2$	0.73	0.27	513	302	$16.41	$0.05
49	KCl-$PbCl_2$	0.48	0.52	407	101	$14.12	$0.14
50	KCl-$PbCl_2$	0.22	0.78	418	82	$14.81	$0.18
51	KCl-$SrCl_2$	0.706	0.294	593	191	$31.33	$0.16
52	KCl-$SrCl_2$	0.573	0.427	584	159	$37.91	$0.24
53	LiCl-$MgCl_2$	0.71	0.29	571	418	$21.56	$0.05
54	LiCl-$MnCl_2$	0.74	0.26	574	334	$28.50	$0.09
55	LiCl-$MnCl_2$	0.44	0.56	537	259	$25.49	$0.10
56	LiCl-NaCl	0.72	0.28	554	414	$59.37	$0.14
57	LiCl-$SrCl_2$	0.643	0.357	492	178	$48.61	$0.27
58	$MgCl_2$-NaCl	0.431	0.569	459	333	$6.55	$0.02
59	$MgCl_2$-$NiCl_2$	0.869	0.131	692	442	$11.18	$0.03
60	$MgCl_2$-$SrCl_2$	0.462	0.538	535	174	$39.44	$0.23
61	$MnCl_2$-NaCl	0.456	0.544	425	230	$16.65	$0.07
62	NaCl-$NiCl_2$	0.697	0.303	573	383	$15.52	$0.04
63	NaCl-$PbCl_2$	0.29	0.71	408	88	$14.37	$0.16
64	NaCl-$SrCl_2$	0.484	0.516	565	152	$42.57	$0.28

CHAPTER 5 RADIATIVE ENHANCEMENT IN CHLORIDE SALTS[6]

5.1 Introduction

Molten inorganic salts hold a great deal of promise as high-temperature heat transfer fluids and thermal storage media in renewable energy applications, and they have found use in nuclear and solar thermal power [25, 130]. In solar energy conversion, the most widespread use has been made of the nitrate salts—namely, the eutectic of potassium nitrate (KNO_3) and sodium nitrate ($NaNO_3$), commonly known as "solar salt." This nitrate eutectic has been used in a variety of parabolic trough- and central receiver- type solar thermal facilities as the storage medium in a two-tank TES configuration [12, 25].

The next generation of solar thermal plants will likely need higher melting materials for their thermal storage systems. Receivers for use in the solar power tower arrangement have reached temperatures as high as 750, 812, and even 950°C [97, 131, 132]. At these elevated temperatures, salts such as sodium chloride (NaCl), potassium chloride (KCl), and the eutectic (minimum melting) mixture of the two salts [(K-Na)Cl] present themselves as nearly ideal storage media candidates, owing to comparatively low cost, high heats of fusion, and melting temperatures in the range of interest (for NaCl, 800.7°C, for KCl, 770.9°C, and for the eutectic, 657°C; see Table 8). It is likely that, as central receivers in the power tower arrangement achieve higher operating temperatures, materials such as these may be used as heat transfer fluids (e.g., in a dual tank storage system) or as phase-change materials (PCMs). The latter provide the potential for increased energy

[6] This chapter has been published previously in the *Journal of Solar Energy Engineering* [129]. Permission for reuse is provided in Appendix B.

storage density for limited ranges of operating temperatures owing to characteristically high heats of fusion, and moreover they are desirable due to their consistent energy delivery at design temperature [23].

These salts, however, are typically hampered by relatively low thermal conductivity (less than 1 W/m-K in the molten state) [133]. To that end, many conductivity enhancement strategies have been explored. These include addition of greater conductivity materials, either as low concentration dispersed additives or in greater amounts as components of salt-based composites [53, 54]. Much work has also been done in the design of the containment—e.g, use of heat pipes or curved slabs to improve conduction and/or convection [47, 134].

This study explores a novel heat transfer enhancement strategy for the storage material itself. At the higher temperatures where these salts would be applied as storage media (>500°C), radiation becomes a significant mode of heat transfer. It is proposed that inclusion of small amounts of infrared- (IR-) absorptive additives in highly IR-transmissive salts (e.g., alkali metal halides) will allow for greater radiative heat transfer, thereby compensating for characteristically low thermal conductivity.

Determining the degree of improvement requires measurement of the absorption coefficient in the spectral range of interest. Unfortunately, traditional spectroscopic methods are ill-suited for work with molten salts: direct transmittance measurements overestimate absorption if they do not capture backscattering, and many window materials are prone to corrosive attack by these molten salts [135]. Another strategy to employ would be attenuated total reflectance spectroscopy [136]; but, here again, owing to the close contact between the reflecting prism and liquid, material compatibility renders this method impractical. The authors therefore developed a new IR-reflectance apparatus (Figure 42) to allow for determination of the spectral absorption

coefficient of the newly formulated storage media in the molten state. The apparatus consisted of an alumina crucible coated alternately at the bottom with a reflective (platinum) or absorptive (graphite) surface, a ceramic heating element housing the crucible, and a combination of zinc sulfide (ZnS) and zinc selenide (ZnSe) windows for containment of the salt and allowance of inert purge gas flow, respectively.

This paper specifically addresses the eutectic mixture of potassium and sodium chloride, (K-Na)Cl. Both KCl and NaCl are highly transmissive in the spectral region of 2.0 to 13.0 micrometers (μm), and it is worth noting that at the melting point of the eutectic (657°C), nearly 90 percent of spectral blackbody emissive power falls within this region, as given by the Planck distribution [61]. Various transition metal chlorides of known solubility in KCl and/or NaCl were investigated as potential absorptive additives, including cuprous chloride (CuCl), cobaltous chloride ($CoCl_2$), ferrous chloride ($FeCl_2$), and nickelous chloride ($NiCl_2$). Using the reflectance apparatus, infrared spectra were obtained for these additives at less than 0.2 weight percent (wt %) concentration in (K-Na)Cl, and improved infrared absorption and radiative transfer properties were demonstrated. Using these spectra, estimations of the absorption coefficient of the additives in the pure salt were calculated. Further, thermophysical properties relevant to TES (i.e., melting temperature, latent heat of fusion) were measured via differential thermal analysis (DTA) for the pure and additive-enhanced PCMs.

5.2 Background

A general treatment of the absorptive properties of inorganic salts is given in Modest's description of the Lorentz model, shown to adequately capture the absorption behavior of ionic crystals [118]. This model predicts that such materials should have one or more absorption bands in the mid- to far- infrared (*Reststrahlen* absorption) and several absorption bands near the

ultraviolet (electronic excitation)—between these absorptive (opaque) regions, ionic crystals are generally transparent. A discussion of the quantum-mechanical considerations behind absorption and emission of photons in these systems is beyond the scope of this paper; for detailed discussions of this topic the reader is referred elsewhere [137-139].

In speaking of the absorptive properties of these materials, and those of KCl and NaCl in particular, it is worthwhile to note the expansive reference work of Touloukian and DeWitt, which collects the radiative properties (reflectance, transmittance, emittance, etc.) of various nonmetallic solids [60]. According to data compiled in this reference, KCl is highly transmissive (transmittance greater than 90%) in the spectral region of 0.4 to 15.0 μm, for crystals 10 to 12 mm thick; analogously, NaCl is highly transmissive in the region of 0.4 to 13.0 μm, for crystals 2.8 to 6.5 mm thick. Other halides are similarly transmissive over much of the infrared, including calcium fluoride, which has also been proposed for TES applications [140]. It bears mentioning that these measurements were made at or near room temperature; the near- to mid- infrared absorption of such crystalline solids, especially if appreciable concentrations of lattice defects or dopants are present within the crystal, can be expected to rise significantly with temperature [118]. (Further information on the radiative properties of materials can be found in other references [62, 65], as well as in various textbooks [61, 118, 141].)

Of course, the high transmissivity of either KCl or NaCl does not guarantee that the mixture of the two will be itself transmissive; indeed, at room temperature, one will notice that the solidified (K-Na)Cl salt is quite opaque to visible radiation, as the cooling solid will self-diffuse to form closely packed lamellae of alternatingly high concentration KCl and high concentration NaCl phases. Importantly, though, the salt regains its high transmissivity as it heated to elevated

temperatures, with a consolute point at approximately 500°C [109]. At this point, the salt becomes a homogeneous solid solution which is transparent to visible radiation.

The (K-Na)Cl eutectic has been studied extensively, and a review of pertinent literature yields the properties data relevant to our study here. A collection of these data is compiled in Table 1 with properties of the pure component salts included for reference. The first entry of the table for the eutectic salt was obtained from the thermophysical properties software FactSage [27]; the second entry presents calculated values obtained from analytical formulations of the system's thermodynamic mixing properties [142]. The remaining entries are experimental data. It can be observed there is significant variability in the data. It is hoped that thermophysical properties data collected for this current study will serve to clarify the validity of some of these values. For the purposes of this study, the molar composition of the eutectic was taken as 50.02:49.98 KCl:NaCl, and the density of the molten salt was taken as 1.58 g/ml. More detailed discussion of the various studies performed and their assertions concerning the composition and melting point of the (K-Na)Cl eutectic salt can be found in the referenced literature [109, 142].

The additives for potential radiative absorption enhancement have been chosen on the basis of two criteria:

- Potential for IR-absorption
- Solubility in the molten salt

With regard to the first criterion, previous work has shown the potential for transition metal oxides—namely Co_3O_4 and CuO—to increase radiative absorption in the ultraviolet, visible and near-IR regions of the electromagnetic spectrum [72]. Further, studies into the middle and far IR show broad-band absorption for such transition metal oxides [143]. While these materials are no doubt promising for infrared absorption, there is an attendant complication to the use of insoluble

additives: maintenance of their suspension in the salt. For PCMs especially, which would likely be sequestered in a containment of some kind (e.g., capsule), continuous agitation may be difficult, and such additives may aggregate and settle.

As such, the second criterion, molten salt solubility, was examined critically during the selection process. It was determined that the four additives ultimately selected—CuCl, $CoCl_2$, $FeCl_2$, and $NiCl_2$—were each miscible in KCl and NaCl as binary solutions; indeed, in the case of $FeCl_2$, there is strong suggestion that it would form a solid state compound with KCl (double salt), K_2FeCl_4, which would allow for improved distribution in both the solid and liquid states [110].

To describe the method for determination of absorptance from reflection-absorption spectroscopy, it is worthwhile to discuss the mathematical basis of the analysis. For a single layer of homogeneous molten salt, as one would expect of the chloride systems considered here, the net radiation method gives the following equation for overall reflectance, R, of the layer [144]:

$$R = \frac{\rho_1 + \rho_2\,(1 - 2\rho_1)\tau^2}{1 - \rho_1\rho_2\tau^2} \tag{5.1}$$

Also, the transmissivity, τ, of the layer will depend on the pathlength and the absorption coefficient, κ, as follows [145].

$$\tau = e^{-\kappa\delta/\cos\theta_i} \tag{5.2}$$

Here, δ is the film thickness, and θ_i is the angle of incidence of the radiation. For the situation under consideration here, we can reasonably specify the thickness of the layer (using a specific mass and known density) and the angle of incidence (set by the geometry of the reflectance apparatus). Thus, for any single reflectance measurement, there are three unknown quantities:

1) The reflectivity at the surface of the salt (i.e., nitrogen-salt interface), ρ_1;
2) The reflectivity at the salt-substrate interface, ρ_2; and
3) The absorption coefficient, κ.

In our case, the reflectivity of the salt-substrate interface is measured separately: the reflective substrate (platinum) is measured relative to a silvered mirror. The absorptive substrate (graphite) is taken to have reflectivity of zero. Hence, from measurement of the reflectance of the salt over graphite, we obtain ρ_1; given this value and the known value of ρ_2, measurement of the reflectance of the salt over the platinum value yields the transmissivity of the salt layer. Given the transmissivity of the pure salt and that of the additive-salt system, the absorption coefficient, κ, of the additive in the pure salt can be calculated directly.

All IR spectra were obtained using a Jasco FTIR-6300 Fourier-transform infrared (FT-IR) spectrometer. In this system, a high-intensity ceramic source was used in conjunction with a mercury cadmium telluride (MCT) detector, effectively limiting the observable spectral range to 7800 – 650 cm^{-1} (although the range into the far infrared is further limited by the window materials and the salts themselves).

The heated sample chamber was provided by Pike Technologies of Madison, Wisconsin. Designed for diffuse reflectance applications, the chamber consists of a heated ceramic sample holder to be used in conjunction with porous alumina crucibles. The heater is capable of reaching 900°C, and the chamber is cooled by chilled water pumped at a rate of approximately 50 ml/min. The cooling water keeps most of the sample chamber at approximately room temperature, so that, for instance, during emission measurements, background radiation interference is minimized. Using a suitable window (in this case, ZnSe), inert gas purge can be passed through the chamber, with the pores of the alumina crucibles allowing the purge gas to pass directly through the (diffuse) powdered sample.

For work with regular reflectance of molten salts, some additional features were introduced to the sample holder. Firstly, porous alumina pans would not allow for liquid samples; therefore,

solid alumina pans were used. However, these pans provide a hindrance to the flow of the inert purge gas. The pans were therefore scored across the bottom in a cross-hatch manner. These grooves allowed for purge gas to flow around the sample and beneath the pan to the purge outlet.

5.3 Methodology

Important study of the reflectance and optical properties of molten nitrates [146], chlorides [69], and carbonates [70] were undertaken by Makino, and a thorough description of their apparatus has been given [146]. The basic strategy of this paper's measurement of radiative properties is similar: regular reflection is measured of molten salt over a reflecting background. However, our study adds the step of performing a separate measurement over black background to elucidate the absorption coefficient.

It was found that for high vapor pressure salts (notably, metal halides), evaporated salt would condense upon and outermost ZnSe window and severely degrade it. Therefore, a second additional feature was introduced: a salt containment window to be placed directly over the sample crucible such that significant amounts of salt vapor would not be allowed to escape. A variety of materials were tested for this purpose; their properties have been presented elsewhere, and these data are presented in Table 9 [147]. KCl, NaCl, potassium bromide (KBr), and calcium fluoride (CaF2), are all promising as window materials, but they are prone to ion exchange with the evolved salt vapors tested here. Hence, they would only serve for one use. (It is possible that these materials could be used as pressed powders, significantly reducing the cost of the window material; the authors are currently exploring this option.) Also, ZnSe, too, showed a high susceptibility to attack by the salts and also by the high temperatures alone. ZnS alone showed the desired resistance to degradation upon multiple uses. While the transmissive range of ZnS crystals is smaller than some of the other materials, it should cover the spectral range relevant here—namely, 2.0 to 13.0 μm, in

which 90 percent of blackbody emissive power at 657°C is captured. (CaF2, on the other hand, would cut off this range on longer wavelength side.) A schematic of the dual-window reflectance cell is shown in Figure 42.

To determine the reflectivity of the platinum backing, it was insufficient to make a simple regular reflectance measurement at room temperature. Rather, the emissivity of the backing was measured against a blackbody radiator, with both sources heated to 680°C. Upon measuring the spectral emissivity, the spectral reflectivity for the opaque surface is easily obtained via the well-known Kirchhoff relations:

$$\rho_\lambda = 1 - \varepsilon_\lambda \tag{5.3}$$

It should be emphasized that the relation above is accurate for spectral quantities—e.g., owing to spectral variability of radiative properties, the same relation does not apply to total reflectivity and emissivity. Also, strictly speaking, this yields the normal incidence spectral reflectivity; due to the relatively small angles of incidence considered here, no correction shall be applied for any directional variation in the following analyses. The blackbody reference used was an IR-563/301 manufactured by Infrared Systems Development Corporation of Winter Park, Florida.

DTA measurements were performed using a TA Instruments SDT-Q600 TGA/DSC. A three-point calibration of the instrument was performed using high purity tin, zinc, and sodium fluoride as calibrants. The cell constant (latent heat) was calibrated using high purity zinc. Samples were placed in platinum pans to prevent the creeping of salt samples during melting and solidification. In each case, samples were melted twice; the second run (after formation of the binary / ternary system) was used to obtain thermophysical properties. Multiple samples for each material were tested, and averaged values obtained. All measurements were made under argon purge flow at a heating rate of 10°C/min.

A novel method was applied to prepare samples for study. Given the potential for the additives to solid solutions or double salts with bulk NaCl and/or KCl, the following strategy was employed:

1) Additives were mixed at a concentration of 0.4 wt % in agate mortar with spectroscopic-grade NaCl in a glovebox under inert gas.
2) The mixtures were heated to approximately 250°C for 24 hours in the glovebox to encourage formation of solid solutions.
3) The heated mixtures were then mixed in agate mortar with the required quantity of KCl (99.997% purity, metals basis). The resultant mixtures were approximately 0.18 wt % additive.
4) Throughout the following analyses they were kept in a vacuum desiccator or drying oven kept at 110°C.

These moisture control steps were important, since three of the four additives considered (excepting CuCl) are known to be very hygroscopic. The concentrations of the salt systems studied are shown in Table 10.

5.4 Results

The measured reflectance of the platinum substrate is shown in Figure 43. The reflectivity is comparatively high, and so will serve the purpose of providing a reflective background to the semi-transparent molten salts.

Next, the salts' spectra were measured. Upon heating, it was observed that the characteristic spectra of the loose powder samples changed dramatically upon melting, thus making it a simple matter to determine when to collect the spectra. That said, the general procedure involved heating the sample / background to approximately 680°C, which ensures the melting

would take place rapidly. Spectra were collected as soon as the melt had occurred, which could be verified by visual examination of the sample.

In Figure 44(a), the spectra obtained for the pure eutectic salt are presented—namely, the reflectance of the overall system (R), the reflectivity of the salt-nitrogen interface (ρ_1), and the calculated transmissivity (τ) from the net radiation method [144]. (The reflectivity of the platinum substrate, ρ_2, is illustrated in Figure 43.) Similar spectra are obtained for each of the salt-additive systems, and these are depicted in Figure 44(b).

Given the transmissivity of the salt systems, it is possible to make an estimation of the absorption coefficient of the additive materials in the pure eutectic salt. For these calculations, the density of the salt is assumed unchanged upon addition of the small concentration (~0.18 wt %) of additive—i.e., the film thickness, δ, is assumed to be constant in each case. The angle of incidence for the geometry considered here is approximately 30.6°. The calculated absorption coefficients for each additive-salt system are presented in Figure 45. Note that these measurements show absorption relative to the pure fused eutectic salt [e.g., see Figure 44(a)], which itself was found to have a transmissivity of approximately 0.9.

The spectra obtained agree qualitatively with expected behavior: the pure eutectic appears mostly transparent. Inclusion of the additives results in a marked decrease in the measured reflectance, especially in the case of $FeCl_2$. From the calculated absorption coefficients, it is clear that the additives increase infrared absorption, and therefore they are promising candidates for heat transfer enhancing additives. One exception is the case of $NiCl_2$ at wavelengths greater than 12 μm. Here, the absorption coefficient is approximately zero, and it is likely that the additive has no effect on the absorption of the pure eutectic in this region. It is also prudent to note here that the $FeCl_2$ measurement was complicated by the formations of oxides, which likely exaggerated the

degree of attenuation in this case. This was the only sample that displayed any evidence of oxide formation—it is possible that the other additives are less prone to this issue, although it may simply have been an error of the experimental apparatus (e.g., greater infiltration of oxygen or moisture into the reflection cell). Further measurements are planned which will take care to void the sample chamber of oxygen / moisture prior to measurement. In any event, this behavior deserves consideration if these materials are to be employed in larger-scale TES units. Oxidation of the material can be avoided, for instance, through atmospheric control, use of a preferential oxidizer (i.e., getter), etc.

The thermophysical properties measured by DSC are presented in Table 11. As can be seen, the heat of fusion and melting point for the pure eutectic system agree well with literature values [142]. Note that while the melting temperatures of the additive-enhanced materials are slightly lower than that of the pure salt (as one would expect by inclusion of a solute), the latent heat of fusion, of primary importance for PCM storage media, seems little impacted. Indeed, in the case of the divalent additives especially, there is an apparent increase in latent heat, although this increase lies well within the error of measurement. It is not unreasonable that latent heat would increase upon addition of small amounts of soluble additive, and this phenomenon is observed in the NaCl-KCl system. Addition of small amounts of KCl to pure NaCl increases the latent heat of fusion, most likely because the presence of the larger impurity potassium ions creates regions of stress that attract and "pin" the moving lattice vacancies required for phase change (i.e., more energy required for melting) [31]. Of course, at higher concentrations, the competing effect of weakening the lattice causes the latent heat to decrease (i.e., less energy required for melting). From the available data, though, it seems that the latent heat is approximately unchanged upon addition of the additive. The melting point, also, is little changed by addition of additives, with the

highest melting point depression, approximately 1.0°C, occurring in the CuCl-(K-Na)Cl system. In either case, the additive does not significantly impact the performance of the PCM as a TES medium.

5.5 Conclusions / Future Work

An IR-reflectance apparatus was developed for testing the radiative absorption of novel inorganic salt thermal storage media in the molten state. The method of collection of the overall layer-substrate reflectance and the salt surface reflectivity by means of two different substrate materials (platinum and graphite) has been demonstrated. The inclusion of transition metal chloride additives shows distinct increases in absorption in the infrared, with only slight impacts on melting temperature and latent heat of fusion.

Further work currently underway includes the collection of spectra from additional samples to determine the error in measurement method, as well as from different concentrations to estimate the concentration dependence of radiative absorption. Part of this study includes working with thinner windows made of pressed halide powders; as mentioned above, these materials would be good for only one use, but they may prove a good choice due to their significantly lower cost, relative to polished crystal optics. It would also be prudent to test the results obtained here with a method based on the emissivity of the substrate / salt system, as has been described by Makino [148]. Such efforts are currently underway. Also, the specific heat capacity of these systems is being measured, in the solid and, if possible, molten states. It is not anticipated, however, that such small concentrations of additives will have a significant impact on this property of the salt.

Radiative transfer in TES systems is valuable area of research, in light of the fact that radiation can play a major role in heat transfer in the next generation of high temperature TES. Spectroscopy, whether through transmission, reflection, or emission measurements, is a direct

means of characterizing the radiative properties of materials needed in these systems. It is hoped that this paper will encourage further work in the field of radiative properties measurement in general and molten salt spectroscopy in particular.

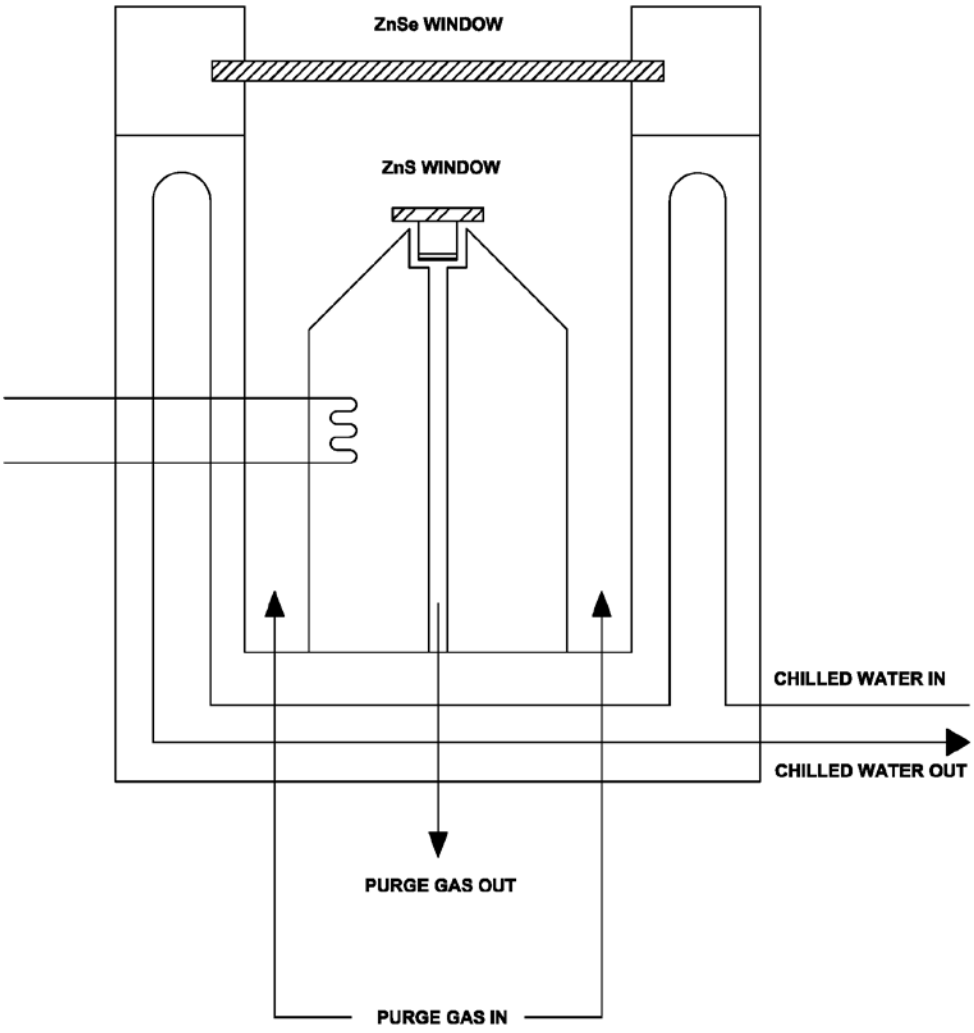

Figure 42 Molten salt reflectance cell.

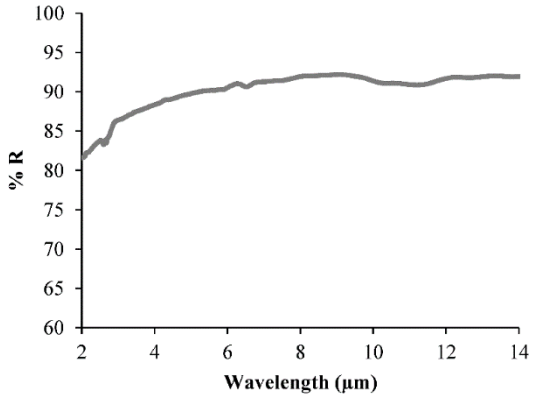

Figure 43 Measured reflectivity of platinum substrate.

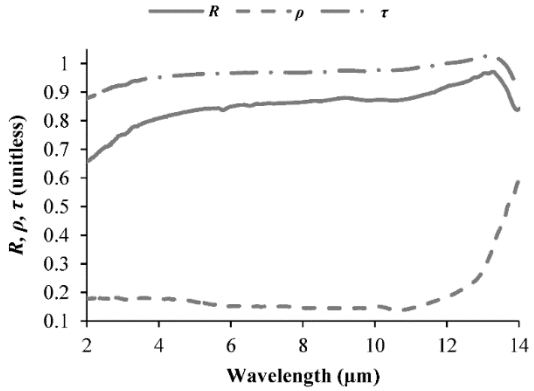

(a)

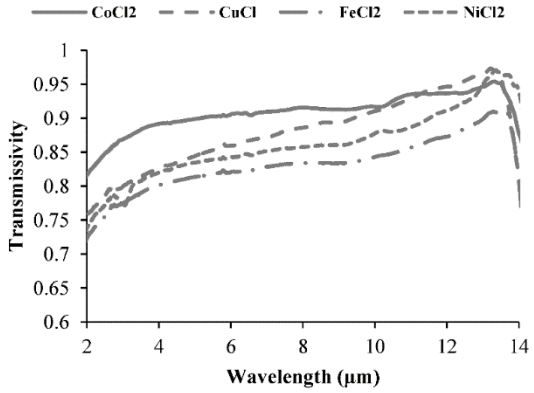

(b)

Figure 44 Transmissivity determination of pure eutectic salt and additive-salt systems. Pure (K-Na)Cl spectra are shown in (a); calculated transmissivities for the additive-salt systems are shown (b).

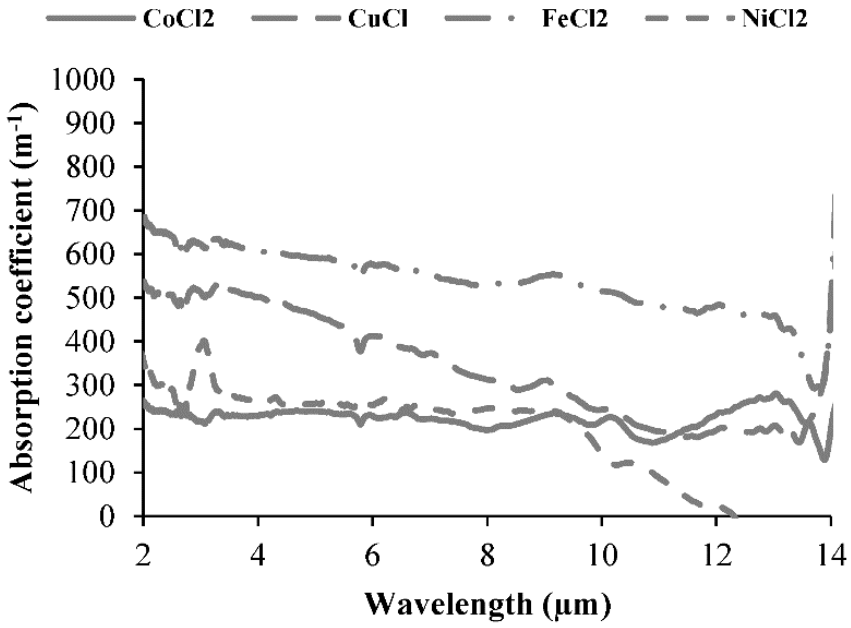

Figure 45 Absorption coefficients of additives in (K-Na)Cl.

Table 8 Thermophysical properties of chloride eutectic salt and constituents

Salt	Mole % (KCl:NaCl)	T_m (°C)	ΔH_{fus} (J/g)	c_p (J/g-K)		Density (g/ml)	
				T = 600°C	*T = 700°C*	*T = 600°C*	*T = 700°C*
KCl [149]	100:0	770.9	353	0.858		1.98	
NaCl [149]	0:100	800.7	482	1.04		2.16	
(K,Na)Cl	50.02:49.98	656.74	306	0.945	1.08	2.08	1.58
[142]	48.5:51.5	657	278	-		-	
[31]	50:50	661	273 ± 8	-		-	
[84]	50:50	658	-	-		-	1.58

Table 9 Window materials considered for molten salt study

Window material	**Transmissive range (cm^{-1}) [147]**	**Transmissive range (μm)**
CaF_2	25,000 – 800	0.40 – 12.5
KBr	40,000 – 200	0.25 – 50
KCl	47,600 – 300	0.210 – 33
NaCl	47,600 – 400	0.210 – 25
ZnS	10,000 – 700	1.0 – 14
ZnSe	22,200 – 500	0.45 – 20

Table 10 Additive concentrations in pure (K-Na)Cl

Additive	**Weight %**	**Mole %**
$CoCl_2$	0.176	0.0986
CuCl	0.176	0.125
$FeCl_2$	0.176	0.101
$NiCl_2$	0.176	0.0988

Table 11 Measured thermophysical properties for pure salt and additive-salt systems. Selected literature data are included for comparison.

	T_m (°C)				ΔH_{fus} (J/g)					
Salt	**Our work**			**Literature [19]**	**Our work**			**Literature [31]**		
(K,Na)Cl	657.2	±	0.2	658	282	±	16	273	±	8
+ 0.18 wt % $CoCl_2$	656.5	±	1.1		290	±	15			
+ 0.18 wt % CuCl	656.2	±	0.2		283	±	6			
+ 0.18 wt % $FeCl_2$	656.8	±	0.2		293	±	27			
+ 0.18 wt % $NiCl_2$	656.5	±	1.2		295	±	14			

CHAPTER 6 STORAGE SYSTEM MODELING

6.1 Introduction

In this chapter, we attempt to quantify the performance enhancement that can result by incorporation of some of the additives discussed previously into the pure PCMs. The main difficulty in these analyses concerns modeling the phase change—namely, solid-to-liquid—as a transient process. Below, we discuss this various approaches to this and other problems in the modeling of these systems.

6.2 Direct Conductivity Enhancement

A simple model for solidification of a material with conductivity enhancing additives has been discussed by Siegel [56]. First, we consider the situation where the PCM takes the geometry of a slab. An energy balance over a differential layer of thickness $d\delta$ yields

$$\Delta H_{fus}\rho_s(1-\phi)\frac{d\delta}{dt} = \frac{T_m - T_c}{\frac{1}{h_c} + \frac{w}{k_w} + \frac{\delta}{k'}} \tag{6.1}$$

In this equation, ϕ represents the volume fraction of high conductivity particles, T_c is the temperature of the cooling fluid (HTF), h_c is the convective transfer coefficient of the HTF, w is the width of the wall, k_w is the conductivity of the wall, and k' is the conductivity of the composite material (PCM). Both ΔH_{fus} and ρ_s represent properties of the pure PCM—that is, without high conductivity additives.

To simplify the problem, we assume the containment wall is thin and has comparatively high thermal conductivity (i.e., $w/k_w \to 0$) and there is comparatively high convective heat

transfer with the HTF (i.e., $1/h_c \rightarrow 0$). Under the stated assumptions, and carrying out the integration, we obtain

$$\delta = \left[\frac{2k'}{1-\phi}\left(\frac{T_m - T_c}{\Delta H_{fus}\rho_s}\right)t\right]^{0.5} \tag{6.2}$$

Similarly, we can examine the heat removed with the CuO-enhanced storage media and the pure salt. The heat removed per unit surface area can be defined as [56]:

$$\frac{Q}{A} = \Delta H_{fus}\rho_s(1-\phi)\delta \tag{6.3}$$

Perhaps a more realistic situation is that of a cylindrical tube. We consider the situation where the HTF flows through a tube with PCM on the outside—that is, a shell-side PCM heat exchanger. In this case [56]:

$$\Delta H_{fus}\rho_s(1-\phi)2\pi r_\delta \frac{d(-r_\delta)}{dt} = \frac{2\pi(T_m - T_c)}{\frac{1}{h_c r_o} + \frac{l}{k_w}\ln\left(\frac{r_o}{r_i}\right) + \frac{l}{k'}\ln\left(\frac{r_\delta}{r_o}\right)} \tag{6.4}$$

where r_δ is the advancing solidification front, r_i in the inner radius of the HTF tube, and r_o is the outer radius of the HTF tube. Under the simplifying assumptions, integrating yields

$$r_\delta^2 \ln\left(\frac{r_\delta}{r_o}\right) - \frac{1}{2}\left(r_\delta^2 - r_o^2\right) = \frac{2k'}{1-\phi}\left(\frac{T_m - T_c}{\Delta H_{fus}\rho_s}\right)t \tag{6.5}$$

To solve for the radius of the solidified layer, r_δ as a function of time, numerical methods are required. Also, the heat removal per unit surface area is formulated as

$$\frac{Q}{A} = \frac{1}{2}\Delta H_{fus}\rho_s(1-\phi)r_o\left[\left(\frac{r_\delta}{r_o}\right)^2 - 1\right] \tag{6.6}$$

Considering the data we obtained in Chapter 3, we can now model the performance enhancement of the higher conductivity composite. The conductivity of the salt-nanoparticle mixture, k', is obtained by extrapolation of the thermal diffusivity data to $T = 306.5$°C, then using the methods described in Section 3.2.2 Results and Discussion to calculate thermal conductivity;

the result is a thermal conductivity of pure $NaNO_3$ of 0.489 W/m-K and that of the CuO-$NaNO_3$ mixture of 0.556 W/m-K. An examination of Equation (6.2) shows that for any size TES unit, the increase in conductivity provided by addition of the CuO nanoparticles will result in a 12% decrease in discharging time.

Using this model, we plot the solid layer growth for the pure PCM (δ_s) and the PCM-additive mixture (δ_m) in Figures 46 and 47, for the slab and cylindrical geometry, respectively.

6.3 Radiative Transfer Enhancement

Owing to the fact that the radiative transfer equation, barring simplifying assumptions, takes the form of an integro-partial differential equation, numerical methods—generally, finite element methods—are needed to quantify the effects of radiative transfer enhancement [61]. The strategy behind radiative heat transfer enhancement is to increase absorption of thermal radiation in the bulk volume of the PCM; in this way, while the PCM is solidifying at the boundary of the container with conduction-limited heat transfer, additional heat is passing to the bulk PCM from the container walls. Furthermore, as the solidification front progresses, the wall is heating the furthest edge of the solidification front with radiation in addition to conduction. For this study, we examine a cylindrical PCM capsule 3 inches in diameter and 2 inches in height.

Using the finite element modeling software COMSOL, we modeled the steady-state radiative heat flux in an effort to optimize the absorption coefficient. For an absorption coefficient of $100m^{-1}$, the dimensionless heat flux is plotted as Figure 48. Simulations were conducted at a variety of absorption coefficients, and these data are plotted in Figure 49. It can be seen that the heat flux increases approximately monotonically with absorption coefficient up to approximately $110m^{-1}$ (the optimum point). At higher absorption coefficient, the heat flux decreases. This behavior corresponds to the radiative transfer passing from the optically “thin” limit to the

optically “thick” limit. In choosing additives and additive concentration, this optimum will serve as a guide.

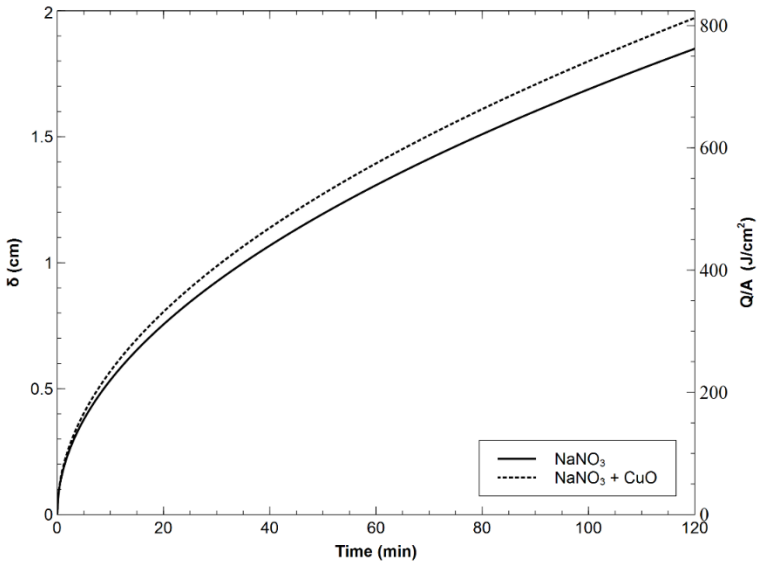

Figure 46 Pure PCM compared with high conductivity composite in slab geometry. Pure PCM layer thickness is δ_s; additive-PCM composite layer growth is δ_m.

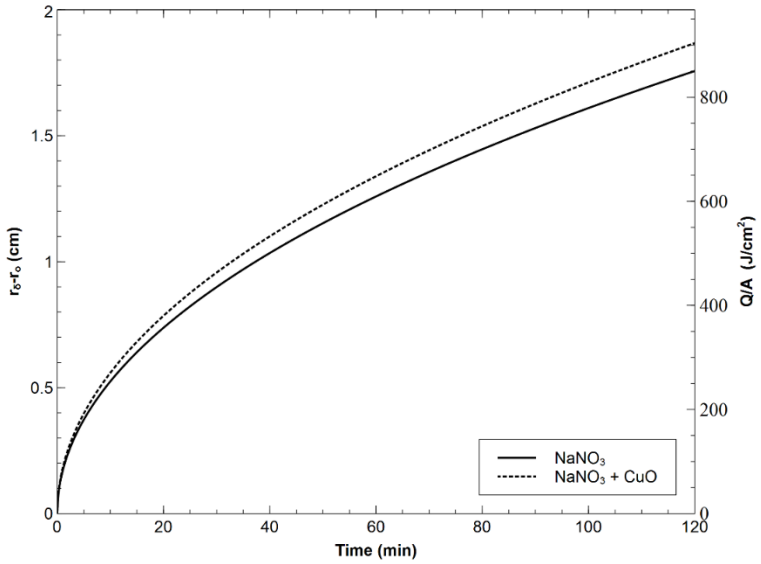

Figure 47 Pure PCM compared with additive enhanced PCM in tube geometry.

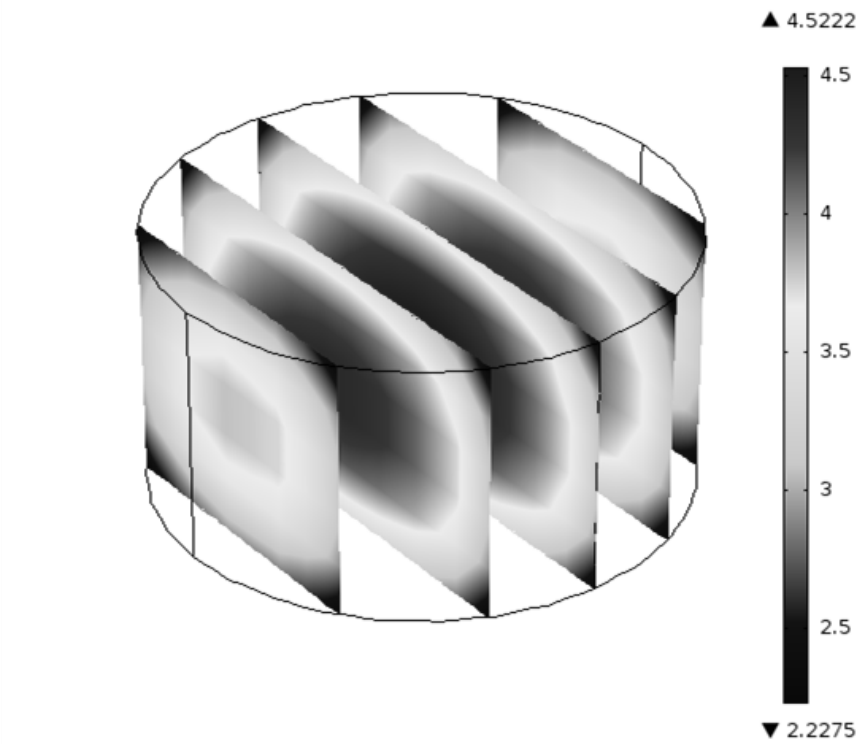

Figure 48 Dimensionless heat flux in PCM capsule with 100 m^{-1} absorption coefficient.

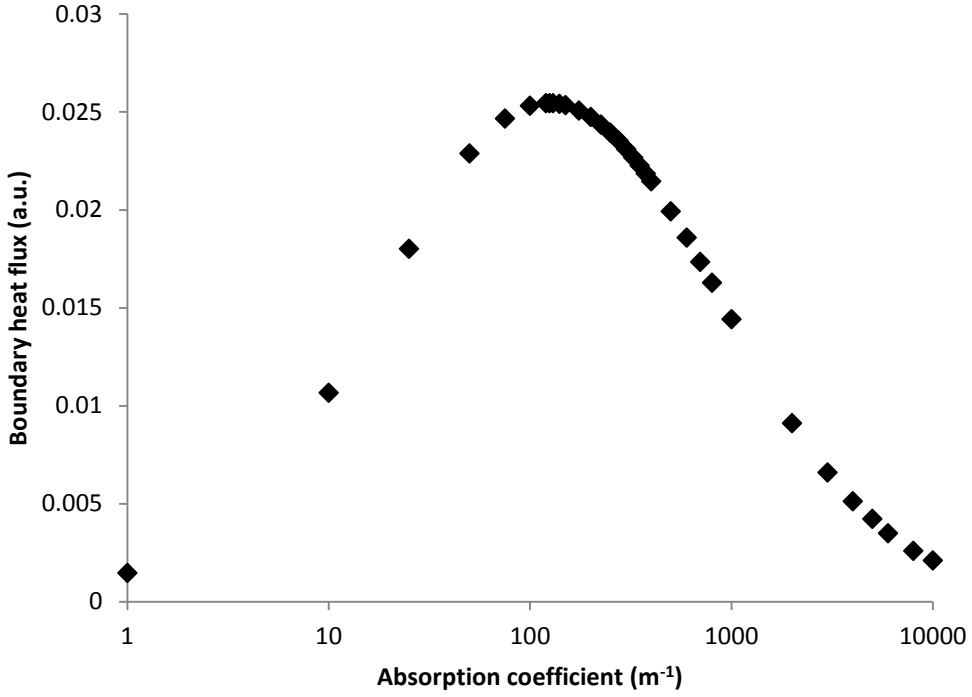

Figure 49 Dimensionless heat flux as a function of absorption coefficient.

CHAPTER 7 CONCLUSIONS AND RECOMMENDATIONS FOR FUTURE WORK

This research was undertaken in an effort to improve heat transfer in inorganic salt based TES media. Two distinct strategies were explored: direct thermal conductivity enhancement through the use of high conductivity particles / additives, and heat transfer enhancement through increase of thermal radiation transfer. With regard to direct thermal conductivity enhancement, CuO nanoparticles were shown to provide a significant increase in thermal conductivity in nitrate salt-based storage media, although the increase was generally more pronounced in the case of KNO_3 or the $(K,Na)NO_3$ eutectic salt than in the case of $NaNO_3$. In a separate study, comparatively small amounts of graphene nanoflakes, when added to $NaNO_3$, showed demonstrably greater thermal diffusivity enhancement, relative to the CuO nanoparticles.

Radiative heat transfer improvement is accomplished by increasing infrared absorption of transparent materials through the addition of optically active media. In this work, the eutectic salt, (K,Na)Cl, which is mostly transparent in the infrared, was shown to have higher infrared absorption with the addition of small amounts (~0.2 wt %) of transition metal chlorides. The increased absorption was quantified using a molten salt reflectance cell.

Mathematical modeling was performed in an effort to elucidate the potential TES performance enhancement upon inclusion of the various additives. In the case of direct conductivity enhancement, it was shown that an improvement in discharge time of approximately 12% was achievable with the addition of only 2 % by volume of CuO nanoparticles to $NaNO_3$ LHTES media. Finite element analysis of the chloride salt as a participating medium was used to assess the ideal absorption coefficient for the highest heat flux at the container wall boundary; with

this information, and given the absorption coefficient of the additives, an optimum additive concentration can be calculated.

Future work on this topic should include transient analysis of the coupled heat transfer involving radiative heat transfer of the additive-salt systems. This would allow for meaningful conclusions to be drawn concerning the performance enhancement of the additives. Further, the problem of scattering and / or anisotropic radiative transfer should be examined, although such an effort would require additional analytical models (e.g., that of Mie) or numerical methods (e.g., Monte Carlo simulation). While scattering should not play a role in the homogeneous chloride salt mixtures—that is, because the molten salt solution is assumed to be uniform in optical properties such as the refractive index—additive particles of differing refractive index, such as oxides, would induce some degree of scattering. If these particles are pursued as potential infrared absorptive media for increase radiative heat transfer, the degree of scattering would have to be known in order to optimize the system.

REFERENCES

[1] U.S. Energy Information Administration (EIA), *Electric Power Monthly with Data for July 2014*, Sep 2014.

[2] American Society of Heating Refrigerating and Air-Conditioning Engineers, *2009 ASHRAE Handbook: Fundamentals*. Atlanta, GA.: ASHRAE, 2009.

[3] D. Y. Goswami, *Principles of solar engineering*, 3rd ed. Boca Raton: Taylor & Francis, 2015.

[4] S. Wilcox, "National Solar Radiation Database 1991-2005 Update: User's Manual," National Renewable Energy Laboratory (NREL), Golden, CO.2007.

[5] M. Leijon, A. Skoglund, R. Waters, A. Rehn, and M. Lindahl, "On the physics of power, energy and economics of renewable electric energy sources - Part I," *Renewable Energy*, vol. 35, pp. 1729-1734, Aug 2010.

[6] M. Medrano, A. Gil, I. Martorell, X. Potau, and L. F. Cabeza, "State of the art on high-temperature thermal energy storage for power generation. Part 2-Case studies," *Renewable & Sustainable Energy Reviews*, vol. 14, pp. 56-72, Jan 2010.

[7] B. Owens, *NREL Parabolic Trough Thermal Energy Storage Workshop*: Platts Research & Consulting, Feb 20 – 21, 2003.

[8] B. Zalba, J. M. Marin, L. F. Cabeza, and H. Mehling, "Review on thermal energy storage with phase change: materials, heat transfer analysis and applications," *Applied Thermal Engineering*, vol. 23, pp. 251-283, Feb 2003.

[9] A. Sharma, V. V. Tyagi, C. R. Chen, and D. Buddhi, "Review on thermal energy storage with phase change materials and applications," *Renewable & Sustainable Energy Reviews*, vol. 13, pp. 318-345, Feb 2009.

[10] I. Dinçer and M. A. Rosen, *Thermal energy storage: Systems and applications*, 2nd ed. Chichester: John Wiley & Sons, 2011.

[11] T. M. I. Mahlia, T. J. Saktisandan, A. Jannifar, M. H. Hasan, and H. S. C. Matseelar, "A review of available methods and development on energy storage; technology update," *Renewable & Sustainable Energy Reviews*, vol. 33, pp. 532-545, May 2014.

[12] S. Kuravi, J. Trahan, D. Y. Goswami, M. M. Rahman, and E. K. Stefanakos, "Thermal energy storage technologies and systems for concentrating solar power plants," *Progress in Energy and Combustion Science,* vol. 39, pp. 285-319, Aug 2013.

[13] J. Stekli, L. Irwin, and R. Pitchumani, "Technical Challenges and Opportunities for Concentrating Solar Power With Thermal Energy Storage," *Journal of Thermal Science and Engineering Applications,* vol. 5, p. 021011, 2013.

[14] D. Barlev, R. Vidu, and P. Stroeve, "Innovation in concentrated solar power," *Solar Energy Materials and Solar Cells,* vol. 95, pp. 2703-2725, Oct 2011.

[15] A. F. Regin, S. C. Solanki, and J. S. Saini, "Heat transfer characteristics of thermal energy storage system using PCM capsules: A review," *Renewable & Sustainable Energy Reviews,* vol. 12, pp. 2438-2458, Dec 2008.

[16] A. Abhat, "Low-Temperature Latent-Heat Thermal-Energy Storage - Heat-Storage Materials," *Solar Energy,* vol. 30, pp. 313-332, 1983.

[17] B. Cardenas and N. Leon, "High temperature latent heat thermal energy storage: Phase change materials, design considerations and performance enhancement techniques," *Renewable & Sustainable Energy Reviews,* vol. 27, pp. 724-737, Nov 2013.

[18] M. O. Steinitz, D. A. Pink, J. P. Clancy, A. N. MacDonald, and I. Swainson, "Sodium nitrate - a difficult discontinuous phase transition," *Canadian Journal of Physics,* vol. 82, pp. 1097-1107, Dec 2004.

[19] G. J. Janz, C. B. Allen, N. P. Bansal, R. M. Murphy, and R. P. T. Tomkins, "Physical Properties Data Compilations Relevant to Energy Storage. II. Molten Salts: Data on Single and Multi-Component Salt Systems," *National Standard Reference Data System, U.S. DEPARTMENT OF COMMERCE,* 1979.

[20] R. Margolis, C. Coggeshall, and J. Zuboy, "Sunshot Vision Study," *US Dept. of Energy,* 2012.

[21] G. Belton and F. Ajami, *Thermochemistry of salt hydrates*. Philadelphia: University of Pennsylvania National Center for Energy Management & Power and Towne School of Civil & Mechanical Engineering, 1973.

[22] M. M. Farid, A. M. Khudhair, S. A. K. Razack, and S. Al-Hallaj, "A review on phase change energy storage: materials and applications," *Energy Conversion and Management,* vol. 45, pp. 1597-1615, Jun 2004.

[23] M. M. Kenisarin, "High-temperature phase change materials for thermal energy storage," *Renewable & Sustainable Energy Reviews,* vol. 14, pp. 955-970, Apr 2010.

[24] G. J. Kolb, "Evaluation of Annual Performance of 2-Tank and Thermocline Thermal Storage Systems for Trough Plants," *Journal of Solar Energy Engineering-Transactions of the ASME,* vol. 133, Aug 2011.

[25] U. Herrmann and D. W. Kearney, "Survey of thermal energy storage for parabolic trough power plants," *Journal of Solar Energy Engineering-Transactions of the ASME,* vol. 124, pp. 145-152, May 2002.

[26] U. Herrmann, B. Kelly, and H. Price, "Two-tank molten salt storage for parabolic trough solar power plants," *Energy,* vol. 29, pp. 883-893, Apr-May 2004.

[27] C. Bale, P. Chartrand, S. Degterov, G. Eriksson, K. Hack, R. B. Mahfoud, *et al.*, "FactSage thermochemical software and databases," *Calphad,* vol. 26, pp. 189-228, 2002.

[28] T. Watanabe, H. Kikuchi, and A. Kanzawa, "Enhancement of Charging and Discharging Rates in a Latent-Heat Storage-System by Use of Pcm with Different Melting Temperatures," *Heat Recovery Systems & Chp,* vol. 13, pp. 57-66, Jan 1993.

[29] A. Hernandez-Guerrero, S. M. Aceves, E. Cabrera-Ruiz, and J. C. Baltazar-Cervanres, "Modeling of the charge and discharge processes in energy storage cells," *Energy Conversion and Management,* vol. 40, pp. 1753-1763, Oct-Nov 1999.

[30] S. I. Sandler, *Chemical, biochemical, and engineering thermodynamics*, 4th ed. Hoboken, N.J.: John Wiley, 2006.

[31] P. Luova and M. Muurinen, *Thermodynamic studies on the systems NaCl-KCl and KBr-KI*, 1967.

[32] S. Pincemin, R. Olives, X. Py, and M. Christ, "Highly conductive composites made of phase change materials and graphite for thermal storage," *Solar Energy Materials and Solar Cells,* vol. 92, pp. 603-613, Jun 2008.

[33] D. Fernandes, "Thermal energy storage: “How previous findings determine current research priorities”," *Energy,* vol. 39, pp. 246–257, 2012.

[34] S. Jegadheeswaran and S. D. Pohekar, "Performance enhancement in latent heat thermal storage system: A review," *Renewable & Sustainable Energy Reviews,* vol. 13, pp. 2225-2244, Dec 2009.

[35] K. Nithyanandam and R. Pitchumani, "Cost and performance analysis of concentrating solar power systems with integrated latent thermal energy storage," *Energy,* vol. 64, pp. 793-810, Jan 1 2014.

[36] J. Fukai, M. Kanou, Y. Kodama, and O. Miyatake, "Thermal conductivity enhancement of energy storage media using carbon fibers," *Energy Conversion and Management,* vol. 41, pp. 1543-1556, Sep 2000.

[37] R. Velraj, R. V. Seeniraj, B. Hafner, C. Faber, and K. Schwarzer, "Heat transfer enhancement in a latent heat storage system," *Solar Energy,* vol. 65, pp. 171-180, Feb 1999.

[38] P. Lamberg, "Approximate analytical model for two-phase solidification problem in a finned phase-change material storage," *Applied Energy,* vol. 77, pp. 131-152, Feb 2004.

[39] P. Lamberg, R. Lehtiniemi, and A. M. Henell, "Numerical and experimental investigation of melting and freezing processes in phase change material storage," *International Journal of Thermal Sciences,* vol. 43, pp. 277-287, Mar 2004.

[40] M. Farid and K. Yacoub, "Performance of Direct Contact Latent-Heat Storage Unit," *Solar Energy,* vol. 43, pp. 237-251, 1989.

[41] Y. H. Wang, J. H. Zhang, J. B. Zang, E. B. Ge, and H. Huang, "Etching and cutting of multi-walled carbon nanotubes in molten nitrate," *Corrosion Science,* vol. 53, pp. 3764-3770, Nov 2011.

[42] Y. B. Tao, Y. L. He, and Z. G. Qu, "Numerical study on performance of molten salt phase change thermal energy storage system with enhanced tubes," *Solar Energy,* vol. 86, pp. 1155-1163, May 2012.

[43] R. Tamme, T. Bauer, J. Buschle, D. Laing, H. Muller-Steinhagen, and W. D. Steinmann, "Latent heat storage above 120 degrees C for applications in the industrial process heat sector and solar power generation," *International Journal of Energy Research,* vol. 32, pp. 264-271, Mar 10 2008.

[44] W. D. Steinmann and R. Tamme, "Latent heat storage for solar steam systems," *Journal of Solar Energy Engineering-Transactions of the ASME,* vol. 130, Feb 2008.

[45] I. M. Bugaje, "Enhancing the thermal response of latent heat storage systems," *International Journal of Energy Research,* vol. 21, pp. 759-766, Jul 1997.

[46] W. D. Steinmann, D. Laing, and R. Tamme, "Development of PCM Storage for Process Heat and Power Generation," *Journal of Solar Energy Engineering-Transactions of the ASME,* vol. 131, Nov 2009.

[47] H. Shabgard, T. L. Bergman, N. Sharifi, and A. Faghri, "High temperature latent heat thermal energy storage using heat pipes," *International Journal of Heat and Mass Transfer,* vol. 53, pp. 2979-2988, Jul 2010.

[48] K. Nithyanandam and R. Pitchumani, "Analysis and optimization of a latent thermal energy storage system with embedded heat pipes," *International Journal of Heat and Mass Transfer,* vol. 54, pp. 4596-4610, Oct 2011.

[49] K. Nithyanandam and R. Pitchumani, "Computational studies on a latent thermal energy storage system with integral heat pipes for concentrating solar power," *Applied Energy,* vol. 103, pp. 400-415, Mar 2013.

[50] Y. Shiina and T. Inagaki, "Study on the efficiency of effective thermal conductivities on melting characteristics of latent heat storage capsules," *International Journal of Heat and Mass Transfer,* vol. 48, pp. 373-383, Jan 2005.

[51] W. H. Zhao, S. Neti, and A. Oztekin, "Heat transfer analysis of encapsulated phase change materials," *Applied Thermal Engineering,* vol. 50, pp. 143-151, Jan 10 2013.

[52] K. S. do Couto Aktay, R. Tamme, and H. Müller-Steinhagen, "Thermal conductivity of high-temperature multicomponent materials with phase change," *International Journal of Thermophysics,* vol. 29, pp. 678-692, 2008.

[53] S. Pincemin, X. Py, R. Olives, M. Christ, and O. Oettinger, "Elaboration of conductive thermal storage composites made of phase change materials and graphite for solar plant," *Journal of Solar Energy Engineering,* vol. 130, Feb 2008.

[54] Z. Acem, J. Lopez, and E. P. Del Barrio, "KNO3/NaNO3 - Graphite materials for thermal energy storage at high temperature: Part I. - Elaboration methods and thermal properties," *Applied Thermal Engineering,* vol. 30, pp. 1580-1585, Sep 2010.

[55] J. Fukai, Y. Hamada, Y. Morozumi, and O. Miyatake, "Improvement of thermal characteristics of latent heat thermal energy storage units using carbon-fiber brushes: experiments and modeling," *International Journal of Heat and Mass Transfer,* vol. 46, pp. 4513-4525, Nov 2003.

[56] R. Siegel, "Solidification of Low Conductivity Material Containing Dispersed High Conductivity Particles," *International Journal of Heat and Mass Transfer,* vol. 20, pp. 1087-1089, 1977.

[57] J. L. Zeng, L. X. Sun, F. Xu, Z. C. Tan, Z. H. Zhang, J. Zhang, *et al.*, "Study of a PCM based energy storage system containing Ag nanoparticles," *Journal of Thermal Analysis and Calorimetry,* vol. 87, pp. 369-373, Jan 2007.

[58] J. Sure, A. R. Shankar, S. Ramya, C. Mallika, and U. K. Mudali, "Corrosion behaviour of carbon materials exposed to molten lithium chloride-potassium chloride salt," *Carbon,* vol. 67, pp. 643-655, Feb 2014.

[59] D. R. Lide and H. P. R. Frederikse, *CRC handbook of chemistry and physics : a ready-reference book of chemical and physical data*, 76th ed / ed. Boca Raton, Fla. ; London: CRC, 1995.

[60] Y. S. Touloukian and D. P. DeWitt, *Thermal radiative properties: nonmetallic solids*. New York,: IFI/Plenum, 1972.

[61] J. R. Howell, R. Siegel, and M. P. Menguc, *Thermal radiation heat transfer*, 5th ed. Boca Raton: Taylor & Francis, 2011.

[62] W. D. Wood, H. W. Deem, and C. F. Lucks, *Thermal radiative properties*. New York,: Plenum Press, 1964.

[63] H. C. Hottel, "Radiant-Heat Transmission," in *Heat transmission, McGraw-Hill series in chemical engineering*, W. H. McAdams, Ed., 3d ed New York: McGraw-Hill, 1954, pp. 55 – 125.

[64] G. G. Gubareff, R. H. Torborg, and J. E. Janssen, *Thermal radiation properties survey : a review of the literature*, 2nd ed. Minneapolis, Minn.: Minneapolis-Honeywell Regulator Co., 1960.

[65] D. Y. Svet, *Thermal radiation : metals, semiconductors, ceramics, partly transparent bodies, and films*. New York: Consultants Bureau, 1965.

[66] Y. S. Touloukian and D. P. DeWitt, "Thermophysical Properties of Matter—the TPRC Data Series. Volume 7. Thermal Radiative Properties-Metallic Elements and Alloys," DTIC Document1970.

[67] Y. S. Touloukian and D. P. DeWitt, "Thermophysical Properties of Matter—the TPRC Data Series. Volume 8. Thermal Radiative Properties-Nonmetallic Solids," DTIC Document1972.

[68] Y. S. Touloukian, D. P. DeWitt, and R. S. Hernicz, "Thermophysical Properties of Matter—the TPRC Data Series. Volume 9. Thermal Radiative Properties-Coatings," DTIC Document1972.

[69] T. Makino, "Thermal radiation properties of molten salts (properties of alkali metal chlorides and conductive-radiative transfer in the salts)," *Heat transfer: Japanese research*, vol. 20, pp. 711-721, 1991.

[70] T. Makino, "Thermal radiation properties of molten salt (properties of alkali metal carbonates)," *Heat transfer: Japanese research*, vol. 21, pp. 331-337, 1992.

[71] N. Arai, Y. Itaya, and M. Hasatani, "Development of a Volume Heat-Trap Type Solar Collector Using a Fine-Particle Semitransparent Liquid Suspension (Fpss) as a Heat Vehicle and Heat-Storage Medium - Unsteady, One-Dimensional Heat-Transfer in a Horizontal Fpss Layer Heated by Thermal-Radiation," *Solar Energy*, vol. 32, pp. 49-56, 1984.

[72] W. D. Drotning, "Optical-Properties of Solar-Absorbing Oxide Particles Suspended in a Molten-Salt Heat-Transfer Fluid," *Solar Energy*, vol. 20, pp. 313-319, 1978.

[73] R. A. Nyquist, C. L. Putzig, M. A. Leugers, and R. O. Kagel, *The handbook of infrared and Raman spectra of inorganic compounds and organic salts*. San Diego: Academic Press, 1997.

[74] A. Hoshi, D. R. Mills, A. Bittar, and T. S. Saitoh, "Screening of high melting point phase change materials (PCM) in solar thermal concentrating technology based on CLFR," *Solar Energy*, vol. 79, pp. 332-339, 2005.

[75] P. D. Myers, Jr., T. E. Alam, R. Kamal, D. Y. Goswami, and E. Stefanakos., "Nitrate salts doped with CuO nanoparticles for thermal energy storage with improved heat transfer," *Applied Energy (Under review)*, 2015.

[76] M. Halmann and K. Zuckerman, "Stability of Molten Nitrate Salts Containing Light Absorbing Additives as Solar Flux Absorbers," *Solar Energy Materials,* vol. 17, pp. 311-318, Jun 1988.

[77] Y. Hwang, J. Lee, C. Lee, Y. Jung, S. Cheong, C. Lee, *et al.*, "Stability and thermal conductivity characteristics of nanofluids," *Thermochimica Acta,* vol. 455, pp. 70-74, 2007.

[78] T. Bauer, D. Laing, and R. Tamme, "Characterization of sodium nitrate as phase change material," *International Journal of Thermophysics,* vol. 33, pp. 91-104, 2012.

[79] N. A. Ghoneim, A. A. Ahmed, and S. Gharib, "Effect of Transition-Metal Oxides on the Thermal-Conductivity of Glass," *Thermochimica Acta,* vol. 71, pp. 43-51, 1983.

[80] H. Rawson, "Nitrate glasses," in *Inorganic glass-forming systems,* 1st ed London, New York: Academic Press, 1967, pp. 213 – 223.

[81] Y. S. Touloukian, R. W. Powell, C. Y. Ho, and P. G. Klemens, "Thermophysical Properties of Matter—the TPRC Data Series. Volume 2. Thermal conductivity: Nonmetallic Solids," *IFI/Plenum, New York,* 1970.

[82] X. W. Wang, X. F. Xu, and S. U. S. Choi, "Thermal conductivity of nanoparticle-fluid mixture," *Journal of Thermophysics and Heat Transfer,* vol. 13, pp. 474-480, Oct-Dec 1999.

[83] D. Shin and D. Banerjee, "Enhancement of specific heat capacity of high-temperature silica-nanofluids synthesized in alkali chloride salt eutectics for solar thermal-energy storage applications," *International Journal of Heat and Mass Transfer,* vol. 54, pp. 1064-1070, Feb 2011.

[84] G. J. Janz, C. B. Allen, N. Bansal, R. Murphy, and R. Tomkins, "Physical properties data compilations relevant to energy storage, 2. Molten salts: Data on single and multi-component salt systems," *NASA STI/Recon Technical Report N,* vol. 80, p. 10643, 1979.

[85] S. Lee, S. U. S. Choi, S. Li, and J. A. Eastman, "Measuring thermal conductivity of fluids containing oxide nanoparticles," *Journal of Heat Transfer-Transactions of the Asme,* vol. 121, pp. 280-289, May 1999.

[86] Linseis Messgeräte GmbH, "Instruction Manual: XFA 500 Xenon Flash Thermal Constant Analyzer."

[87] W. Parker, R. Jenkins, C. Butler, and G. Abbott, "Flash method of determining thermal diffusivity, heat capacity, and thermal conductivity," *Journal of applied physics,* vol. 32, pp. 1679-1684, 1961.

[88] P. S. Gaal, M. Thermitus, and D. E. Stroe, "Thermal conductivity measurements using the flash method," *Journal of Thermal Analysis and Calorimetry,* vol. 78, pp. 185–189, 2004.

[89] ASTM Standard, "E1461-01, 2001," *Standard Test Method for Thermal Diffusivity by the Flash Method*.

[90] M. E. Brown, *Handbook of thermal analysis and calorimetry. Vol. 1: Principles and practice*. Amsterdam: Elsevier Science, 1998.

[91] C. M. Guttman and J. H. Flynn, "On the drawing of the base line for differential scanning calorimetric calculation of heats of transition," *Analytical Chemistry*, vol. 45, 1973.

[92] F. A. Miller and C. H. Wilkins, "Infrared Spectra and Characteristic Frequencies of Inorganic Ions - Their Use in Qualitative Analysis," *Analytical Chemistry*, vol. 24, pp. 1253-1294, 1952.

[93] G. Janz, F. Kelley, and J. Perano, "Melting and Pre-Melting Phenomena in Alkali Metal Nitrates," *Journal of Chemical & Engineering Data*, vol. 9, pp. 133-136, 1964.

[94] J. Buongiorno, "Convective transport in nanofluids," *Journal of Heat Transfer-Transactions of the ASME*, vol. 128, pp. 240-250, Mar 2006.

[95] R. B. Bird, W. E. Stewart, and E. N. Lightfoot, *Transport phenomena*, Rev. 2nd ed. New York: J. Wiley, 2007.

[96] P. D. Myers, Jr., A. Bhardwaj, D. Y. Goswami, and E. Stefanakos, "Chloride salt systems for high temperature thermal energy storage: Properties and applications," *Journal of Solar Energy Engineering (Under review)*, 2015.

[97] B. Hoffschmidt, F. M. Tellez, A. Valverde, J. Fernandez, and V. Fernandez, "Performance evaluation of the 200-kW(th) HiTRec-II open volumetric air receiver," *Journal of Solar Energy Engineering*, vol. 125, pp. 87-94, Feb 2003.

[98] N. Lior, P. Ayyaswamy, J. Oleary, K. Kauffman, H. Yeh, and H. Lorsch, "Thermal energy storage considerations for solar-thermal power generation," in *11th Intersociety Energy Conversion Engineering Conference*, 1976, pp. 613-622.

[99] M. L. Yang, X. X. Yang, X. P. Yang, and J. Ding, "Heat transfer enhancement and performance of the molten salt receiver of a solar power tower," *Applied Energy*, vol. 87, pp. 2808-2811, Sep 2010.

[100] A. Rovira, M. J. Montes, M. Valdes, and J. M. Martinez-Val, "Energy management in solar thermal power plants with double thermal storage system and subdivided solar field," *Applied Energy*, vol. 88, pp. 4055-4066, Nov 2011.

[101] H. E. Reilly and G. J. Kolb, "An evaluation of molten-salt power towers including results of the solar two project," Sandia National Labs., Albuquerque, NM (US); Sandia National Labs., Livermore, CA (US)2001.

[102] K. H. Stem, "High temperature properties and decomposition of inorganic salts Part 3. Nitrates and nitrites," *J. Phys. Chem. Ref. Data*, vol. 1, 1972.

[103] A. Ferrara, R. Haslett, and J. Joyce, "Molten salt thermal energy storage for utility peaking loads," in *12th Intersociety Energy Conversion Engineering Conference*, 1977, pp. 547-554.

[104] D. Y. Goswami, F. Kreith, and J. F. Kreider, *Principles of solar engineering*, 2nd ed. Philadelphia ; London: Taylor & Francis, 2000.

[105] Y. S. Touloukian and E. H. Buyco, "Thermophysical Properties of Matter—the TPRC Data Series. Volume 5. Specific Heat-Nonmetallic Solids," DTIC Document1970.

[106] G. J. Janz, *Molten salts handbook*. New York,: Academic Press, 1967.

[107] G. J. Janz, C. B. Allen, J. R. Downey, and R. Tomkins, "Physical properties data compilations relevant to energy storage, 1. Molten salts: Eutectic data," *NASA STI/Recon Technical Report N*, vol. 78, p. 31589, 1978.

[108] G. J. Janz and R. Tomkins, "Physical Properties Data Compilations Relevant to Energy Storage, 4. Molten Salts: Data on Additional Single and Multicomponent Salt Systems.(Pamphlet)," *National Bureau of Standards, 861*, p. 1981, 1981.

[109] J. Sangster and A. D. Pelton, "Phase-Diagrams and Thermodynamic Properties of the 70 Binary Alkali-Halide Systems Having Common Ions," *Journal of Physical and Chemical Reference Data*, vol. 16, pp. 509-561, 1987.

[110] V. I. Posypajko, E. A. Alekseeva, and H. B. Bell, *Phase equilibria in binary halides*. New York: IFI/Plenum, 1987.

[111] E. M. Levin, *Phase diagrams for ceramists*. Columbus, Ohio,: American Ceramic Society, 1956.

[112] A.-N. P. E. Diagram, "CD-ROM Database," ed: Version, 2005.

[113] C. W. Bale, P. Chartrand, S. A. Decterov, G. Eriksson, K. Hack, R. B. Mahfoud, *et al.*, "FactSage Thermochemical Software and Databases," *Calphad Journal*, vol. 62, pp. 189-228, 2002.

[114] C. Bale, E. Bélisle, P. Chartrand, S. Decterov, G. Eriksson, K. Hack, *et al.*, "FactSage thermochemical software and databases—recent developments," *Calphad*, vol. 33, pp. 295-311, 2009.

[115] P. Patnaik, *Handbook of inorganic chemicals*. New York: McGraw-Hill, 2003.

[116] (Oct - Dec). Available: http://scifinder.cas.org

[117] Y. Abe, M. Kamimoto, Y. Takahashi, R. Sakamoto, K. Kanari, and T. Ozawa, "Peak load coverage by molten salts latent thermal storage," in *Intersociety energy conversion engineering conference. 19*, 1984, pp. 1114-1119.

[118] M. F. Modest, *Radiative heat transfer*, 2nd ed. Amsterdam ; Boston: Academic Press, 2003.

[119] K. Vignarooban, P. Pugazhendhi, C. Tucker, D. Gervasio, and A. Kannan, "Corrosion resistance of Hastelloys in molten metal-chloride heat-transfer fluids for concentrating solar power applications," *Solar Energy,* vol. 103, pp. 62-69, 2014.

[120] Y. Zhou, J. Chen, Y. Xu, and Z. Liu, "Effects of Cr, Ni and Cu on the Corrosion Behavior of Low Carbon Microalloying Steel in a Cl-Containing Environment," *Journal of Materials Science & Technology,* vol. 29, pp. 168-174, 2013.

[121] N. Hiramatsu, Y. Uematsu, T. Tanaka, and M. Kinugasa, "Effects of alloying elements on NaCl-induced hot corrosion of stainless steels," *Materials Science and Engineering: A,* vol. 120, pp. 319-328, 1989.

[122] J. Lehmusto, P. Yrjas, B.-J. Skrifvars, and M. Hupa, "High temperature corrosion of superheater steels by KCl and K_2CO_3 under dry and wet conditions," *Fuel Processing Technology,* vol. 104, pp. 253-264, 2012.

[123] H. Evans, D. Hilton, and R. Holm, "Chromium-depleted zones and the oxidation process in stainless steels," *Oxidation of metals,* vol. 10, pp. 149-161, 1976.

[124] B. P. Mohanty and D. A. Shores, "Role of chlorides in hot corrosion of a cast Fe–Cr–Ni alloy. Part I: experimental studies," *Corrosion science,* vol. 46, pp. 2893-2907, 2004.

[125] A. R. Shankar and U. K. Mudali, "Corrosion of type 316L stainless steel in molten LiCl–KCl salt," *Materials and corrosion,* vol. 59, pp. 878-882, 2008.

[126] M. Uusitalo, P. Vuoristo, and T. Mäntylä, "High temperature corrosion of coatings and boiler steels below chlorine-containing salt deposits," *Corrosion Science,* vol. 46, pp. 1311-1331, 2004.

[127] B. Mordyuk, G. Prokopenko, M. Vasylyev, and M. Iefimov, "Effect of structure evolution induced by ultrasonic peening on the corrosion behavior of AISI-321 stainless steel," *Materials Science and Engineering: A,* vol. 458, pp. 253-261, 2007.

[128] K. Kwong, A. Petty, J. Bennett, R. Krabbe, and H. Thomas, "Wear mechanisms of chromia refractories in slagging gasifiers," *International Journal of Applied Ceramic Technology*, vol. 4, pp. 503-513, 2007.

[129] P. D. Myers, Jr., D. Y. Goswami, and E. Stefanakos, "Molten salt spectroscopy for quantification of radiative absorption in novel metal chloride-enhanced thermal storage media," *Journal of Solar Energy Engineering,* vol. 137, p. 041002, 2015.

[130] D. Kearney, U. Herrmann, P. Nava, P. Kelly, R. Mahoney, J. Pacheco, *et al.*, "Assessment of a molten salt heat transfer fluid in a parabolic trough solar field," *Journal of Solar Energy Engineering*, vol. 125, pp. 170-176, May 2003.

[131] G. Koll, P. Schwarzbözl, K. Hennecke, T. Hartz, M. Schmitz, and B. Hoffschmidt, "The solar tower Jülich—A research and demonstration plant for central receiver systems," in *Proceedings of the 2009 SolarPaces Conference, Berlin*, 2009.

[132] R. Buck, T. Brauning, T. Denk, M. Pfander, P. Schwarzbozl, and F. Tellez, "Solar-hybrid gas turbine-based power tower systems (REFOS)," *Journal of Solar Energy Engineering*, vol. 124, pp. 2-9, Feb 2002.

[133] M. V. Smirnov, V. A. Khokhlov, and E. S. Filatov, "Thermal-Conductivity of Molten Alkali-Halides and Their Mixtures," *Electrochimica Acta*, vol. 32, pp. 1019-1026, Jul 1987.

[134] H. Koizumi and Y. H. Jin, "Performance enhancement of a latent heat thermal energy storage system using curved-slab containers," *Applied Thermal Engineering*, vol. 37, pp. 145-153, May 2012.

[135] T. R. Griffiths, "Molten Salt Spectroscopy," in *Molten Salt Techniques*, ed: Springer, 1984, pp. 79-135.

[136] N. J. Harrick, *Internal reflection spectroscopy*. New York,: Interscience Publishers, 1967.

[137] F. Abelès, *Optical properties of solids*. Amsterdam ; London: North-Holland, 1972.

[138] H. M. Crosswhite and H. W. Moos, *Optical Properties of Ions in Crystals*. S.l.: Interscience Pubs., 1967.

[139] B. Di Bartolo, *Optical properties of ions in solids*. New York: Plenum Press, 1975.

[140] M. Ibrahim, P. Sokolov, T. Kerslake, and C. Tolbert, "Experimental and computational investigations of phase change thermal energy storage canisters," *Journal of Solar Energy Engineering*, vol. 122, pp. 176-182, Nov 2000.

[141] M. Q. Brewster, *Thermal radiative transfer and properties*. New York: Wiley, 1992.

[142] D. R. Waldbaum, "Thermodynamic Mixing Properties of NaCl-KCl Liquids," *Geochimica et Cosmochimica Acta*, vol. 33, pp. 1415-&, 1969.

[143] D. W. Sheibley and M. H. Fowler, "Infrared spectra of various metal oxides in the region of 2 to 26 microns," National Aeronautics and Space Administration (NASA) Lewis Research Center, Cleveland, Ohio,1966.

[144] R. Siegel, "Net Radiation Method for Transmission through Partially Transparent Plates," *Solar Energy*, vol. 15, pp. 273-276, 1973.

[145] O. S. Heavens, *Optical properties of thin solid films*. New York,: Dover Publications, 1965.

[146] T. Makino, T. Maeda, M. Edamura, and A. Yoshida, "Thermal radiation properties of molten salts. 1st Report. Properties of alkaline metal nitrates," *Transactions of the Japan Society of Mechanical Engineers Series B*, vol. 56, pp. 3805-3809, 1990.

[147] B. Schrader, *Infrared and raman spectroscopy : methods and applications*. Weinheim: VCH, 1995.

[148] T. Makino, "Present Research on Thermal-Radiation Properties and Characteristics of Materials," *International Journal of Thermophysics*, vol. 11, pp. 339-352, Mar 1990.

[149] I. Barin, O. Knacke, and O. Kubaschewski, *Thermochemical properties of inorganic substances: supplement*. Berlin ; New York: Springer-Verlag, 1977.

APPENDIX A. NOMENCLATURE

A.1 Acronyms

$ASHRAE$	American Society of Heating Refrigerating and Air-Conditioning Engineers
CSP	Concentrating solar power
DSC	Differential scanning calorimetry
EIA	Energy Information Administration (U.S.)
$FTIR$	Fourier-transform infrared (spectroscopy)
HTF	Heat transfer fluid
IR	Infrared
$LCOE$	Levelized cost of electricity
LFA	Laser flash analysis
$LHTES$	Latent heat thermal energy storage
$NREL$	National Renewable Energy Laboratory
$NSRDB$	National Solar Radiation Database (NREL)
TES	Thermal energy storage
TGA	Thermo-gravimetric analysis
MCT	Mercury cadmium telluride
PCM	Phase-change material

A.2 Symbols

c	Speed of light
c_p	Specific heat capacity
$c_{p,l}$	Specific heat capacity of the liquid phase
$c_{p,s}$	Specific heat capacity of the solid phase
d	Sample thickness

$e_{b\lambda}$	Spectral emissive power of a blackbody
h	Planck constant
ΔH_{fus}	Latent heat of fusion
I	Radiant intensity
I_{bN}	Solar irradiance, beam normal
$I_{b\lambda}$	Spectral blackbody radiant intensity
I_{λ}	Spectral radiant intensity
I_i	Irradiance incident on surface i
k_s	Thermal conductivity
m	Mass
$\dot{m}$	mass flow rate
P	Pressure
Q	Heat
Q_{cond}	Conductive heat flux
Q_{conv}	Convective heat flux
Q_r	Radiative heat flux
q	Heat flux
R_i	Radiosity of surface i
T	Temperature
T_m	Melting temperature
T_{∞}	Ambient temperature
$t_{0.5}$	Time to reach half of the maximum temperature

A.2 Greek Letters

α	Thermal diffusivity
α_i	Absorptivity of surface i
ϵ	Emissivity
ϵ_{eff}	Effective emissivity
ϵ_{λ}	Spectral emissivity
ϵ_w	Emissivity of wall surface

κ	Boltzmann constant
λ	Wavelength
ρ_i	Reflectivity of surface i
ρ	Density
ρ_l	Density, liquid phase
ρ_s	Density, solid phase
σ	Stefan-Boltzmann constant
τ_i	Transmissivity of surface i

APPENDIX B. COPYRIGHT PERMISSIONS

Below is permission for the use of material in Chapter 5.

Philip Myers <philipmyers@mail.usf.edu>

Permission form, "Molten salt spectroscopy for quanitification of radiative absorption ..."

Beth Darchi <DarchiB@asme.org> Fri, May 29, 2015 at 1:56 PM
To: Philip Myers <philipmyers@mail.usf.edu>

Dear Prof. Myers,

It is our pleasure to grant you permission to publish **any part or all of** the ASME paper "Molten Salt Spectroscopy for Quantification of Radiative Absorption in Novel Metal Chloride-Enhanced Thermal Storage Media," by Philip D. Myers, Jr.; D. Yogi Goswami; Elias Stefanakos, J. Sol. Energy Eng. 2015; 137(4), as cited in your letter in a PhD Dissertation entitled Additives for heat transfer enhancement in high temperature ... to be published by University of South Florida.

Permission is granted for the specific use as stated herein and does not permit further use of the materials without proper authorization. Proper attribution must be made to the author(s) of the materials. **Please note:** if any or all of the figures and/or Tables are of another source, permission should be granted from that outside source or include the reference of the original source. ASME does not grant permission for outside source material that may be referenced in the ASME works.

As is customary, we request that you ensure proper acknowledgment of the exact sources of this material, the authors, and ASME as original publisher. Acknowledgment must be retained on all pages printed and distributed.

Many thanks for your interest in ASME publications.

Sincerely,

Beth Darchi
Publishing Administrator
ASME
2 Park Avenue, 6th Floor
New York, NY 10016-5990
Tel 1.212.591.7700
darchib@asme.org

ABOUT THE AUTHOR

Philip D. Myers, Jr., received his bachelor's degree in chemical engineering from the University of Delaware in 2005 and his master's degree in chemical engineering from the University of South Florida in 2012.

In 2006, he accepted a position as a post-bachelor's research associate at the Army Research Laboratory at Aberdeen Proving Ground, Aberdeen, Maryland, where his work included the development of environmentally friendly low-VOC materials. From 2007 to 2010, he worked as an engineering analyst for the consultant company Black & Veatch, whose clients included the U.S. EPA. His graduate work was undertaken at the USF Clean Energy Research Center under the guidance of Dr. D. Yogi Goswami and Dr. Elias Stefanakos. His Ph.D. research focused on the development and characterization of novel thermal energy storage media for use in high-temperature solar thermal power applications. He also assisted in the revision of Dr. Goswami's textbook, *Principles of Solar Energy Engineering* (3rd Ed.), and co-authored the solutions manual for that text.